


การใช้งานผลึกขนาดนาโนเมตรของไทเทเนียมไดออกไซด์ที่ดัดแปลงโดยกระบวนการเย็น

ตัวอย่างรวดเร็วสำหรับตัวเร่งปฏิกิริยาและตัวรองรับของตัวเร่งปฏิกิริยา



นาย ปิยะวัฒน์ สุขศรีรุ่งเจริญ

วิทยานิพนธ์นี้เป็นส่วนหนึ่งของการศึกษาตามหลักสูตรปริญญาวิทยาศาสตรดุษฎีบัณฑิต

สาขาวิชาวิศวกรรมเคมี ภาควิชาวิศวกรรมเคมี

คณะวิศวกรรมศาสตร์ จุฬาลงกรณ์มหาวิทยาลัย

ปีการศึกษา 2550

ลิขสิทธิ์ของจุฬาลงกรณ์มหาวิทยาลัย

APPLICATIONS OF TITANIUM DIOXIDE NANOCRYSTAL MODIFIED BY
QUENCHING PROCESSES FOR CATALYST AND CATALYST SUPPORT



Mr. Piyawat Supphasrirongjaroen

A Dissertation Submitted in Partial Fulfillment of the Requirements
for the Degree of Doctor of Engineering Program in Chemical Engineering

Department of Chemical Engineering

Faculty of Engineering

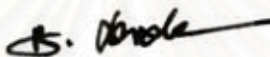
Chulalongkorn University

Academic Year 2007

Copyright of Chulalongkorn University

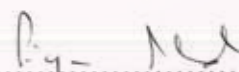
Thesis Title APPLICATIONS OF TITANIUM DIOXIDE NANOCRYSTAL
 MODIFIED BY QUENCHING PROCESSES FOR CATALYST
 AND CATALYST SUPPORT
By Mr. Piyawat Suphasrirongjaroen
Field of Study Chemical Engineering
Thesis Advisor Professor Piyasan Prasertthdam, Dr.Ing.
Thesis Co-Advisor Assistant Professor Duangkamol Na Ranong, D.Eng.

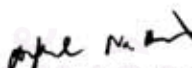
Accepted by the Faculty of Engineering, Chulalongkorn University in Partial
Fulfillment of the Requirements for the Doctor's Degree



.....Dean of the Faculty of Engineering
(Associate Professor Boonsom Lerdhirungwong, Dr.Ing.)


THESIS COMMITTEE


.....Chairman
(Assistant Professor Montree Wongsri, D.Sc.)


.....Thesis Advisor
(Professor Piyasan Prasertthdam, Dr.Ing.)


..... Thesis Co-Advisor
(Assistant Professor Duangkamol Na Ranong, D.Eng.)


..... Member
(Akawat Sirisuk, Ph.D.)


.....Member
(Assistant Professor Bunjerd Jongsomjit, Ph.D.)


.....External Member
(Assistant Professor Okorn Mekasuwandumrongt, D.Eng.)

ปิยะวัฒน์ ศุภศรีรุ่งเจริญ : การใช้งานผลึกขนาดนาโนเมตรของไทเทเนียมไดออกไซด์ที่ดัดแปลง โดยกระบวนการเย็นตัวอย่างรวดเร็วสำหรับตัวเร่งปฏิกิริยาและตัวรองรับของตัวเร่งปฏิกิริยา (APPLICATIONS OF TITANIUM DIOXIDE NANOCRYSTAL MODIFIED BY QUENCHING PROCESSES FOR CATALYST AND CATALYST SUPPORT) อ. ที่ปรึกษา: ศ.ดร.ปิยะสาร ประเสริฐธรรม, อ.ที่ปรึกษาร่วม: ผศ.ดร.ดวงกมล ณ ระนอง, 114 หน้า.

วิทยานิพนธ์ฉบับนี้ ศึกษาถึงการใช้งานผลึกขนาดนาโนเมตรของไทเทเนียมไดออกไซด์ที่ดัดแปลงโดยกระบวนการเย็นตัวอย่างรวดเร็ว สำหรับตัวเร่งปฏิกิริยา และตัวรองรับของตัวเร่งปฏิกิริยา โดยสังเคราะห์ผลึกขนาดต่างๆ ของไทเทเนียมไดออกไซด์และสังเคราะห์ผลึกไทเทเนียมไดออกไซด์ที่เติมโลหะชนิดที่สองด้วยวิธีโซลโวลเทอร์มอล และนำเข้าสู่กระบวนการเย็นตัวอย่างรวดเร็วในตัวกลางชนิดต่างๆ ในการพิสูจน์เอกลักษณ์ของตัวเร่งปฏิกิริยาทำการศึกษา โดยใช้การดูดซับทางกายภาพด้วยไนโตรเจน การกระเจิงรังสีเอ็กซ์ การส่องผ่านด้วยกล้องจุลทรรศน์อิเล็กตรอน การหลุดออกของคาร์บอนไดออกไซด์แบบโปรแกรมอุณหภูมิ อิเล็กตรอนสปีนเรโซแนนซ์ และเอ็กซ์เรย์โฟโต้อิเล็กตรอนสเปกโตรสโคปี ความว่องไวในการเร่งปฏิกิริยาเชิงแสงของตัวเร่งปฏิกิริยาไทเทเนียมไดออกไซด์ ได้ทดสอบในปฏิกิริยาการสลายตัวของเอทิลีนภายใต้การภาวะฉายแสงอัลตราไวโอเล็ต ผลการศึกษา พบว่า การเย็นตัวอย่างรวดเร็วในตัวกลางต่างชนิดกัน ทำให้ผลึกไทเทเนียมไดออกไซด์มีความบกพร่องบนพื้นผิวแตกต่างกัน ผลึกที่มีความบกพร่องบนพื้นผิวมากจะมีความว่องไวในการทำปฏิกิริยาสูง ผลึกไทเทเนียมไดออกไซด์ที่มีขนาดเล็กจะได้ผลจากการกระบวนการเย็นตัวอย่างรวดเร็วมากกว่าผลึกที่มีขนาดใหญ่ นอกจากนี้ พบว่าการเลือกเติมโลหะชนิดที่สองที่เหมาะสม จะช่วยเพิ่มความสามารถในการเร่งปฏิกิริยาของผลึกไทเทเนียมไดออกไซด์ สำหรับการใช้งานผลึกขนาดนาโนเมตรของไทเทเนียมไดออกไซด์สำหรับตัวรองรับตัวเร่งปฏิกิริยา พบว่าผลของกระบวนการเย็นตัวอย่างรวดเร็ว มีแนวโน้มส่งผลดีในการช่วยให้ตัวเร่งปฏิกิริยามีความว่องไวมากขึ้น สำหรับปฏิกิริยาไฮโดรจิเนชันของคาร์บอนไดออกไซด์

ภาควิชา.....วิศวกรรมเคมี..... ลายมือชื่อนิสิต..... ปิยะวัฒน์ ศุภศรีรุ่งเจริญ.....
 สาขาวิชา.....วิศวกรรมเคมี..... ลายมือชื่ออาจารย์ที่ปรึกษา.....
 ปีการศึกษา.....2550..... ลายมือชื่ออาจารย์ที่ปรึกษาร่วม.....

##4771818521: MAJOR CHEMICAL ENGINEERING

KEY WORD: TITANIUM (IV) OXIDE/ SOLVOTHERMAL METHOD/ SURFACE DEFECT/ PHOTOCATALYTIC OXIDATION OF ETHYLENE

PIYAWAT SUPPHASRIRONGJAROEN: APPLICATIONS OF TITANIUM DIOXIDE NANOCRYSTAL MODIFIED BY QUENCHING PROCESSES FOR CATALYST AND CATALYST SUPPORT. THESIS ADVISOR: PROF. PIYASAN PRASERTHDAM, Dr.Ing., THESIS COADVISOR: ASST. PROF. DUANGKAMOL NA RANONG, D.Eng., 114 pp.

In this work, pure anatase nano-TiO₂ with various crystallite sizes and metal-doped TiO₂ were synthesized by solvothermal method. The catalysts were subjected to a rapid quenching in various media such as H₂O, 30%wt H₂O₂, air, and liquid N₂ as a post-synthesis treatment. In order to identify the characteristics, all catalysts were characterized using N₂ physisorption, XRD, SEM, CO₂-TPD, ESR, and XPS. The photocatalytic activities of TiO₂ catalysts were evaluated for the degradation of ethylene under UV illumination. It was found that photocatalytic activity of the nano-sized TiO₂ quenched in different media is evidently different. It is likely that quenching process can modify surface properties of the TiO₂ samples i.e., enhancing the amount of surface defects (Ti³⁺) so that higher photocatalytic activity was obtained. The effect of quenching was more pronounced on the smaller crystallite size TiO₂ than on the larger ones. In addition, the selection of a suitable second metal doping can enhance photocatalytic activity of the TiO₂. Moreover, the quenching processes tended to have positive effect on activity for CO hydrogenation reaction.

Department.....Chemical Engineering.....	Student's signature..... <i>Piyawat Supphasrirongjaroen</i>
Field of study....Chemical Engineering.....	Advisor's signature..... <i>Piyasan Praserttham</i>
Academic year.....2007.....	Co-Advisor's signature..... <i>Duangkamol Na Ranong</i>

ACKNOWLEDGEMENTS

This dissertation would not have been possible to complete without the support of the following individuals. Firstly, He would like to express his greatest gratitude to his advisor and co-advisor, Professors Piyasan Praserttham and Assistant Professor Duangkamol Na-Ranong, for their invaluable guidance during the course of this work. In addition, I am also very grateful to Dr. Montree Wongsr, for his kind supervision over this thesis as the chairman, Assistant Professor Bunjerd Jongsomjit, Dr. Akawat Sirisuk and Assistant Professor Okorn Mekasuwandumrongt, members of the thesis committee for their kind cooperation.

The financial supports from the Chulalongkorn University Graduate Scholarship to Commemorate the 72nd Anniversary of his Majesty King Bhumibol Adulyadej, The 90th Anniversary of Chulalongkorn University Fund (Ratchadaphiseksomphot Endowment Fund), Thailand Research Fund (TRF) and the Commission on Higher Education (CHE) are also gratefully acknowledged.

Many thanks for kind suggestions and useful help to Assistant Professor Joongjai Panpranot, Dr. Kongkiat Suriye, Miss. Malin Mungmart and many friends in the Center of Excellence on Catalysis and Catalytic Reaction Engineering who always provide the encouragement and assistance along the thesis study.

Most of all, I would like to express my highest gratitude to my parents, my brother and my sister who always pay attention to me all the times for suggestions, support and encouragement.

CONTENTS

	Page
ABSTRACT (IN THAI).....	iv
ABSTRACT (IN ENGLISH).....	v
ACKNOWLEDGEMENTS.....	vi
CONTENTS.....	vii
LIST OF TABLES.....	xi
LIST OF FIGURES.....	xii
CHAPTER	
I INTRODUCTION.....	1
II LITERATURE REVIEWS.....	5
2.1 Titanium dioxide for use as photocatalysts	5
2.2 Metal-doped TiO ₂ for use as photocatalysts.....	7
2.2.1 Si-doped TiO ₂	7
2.2.2 Zr-doped TiO ₂	9
2.3 Titanium dioxide for use as catalyst support.....	10
III THEORY.....	12
3.1 Quenching process	12
3.1.1 Classification of quenching methods and techniques...	12
3.1.2 Quenching media and techniques.....	13
3.2 Titanium (IV) oxide	15
3.2.1 Physical and Chemical Properties.....	15
3.2.2 Preparation procedure of TiO ₂	18
3.2.2.1. Solution routes.....	18
3.2.2.2. Gas phase methods.....	19
3.2.3 Applications of titanium dioxide.....	20
3.3 Photocatalytic process	21
3.4 CO-hydrogenation.....	24
3.5 Co-based catalysts.....	29

	Page
IV EXPERIMENTAL.....	30
4.1 Catalyst preparation.....	30
4.1.1 Synthesis of TiO ₂	30
4.1.2 Synthesis of metal-doped TiO ₂	31
4.1.3 Quenching treatment.....	32
4.1.4 Synthesis of Co/TiO ₂ catalyst.....	32
4.2 Catalyst characterization.....	32
4.2.1 TiO ₂ photocatalyst.....	33
4.2.1.1 X-ray diffractometry (XRD).....	33
4.2.1.2 Specific surface area measurement.....	33
4.2.1.3 Transmission electron microscope (TEM).....	34
4.2.1.4 Scanning electron microscopy (SEM).....	34
4.2.1.5 Temperature programmed desorption of carbon dioxide (CO ₂ -TPD).....	34
4.2.1.6 Electron spin resonance spectroscopy (ESR).....	34
4.2.1.7 X-ray photoelectron spectroscopy (XPS).....	35
4.2.2 Supported metal catalyst.....	35
4.2.2.1 Scanning electron microscopy and energy dispersive X-ray spectroscopy.....	35
4.2.2.2 Temperature-programmed reduction (TPR).....	35
4.2.2.3 Hydrogen pulse chemisorption.....	36
4.2.2.4 X-ray photoelectron spectroscopy (XPS).....	36
4.3 Reactivity measurements.....	37
4.3.1 Photocatalytic reaction.....	37
4.3.1.1 Chemicals and reagents.....	37
4.3.1.2 Instruments and apparatus.....	37
4.3.1.3 Procedures.....	39
4.3.2 CO-hydrogenation reaction.....	40
4.3.2.1 Material.....	40
4.3.2.2 Instruments and apparatus.....	40

	Page
4.3.2.3 Procedures	41
RESEARCH METHODOLOGY	
V RESULTS AND DISSCUSSION.....	44
5.1 Titanium dioxide as photocatalyst.....	45
5.1.1 Effect of quenching medium on photocatalytic activity of nano-TiO ₂ prepared by solvothermal method.....	45
5.1.1.1 Synthesis of Titanium (IV) oxide in toluene....	45
5.1.1.2 Specific surface area and crystal structure.....	46
5.1.1.3 Temperature programmed desorption of carbon dioxide (CO ₂ -TPD).....	48
5.1.1.4 X-ray Photoelectron spectroscopic (XPS) measurements.....	49
5.1.1.5 Photocatalytic activity of the nano-TiO ₂ quenched in different media.....	52
5.1.2. Dependence of quenching process on the photocatalytic activity of solvothermal-derived TiO ₂ with various crystallite sizes.....	55
5.1.2.1 Textural properties of the TiO ₂ photocatalysts..	55
5.1.2.2 Temperature programmed desorption of carbon dioxide (CO ₂ -TPD).....	58
5.1.2.3 Photocatalytic activity of the nano-TiO ₂ quenched in different media.....	61
5.1.3 Effect of Si and Zr addition on the surface defect and photocatalytic activity of the solvothermal-derived TiO ₂ ...	62
5.1.3.1 Textural properties of the TiO ₂ photocatalysts...	62
5.1.3.2 Electron spin resonance spectroscopy (ESR) study.....	65
5.1.3.3 X-ray photoelectron spectroscopy (XPS) study..	67
5.1.3.4 Photocatalytic activity test.....	70

	Page
5.2 Titanium dioxide as catalyst support.....	71
5.2.1 Catalytic behaviors of quenched TiO ₂ -supported cobalt Fischer–Tropsch catalysts for carbon monoxide hydrogenation.....	71
5.2.1.1 Characteristics of catalyst	71
5.2.1.2 Catalytic properties.....	78
VI CONCLUSIONS AND RECOMMENDATIONS.....	79
6.1 Conclusions.....	79
6.1.1 Titanium dioxide as photocatalyst.....	79
6.1.2 Titanium dioxide as catalyst support.....	80
6.2 Recommendations for future studies.....	81
REFERENCES.....	82
APPENDICES.....	88
APPENDIX A: CALCULATION FOR CATALYST PREPARATION.....	89
APPENDIX B: CALCULATION OF THE CRYSTALLITE SIZE.....	91
APPENDIX C: CALCULATION FOR TOTAL H ₂ CHEMISSORPTION.....	94
APPENDIX D: THE OPERATING CONDITIONS OF GAS CHROMATOGRAPHYAND CALIBRATION CURVES.....	95
APPENDIX E: CALCULATION OF CO CONVERSION REACTION RATE AND SELECTIVITY.....	101
APPENDIX F: LIST OF PUBLICATIONS.....	102
VITA.....	114

LIST OF TABLES

Table	Page
3.1 Crystallographic properties of anatase, brookite, and rutile.....	17
4.1 Chemicals used in synthesis of TiO ₂	30
4.2 Chemicals used in of metal-doped TiO ₂	31
4.3 Operating conditions for gas chromatograph for photocatalytic reaction	39
4.4 Operating condition for gas chromatograph for CO-hydrogenation	42
5.1 Specific surface areas and crystallite sizes of titania under various quenching conditions	47
5.2 The amount of Ti ³⁺ surface defects of TiO ₂ catalysts from XPS measurements.....	54
5.3 Phase compositions and structural properties of the TiO ₂ synthesized by solvothermal method after quenching in various media.....	57
5.4 Physical properties and activities of Si- and Zr-doped TiO ₂ samples synthesized by solvothermal method.....	64
5.5 XPS binding energies (eV) and FWHM (eV) values of Si- and Zr-doped TiO ₂ catalysts.....	68
5.6 Crystallite sizes and BET surface areas of quenched titania support.....	72
5.7 Characteristics of various Co/TiO ₂ catalysts.....	72
5.8 Reaction study during CO hydrogenation of catalyst samples pretreated under various quenching conditions.....	78
D1. The operating condition for gas chromatograph.....	95
D2. Conditions use in Shimadzu modal GC-8A and GC-14B.....	98

LIST OF FIGURES

Figure	Page
3.1 Crystal structures of anatase (a), rutile (b), and brookite (c).....	16
3.2 Band-gap diagram formation of holes (h^+) and electrons (e^-) upon UV irradiation of semiconductor surface.....	21
3.3 Main processes occurring on a semiconductor particle: (a) electron–hole generation; (b) oxidation of donor (D); (c) reduction of acceptor (A); (d) and (e) electron–hole recombination at surface and in bulk, respectively....	22
4.1 Photoreactor for experiment.....	38
4.2 Flow diagram of CO hydrogenation system.....	43
5.1 Mechanism of reaction in toluene for the titania product	45
5.2 The XRD patterns of the TiO_2 obtained from quenching in various media; (A) liquid N_2 , (B) H_2O at RT, (C) H_2O at 373 K, (D) 30% wt H_2O_2 at RT, (E) 30% wt H_2O_2 at 373 K, (F) air at RT and (G) air at 77 K.....	46
5.3 Thermal desorption spectra for CO_2 adsorbed on TiO_2 quenched in different media; (A) liquid N_2 , (B) H_2O at RT, (C) H_2O at 373 K, (D) 30% wt H_2O_2 at RT, (E) 30% wt H_2O_2 at 373 K, (F) air at RT and (G) air at 77 K.....	48
5.4 Overview X-ray photoelectron spectra in the case of TiO_2 sample quenched in 30% wt hydrogen peroxide at room temperature.....	49
5.5 Ti 2p XPS spectra for TiO_2 sample quenched in 30% wt hydrogen peroxide at room temperature.....	50
5.6 O 1s XPS spectra for TiO_2 sample quenched in 30% wt hydrogen peroxide at room temperature.....	51
5.7 Results of photocatalytic testing comparing the activities of different TiO_2 samples.....	52
5.8 Ethylene conversions as a function of surface Ti^{3+} on the TiO_2 samples quenched in different media.....	53
5.9 The XRD patterns of the various TiO_2 samples after quenching in air at room temperature: (a) 9 nm, (b) 11 nm, (c) 13 nm.....	56

Figure	Page
5.10 TEM micrographs of TiO ₂ -9 nm and TiO ₂ -13 nm (non-quenched).....	58
5.11 CO ₂ temperature programmed desorption results of the TiO ₂ 11 nm quenched in different media; (A) Air at 373 K, (B) Air at RT, (C) H ₂ O at 373 K, (D) H ₂ O at RT, (E) H ₂ O ₂ at 373 K, (F) H ₂ O ₂ at RT (RT = room temperature).....	59
5.12 Ti ³⁺ /Ti ⁴⁺ calculated from CO ₂ -TPD results of the TiO ₂ -11 nm quenched in different media: (A) Air at 373 K, (B) Air at RT, (C) H ₂ O at 373 K, (D) H ₂ O at RT, (E) H ₂ O ₂ at 373 K, (F) H ₂ O ₂ at RT (RT = room temperature)..	60
5.13 Results of the photocatalytic activities of TiO ₂ samples quenched in different media.....	62
5.14 X-ray diffraction patterns of pure TiO ₂ and metal doped-TiO ₂	63
5.15 ESR spectra of (a) 0.002 Si-doped TiO ₂ , (b) 0.005 Si- doped TiO ₂ , (c) 0.1 Si- doped TiO ₂ , (d) 0.002 Zr- doped TiO ₂ , (e) 0.005 Zr- doped TiO ₂ , (f) 0.1 Zr- doped TiO ₂	66
5.16 Ti 2p XPS spectra of various TiO ₂ samples: (a) TiO ₂ -RT, (b) 0.1-(Zr)-TiO ₂ -RT, (c) 0.1-(Si)-TiO ₂ -RT.....	69
5.17 XRD patterns of sample pretreated under various quenching conditions; (a) TiO ₂ supports and (b) Co/TiO ₂ catalysts.....	73
5.18 a) SEM micrograph and EDX mapping of Co/TiO ₂ quenched in air.....	74
5.18 b) SEM micrograph and EDX mapping of Co/TiO ₂ quenched in water at room temperature.....	75
5.18 c) SEM micrograph and EDX mapping of Co/TiO ₂ quenched in water at room temperature.....	76
5.19 Temperature-programmed reduction of the catalyst samples (a) 20%Co/TiO ₂ -Air; (b) 20%Co/TiO ₂ -H ₂ O; (c) 20%Co/TiO ₂ -H ₂ O 100....	77
A.1 The 101 diffraction peak of titania for calculation of the crystallite size.....	92
A.2 The plot indicating the value of line broadening due to the equipment. The data were obtained by using α -alumina as standard.....	93

Figure	Page
D.1 The calibration curve of ethylene.....	96
D.2 The calibration curve of methane.....	98
D.3 The calibration curve of ethylene.....	99
D.4 The chromatograms of catalyst sample from thermal conductivity detector, gas chromatography Shimadzu model 8A (Molecular sieve 5A column)....	99 100



สถาบันวิทยบริการ
จุฬาลงกรณ์มหาวิทยาลัย

CHAPTER I

INTRODUCTION

Titanium dioxide (TiO₂ or titania) belongs to the family of transition metal oxides. TiO₂ has received a great deal of attention due to its chemical stability, non-toxicity, low cost, high photostability and redox selectivity, and other advantageous properties (Ohtani *et al.*, 1997). Titania is used in catalytic reactions acting as a promoter, a carrier for metals and metal oxides, an additive, or as a catalyst. Reactions carried out with TiO₂ catalysts include selective reduction of NO_x to N₂ (Hu and Apple, 1996; Amridis *et al.*, 1999), effective decomposition of VOCs (including dioxins (Blanco *et al.*, 1997) and chlorinated (Busca and Angeles, 2002) compounds.) H₂S oxidation to S (Chun *et al.*, 1998), CO oxidation by O₂ (Fan *et al.*, 2003), and Fischer–Tropsch synthesis (Li *et al.*, 2002). Titania has three naturally occurring polymorphs, namely, anatase (tetragonal), brookite (orthorhombic), and rutile (tetragonal). Rutile is the most stable form of titanium dioxide. Two different crystal structures of TiO₂, rutile and anatase, are commonly used in photocatalysis, with anatase showing a higher photocatalytic activity. Anatase type titania has been used as a catalyst for photodecomposition and solar energy conversion, because of its high photoactivity (Lason and Falconer, 1994; Kamat and Dimitrijevic, 1990; Herrmann *et al.*, 1997; Fox and Dulay, 1993; Fujishima *et al.*, 1999). On the other hand, rutile-type titania has been used for white pigment materials, because of its good scattering effect, which protects materials from ultraviolet light.

Titania nanocrystal is usually prepared by sol-gel (Zaharescu *et al.*, 1997), gas-synthesis (Morrison *et al.*, 1997) and solvothermal process (Kominami *et al.*, 1999). Although the sol-gel method is widely used to prepare nanometer TiO₂, calcination process will inevitably cause the grain growth and reduction in specific surface area of particles and even induce phase transformation. Solvothermal synthesis, in which chemical reactions can occur in aqueous or organic media under the self-produced pressure at low temperature, (usually lower than 250 °C) can solve those problems encountered during sol-gel process.

TiO₂ semiconductor photocatalysts have the potential to oxidize a wide range of organic compounds, including chlorinated organic compounds, such as dioxins, into harmless compounds such as CO₂ and H₂O by irradiation with UV light (Blount and Falconer, 2001). In general, a photocatalytic reaction involves various processes on the TiO₂ surface such as oxidation reaction by photo-generated holes, reduction reaction by photo-generated electrons, diffusion of electrons and holes, and electron-hole recombination (Hoffmann *et al.*, 1995). UV light excites the electrons from the valence band to the conduction band of the TiO₂, leaving holes in the valence band. These electrons and holes can then initiate redox reactions with molecular species adsorbed on the surfaces of the catalysts.

The photocatalytic activity of TiO₂ strongly depends on preparation methods and post-treatment conditions since they have a decisive influence on crystal structure, particle size, surface area, pore size, density of OH groups, surface acidity, number and nature of trap sites incident light intensity, porosity and surface characteristics of the TiO₂ (Serpone, 1997). It has been reported that photocatalytic activity is increased with the decrease in titania particle size, especially into nanometerscale, because of high surface area and short interface migration distances for photoinduced holes and electrons (Xu *et al.*, 1999).

The surface characteristics may be modified by several pre-treatments of the photocatalyst such as sulfation, reduction with hydrogen, and halogenation in order to enhance the photocatalytic activity. TiO₂ always exists structural defects on the surface and inside the titania particles (Torimoto *et al.*, 1996). Although, the bulk defect is important factor to control level of perfect crystal, the surface defect is more important than bulk structure in field of surface science such catalyst and support. It has been known that surface defects play a fundamental role in the interaction of molecules with oxide surfaces, since defects act as active sites for the adsorption and dissociation of molecules on the surface (Diebold, 2003). In TiO₂ surfaces, these defects, mainly Ti³⁺ species (oxygen vacancies), play an important role in the photo-oxidation of organic species on the TiO₂ photo-catalyst (Shklover *et al.*, 1997). The use of a variety of

techniques including X-ray photoelectron spectroscopy (XPS) (Diebold, 2003), O₂ photodesorption (Rusu and Yates, 1997), electron spin resonance (ESR) (Nakaoka and Nosaka, 1997) and CO₂-temperature programmed reduction (TPD) (Thompson et al., 2003) can monitor the surface defect of titania.

Due to its tremendous technological importance, surface properties of TiO₂ have been extensively investigated in order to understand its photocatalytic properties. Some success in enhancing the photocatalytic activity has been achieved by several methods, such as using nano-sized semiconductor crystallites instead of bulk materials (Maira *et al.*, 2000) and modifying photocatalysts by sulfation (Corma *et al.*, 1996), reduction with hydrogen (Liu *et al.*, 2003), halogenation (Amama *et al.*, 2002), doping with ions (Yu *et al.*, 2002), or coupling TiO₂ to other oxides. These improvement methods reported in the literature are time-consuming, high cost, and rather complicated. An alternative pre-treatment technique for create defect sites on TiO₂ surface is quenching process. This possible an effective method for improve photocalytic activity of the TiO₂ because in the literature find the variety of the surface defects, strains and reconstructions caused by the process of annealing or quenching (Henderson, 1996).

Therefore, we focus on the study of effects of quenching processes on the properties and photocatalytic activities of titania and metal doped on titania prepared via a solvothermal method. Photocatalytic oxidation is employed as a main model reaction to determine photocatalytic activity of these catalysts under UV irradiation. The main goal of this research is to investigate and understand the effects of various factors on the photocatalytic activities of titania and metal doped on titania. The study included the effects of quenching media on the photocatalytic activities in photocatalytic oxidation of ethylene, the effect of different temperature of quenching media on the photocatalytic activities in gas-phase reaction of TiO₂.

The objectives of this research are as follows:

1. To study the preparation of titania and metal doped on titania using a solvothermal method.
2. To study the effect of quenching processes, namely, type and temperature of quenching media, on crystallite size, phase, and photocatalytic activity of titania and metal doped on titania prepared by solvothermal method.
3. To study effects of using quenched titania as catalyst support in CO hydrogenation reaction

This thesis is arranged as follows:

Chapter I mentions the introduction of this work

Chapter II presents literature reviews of previous works related to this research.

Chapter III explains the principle of catalyst preparation via solvothermal method and basic information about titania such as physical properties as well as the principles of photocatalytic process. In addition, basic theory about CO hydrogenation and Co-catalyst are described.

Chapter IV describes synthesis of titania and metal doped on titania employed in this research, experimental apparatus and characterization equipments.

Chapter V describes experimental results and discussion of this research.

Chapter VI presents overall conclusions of this research and recommendations for future work.

CHAPTER II

LITERATURE REVIEWS

This chapter reviews the work about several synthesis of titania and improvement of titania properties. A researcher has been found the advantage and drawback which not only the synthesis method but also in titania properties. Their works is very useful to apply titania in several ways such as, the photocatalytic reaction, electronic equipment, industrial etc. and learn to develop technical for modify and apply in the future.

2.1 Titanium dioxide for use as photocatalysts

Kominami *et al.* (1999) studied new synthesis method for nanosized by hydrolysis of titanium (IV) *n*-butoxide (TNB) in toluene and add water in the gap of autoclave. Titania was prepared in various conditions, found that anatase and amorphous formed in the reaction. When they calculate surface area in assumption that the particles were nonporous spheres for compared the specific surface area from BET measurement which test contaminate amorphous phase in the as-prepared titania. They found that when the reaction time was prolonged, the crystallite size was gradually increased and the effect of the combustion heat of the organic moieties locally raises the surface temperature of crystals, which can accelerate the crystallization and/or sintering of TiO₂ crystals (or particle) from the calcinations and the decrease in surface area from BET was probably due to sintering of single crystals.

Kim *et al.* (2003) had synthesized nanocrystalline TiO₂ in toluene by a solvothermal route. Weight ratios of titanium isopropoxide (TIP) to toluene prepared in the mixture are 5/100, 10/100, 20/ 100, 30/100 and 40/100. After synthesis at 250 °C for 3 h with solutions at the weight ratios 10/100, 20/100 and 30/100 nanocrystalline TiO₂ particles were formed. They found that average size of the nanocrystalline particle increases as increasing the amount of TIP precursor in this composition range.

Payakgul *et al.* (2005) studied effects of reaction medium on the synthesis of TiO₂ nanocrystals by thermal decomposition of titanium (IV) *n*-butoxide. They used 1,4-butanediol or toluene as organic solvent for titania synthesis. They found that the products synthesized in toluene agglomerated into spherical micron-sized particle, which is called secondary particle. On the other hand, in case of reaction in 1,4-butanediol, irregular aggregates of nanometer particles are observed for all reaction holding period investigated. They suggested that the product synthesized in toluene may contain small amount of amorphous-like phase, while titania synthesized in 1,4-butanediol is crystalline. In addition, they found that anatase products obtained from the reaction in toluene start transforming into rutile at lower calcination temperature than the products obtained in 1,4-butanediol. They concluded that anatase titania synthesized via different routes, i.e. direct crystallization or solid state transformation of amorphous intermediate, contains different amount of defect structures in the crystals.

Nakaoka *et al.* (1997) studied ESR investigation into the effects of heat treatment and crystal structure on radicals produced over irradiated TiO₂ powder. Electron spin resonance measurements were carried out at 77 K under irradiation for anatase TiO₂ powders treated by heating at various temperatures in the air. For the untreated powder photoproducted holes were trapped at the surface forming Ti⁴⁺O⁻Ti⁴⁺OH⁻ radicals, while, for the heated powder, they were trapped as Ti⁴⁺O²⁻ Ti⁴⁺O⁻ radicals at the surface. Photoproducted electrons were trapped as Ti⁴⁺ at the surface of the unheated powder, while they trapped at the inner part of the heat-treated powder. These differences could be explained by the desorption of surface hydroxyl groups and the change in the surface structure accompanied by the crystalline growth. No photoproducted radicals were detected for rutile TiO₂ powder, which may explain the low photocatalytic activity of this crystalline structure.

2.2 Metal-doped TiO₂ for use as photocatalysts

Metal-doped TiO₂ can be used as photocatalysts. The influence of dissolved metal impurity ions on the photocatalytic properties of TiO₂ has become another interesting area of semiconductor modification. The benefit of transition metal doping species is the improved trapping of electrons to inhibit electron-hole recombination during illumination. The concentration of the beneficial transition metal dopants is very small and large concentrations are detrimental.

Silica–titania nanocomposites are more efficient photocatalysts than pure TiO₂. The increase in photocatalytic efficiency has been attributed to the improved adsorption and concentration of the reactants near the active centers. At the same time, silica acts as the carrier of titania and helps to obtain a large surface area as well as suitable porous structure. Titanium and zirconium belong to the same group (IVB) of elements, both oxides TiO₂ and ZrO₂ are n-type semiconductors with similar physicochemical properties. Doping of TiO₂ with metal elements produces crystal defects and surface modifications, which can change its photocatalytic properties. Therefore, the Si-doped TiO₂ and Zr-doped TiO₂ are discussed in this research.

2.2.1 Si-doped TiO₂

Jung *et al.* (1999) studied preparation anatase-phase titania by embedding silica and photocatalytic activity for the decomposition of trichloroethylene. Nanophase titania particles were prepared by the sol–gel process using two different precursors; titanium isopropoxide (TTIP) and titanium ethoxide (TEOT). Silica-embedded titania particles was also prepared from TEOT and tetra-ethyl-ortho-silicate (TEOS). In the case of nanophase titania particles prepared from TTIP, the rutile/anatase mixed phase had higher photoactivity than the pure anatase in the decomposition of TCE. However, in the nanophase titania prepared from TEOT, the photoactivity was increased with the heat treatment temperature until rutile phase began to be formed. The surface area was decreased with the heat treatment temperature. The photoactivity of the pure anatase

titania prepared from TEOT was higher than that of Degussa P25 and the anatase/rutile mixed titania prepared from TTIP. Therefore, we concluded that, in order to achieve high photocatalytic activity, it was important to prepare titania particles at high temperature, preferably without forming rutile phase but not necessarily. This conclusion was confirmed by the experimental result that the silica-embedded titania particle of pure anatase phase had higher photoactivity than that of Degussa P25 and the pure anatase titania prepared from TEOT. The embedding of small amount of silica into anatase titania matrix enhanced the thermal stability of nanophase titania particle resulting in the suppression of the phase transformation from anatase to rutile phase. This thermal stability enables us to calcine the silica-embedded particles at higher temperature without accompanying the phase transformation and to reduce the bulk defects, which are responsible for the low photocatalytic activity.

Cheng *et al.* (2003) have studied preparation and characterization of silica-doped titania photocatalyst through sol-gel method. Five kinds of $X\text{SiO}_2/\text{TiO}_2$ nanopowders (X denotes wt.%) were prepared by the sol-gel process. $\text{Ti}(\text{O}i\text{Bu})_4$ and TEOS were used as precursors of titania and silica, respectively. The samples were calcined at the temperatures ranging from 400 °C to 950 °C for two hours. They reported that the suitable addition of silica into titania can effectively suppress the phase transformation of titania from anatase to rutile and prevent the growth of titania grains. The optimum material for higher photoactivity is 30 $\text{SiO}_2/\text{TiO}_2$ sample fired at 800 °C with a grain size of 12 nm. By comparison of all sectors, it is found that oxygen vacancies play a dominant role in the higher photoactivity of the 30 $\text{SiO}_2/\text{TiO}_2$ sample sintered at 800 °C. In addition, presence of Ti^{3+} , as detected by EPR and XPS proved the occurrence of deoxidization in silica/titania samples after heat treatment and the existence of oxygen vacancies in the nanoparticles. All these effects contributed to the higher photocatalytic activity Pd silica-doped titania powders.

2.2.2 Zr-doped TiO₂

Hirano *et al.* (2002) studied direct formation of zirconia-doped titania with stable anatase-type structure by thermal hydrolysis. They found that the ZrO₂ content in the starting solution increased, a shift of the diffraction peak of the as-precipitated anatase-type TiO₂ to lower diffraction angle was observed. In heat treatment, they found a small amount of tetragonal ZrO₂ was detected after heat treatment at >950°C and the anatase structure was fully maintained when ZrO₂ was doped in the titania, even after heat treatment at 1000°C. They reported that the hydrothermally precipitated anatase particles with nanosized crystallites can produce solid solution with large amount of ZrO₂ than those with high crystallinity and large crystallite size after heat treatment at 950° - 1000°C.

Hirano *et al.* (2003) studied photoactivity and phase stability of ZrO₂-doped anatase-type TiO₂ directly formed as nanometer-sized particles by hydrolysis under hydrothermal conditions. They synthesized anatase-type TiO₂ doped with 4.7 and 12.4 mol% ZrO₂ that were directly precipitated as nanometer-sized particles from acidic precursor solutions of TiOSO₄ and Zr(SO₄)₂. The enhancement in photocatalytic activity of the ZrO₂-doped TiO₂ might be explained by the increase in concentration oxygen vacancies in the structure defects such as vacancies in the lattice, particularly on the surface to partially offset the lattice strain. Therefore, oxygen could escaped from the surface of the lattice to trap photogenerated holes. Moreover, the anatase-type TiO₂ doped with ZrO₂ showed high phase stability and maintained anatase-type structure even after heating at 1000°C for one hour.

Marinas *et al.* (2006) studied different titania-based systems doped with diverse transition metals were synthesized by the sol-gel method. Titanium tetraisopropoxide (TTIP) was used as the titanium source whereas precursors for doping-metals were the corresponding acetylacetonates. In preparation step, the gel was divided into two equivalent portions. One of them was magnetically stirred for 24 h whereas the other was treated with ultrasonic irradiation. All the samples were tested for gas phase selective

photooxidation of 2-propanol. They found that irrespective of the aging method, the addition of Pd, Pt and Ag improved the catalytic performance of bare-TiO₂, whereas doping with Fe and Zr had a detrimental effect on activity. In the case of Zn-containing systems, the addition of Zn was either detrimental or beneficial depending on the aging being carried out under magnetic stirring or sonication, respectively.

Lukáč *et al.* (2007) studied influence of Zr as TiO₂ doping ion on photocatalytic degradation of 4-chlorophenol. Nanosized Zr-doped TiO₂ photocatalysts were prepared using the homogenous co-precipitation method from aqueous solutions containing TiOSO₄ and ZrCl₄ by urea as a precipitation agent, with subsequently annealing at various temperatures of 400–1100 °C. They found that catalysts annealed between 800 and 900 °C are more efficient than the standard photocatalyst Degussa P25. The most photoactive catalyst annealed at 900 °C contains 87 wt.% of anatase and 13 wt.% of rutile. In addition, they proposed that the improved photocatalytic activity of TiO₂ by Zr-doping is probably due to mutually working effects. Electrons are trapped more effectively on Zr⁴⁺ than Ti⁴⁺ sites and the oxygen vacancies facilitate the transport of charge carriers to the surface reactive sites.

2.3 Titanium dioxide for use as catalyst support

Titanium dioxide (TiO₂) is commonly used as a carrier or support for catalytic materials due to its high surface areas, high thermal stability and high mechanical resistance. Thus, an active catalytic phase such as metal or metal oxide species can be highly dispersed on the high surface area supports. It is noted that high dispersion of the active catalytic phase may lead to great accessibility to utilize the active sites for surface reaction.

Kaluža *et al.* (2007) studied effect of support type on the magnitude of synergism and promotion in CoMo sulphide hydrodesulphurisation catalyst. They prepared the Co, Mo and CoMo catalysts in different Co/Mo ratios supported on SiO₂, ZrO₂, TiO₂, Al₂O₃,

active carbon and MgO. The order of activity of monometallic Mo catalysts was $\text{MoO}_3/\text{TiO}_2 > \text{MoO}_3/\text{C} > \text{MoO}_3/\text{ZrO}_2 > \text{MoO}_3/\text{SiO}_2 > \text{MoO}_3/\text{Al}_2\text{O}_3 > \text{MoO}_3/\text{MgO}$. The order of promotion of $\text{MoO}_3/\text{support}$ by Co addition was $\text{CoMo}/\text{MgO} > \text{CoMo}/\text{C} > \text{CoMo}/\text{Al}_2\text{O}_3 > \text{CoMo}/\text{TiO}_2 > \text{CoMo}/\text{ZrO}_2 > \text{CoMo}/\text{SiO}_2$.

Sandoval *et al.* (2007) studied gold nanoparticles supported on reducible (TiO_2 and CeO_2) and non-reducible oxides (Al_2O_3 and SiO_2) with comparable gold particle size (2.5–3.5 nm) as catalysts in the WGS reaction. Metal loading was fixed to 4 and 8 wt.%. The WGS reaction was studied in the temperature range from 50 to 400 °C in a flow reactor at atmospheric pressure. Before reaction the samples were calcined at 200, 300 or 400 °C to study the effect of calcination temperature in the catalyst activity. The Au/CeO_2 catalyst showed an enhanced reduction at low-temperatures as evidenced by the H/Au ratio. They found that when supported on TiO_2 and CeO_2 , the activity of gold nanoparticles was much higher than the one observed when supported on Al_2O_3 and SiO_2 being the Au/SiO_2 catalyst practically inactive.

From the previous literature reviews, some success in enhancing the photocatalytic activity of TiO_2 has been achieved by several methods such as sulfation, reduction with hydrogen, and halogenation. However, no one use quenching technique in order to modify the properties of TiO_2 . Therefore, an alternative quenching pre-treatment for create defect sites on TiO_2 surface is chosen study in this research.

สถาบันวิทยบริการ
จุฬาลงกรณ์มหาวิทยาลัย

CHAPTER III

THEORY

3.1 Quenching process (Boyer, 1988)

Quenching is a critical process that determines the final product of transformations of many materials. For the purposes of this proposal, it is defined as the mechanism of “rapid cooling” of metals. Quenching consists of cooling from a relatively high temperature to a fairly low temperature in a short period of time. The temperature differential and the rate of cooling may vary greatly, depending on the material being heated and on the required cooling rate. The temperature of the medium in which the article is then placed (quenched) may vary from that of ice water (0°C, or 32°F) to more than several hundreds of degrees Fahrenheit. Furthermore, the cooling power of the quenching medium may vary from as slow as that of still air to that of a violently agitated aqueous solution.

3.1.1 Classification of quenching methods and techniques

These modifications have resulted in the arbitrary assignment of specific names to various quenching methods, such as direct quenching, fog quenching, and gas quenching.

Direct quenching refers to direct cooling (usually by a liquid quench) of the metal from its heat treating temperature to, or at least to near, ambient temperature.

Selective quenching is used when pre-selected areas of the workpiece must remain relatively unaffected by the quenching medium. This can be accomplished by insulating the area to be protected, or by allowing the quenchant to contact only those areas of the part that are to be quenched.

Time quenching is used when the cooling rate of the part being quenched must be changed abruptly at some time during the cooling cycle. The change in cooling rate may entail either an increase or a decrease in temperature, depending on which is needed to attain the desired results.

Spray quenching. With this method, streams of quenching liquid are directed at high pressure (up to 0.8 MPa, or 120 psi) to local areas of the workpiece. The cooling rate is rapid and uniform over the entire temperature range of the quenching cycle.

Fog quenching utilizes a fine fog or mist of liquid droplets and a gas carrier as cooling agents. This method of quenching, although similar to spray quenching, is less effective, because the quenching mist or fog is not readily adapted to rapid removal or replacement by cooler fog or mist once it has been heated by contact with the part being quenched.

Gas quenching. The term gas quenching includes cooling of metal parts in still or moving air, as well as in still or moving inert gases, such as nitrogen or argon, and active gas mixtures such as protective atmospheres.

3.1.2 Quenching media and techniques

Many different media have been used for quenching. The most commonly used are included in the list below, including some that are used only to a very limited extent for specific applications:

- Water
- Brine solutions (aqueous)
- Caustic solutions (aqueous)
- Polymer solutions
- Oils
- Molten salts

- Molten metals
- Gases (still or moving)
- Fog quenching
- Dry dies (commonly water cooled, or cold slabs)

Only liquid quenching and gas quenching that concerns our work thus other quenching media will not mentioned in details. The details of liquid quenching and gas quenching are following

Water Quenching

Water was the original quenching medium used in commercial practice. Its other advantages are that it is inexpensive and readily available; it is easily disposed of without attendant problems of pollution or health hazard. Consequently, the quenching system can be extremely simple. One disadvantage of water as a quench is that its rapid cooling rate persists throughout the lower temperature range, in which distortion or cracking is like to occur. To reduce to temperature sensitivity of water, a wide variety of additives have been tried. The two most practical and effective additives are salt (sodium or calcium chloride and caustic (sodium or potassium hydroxide). Both of these materials increase the uniformity of the water quench without detracting from its cooling power. However these additives in themselves create certain drawback: including requirements for a closed system.

Gas Quenching

Gas quenching in its simplest form consists of removing a part from the furnace and allowing it to cool in still air; the only circulation is created by natural convection around the hot workpiece. In gas quenching, the workpiece is placed directly into the gas quenching zone or chamber, and heat is rapidly extracted from the metal by a fast-moving stream of gas. Various gases, ranging from air to complex mixtures, may be used for cooling, depending on process requirements.

In general, the quenching techniques in common use are:

- Immersion in a single quenchant (air or liquid) and cooling to near room temperature (usually slightly above) without interruption.
- Use of two quenching mediums on a timed basis, such as a partial quench in water, followed by oil; quench or quenching in molten salt, followed by finishing in air.
- Isothermal quenching, that is, predetermined temperature, then temperature until the phase completed.
- Spray quenching which usually uses an aqueous medium. This technique is most frequently used for quenching of induction- or flame-hardened parts, although it can be used for quenching of furnace- heated workpieces. Spray quenching offers the advantage of instantaneous control in timing as well as pressure regulation.

3.2 Titanium (IV) oxide

3.2.1 Physical and Chemical Properties

Titanium (IV) dioxide (TiO_2) belongs to the family of transition metal oxides. TiO_2 has received a great deal of attention due to its chemical stability, non-toxicity, low cost, and other advantageous properties. TiO_2 is also used in catalytic reactions acting as a promoter, a carrier for metals and metal oxides, an additive, or as a catalyst. The structures of rutile, anatase and brookite can be discussed in terms of (TiO_2^{6-}) octahedrals. Brookite is extremely difficult to synthesize in the laboratory but both anatase and rutile can be readily prepared. However, only rutile and anatase play role in the applications of TiO_2 and are of any interest here as they have been studied with surface science techniques. The three crystal structures differ by the distortion of each octahedral and by the assembly patterns of the octahedral chains (Figure 3.1).

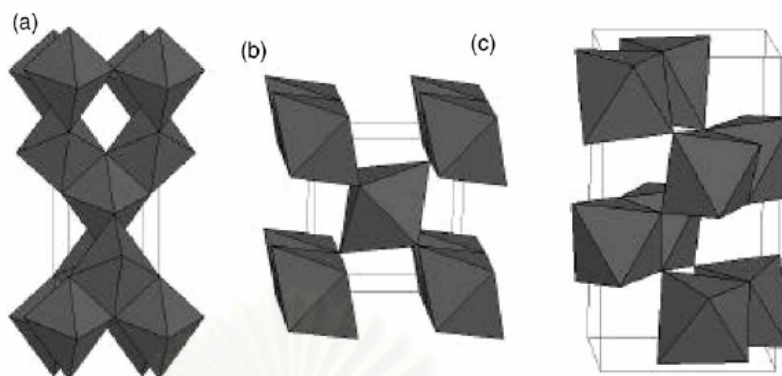


Figure 3.1 Crystal structures of anatase (a), rutile (b), and brookite (c).

(O. Carp *et al.*, 2004)

Both crystal structures, anatase and rutile, are commonly used as photocatalyst, with anatase showing a greater photocatalytic activity for most reactions. It has been suggested that this increased photoreactivity is due to anatase's slightly higher Fermi level, lower capacity to adsorb oxygen and higher degree of hydroxylation (i.e., number of hydroxy groups on the surface). Reactions in which both crystalline phases have the same photoreactivity or rutile a higher one are also reported. Furthermore, there are also studies which claim that a mixture of anatase (70–75%) and rutile (30–25%) is more active than pure anatase.

Anatase appears to be the more active of the two phases studied. This is probably due to differences in the extent and nature of the surface hydroxyl groups present in the low temperature anatase structure. Furthermore, the photoactivity enhancement can be related to the Fermi level of anatase which is about 0.2 eV higher than that of rutile. (Maruska and Kato, 1983). The band gap energy of a semiconductor corresponds to the minimum energy of light required to make the material electrically conductive. The band gap energy of anatase is 3.2 eV, which corresponds to UV light with wavelength of 388 nanometers, while the band gap energy for the rutile type is 3.0 eV, corresponding to violet light that has a wavelength of 413 nanometers.

The transformation from anatase to rutile is accompanied by the evolution of ca. 12.6 kJ/mol (3.01 kcal/mol), but the rate of transformation is greatly affected by temperature and by the presence of other substance which may either catalyze or inhibit the reaction. During the transformation, anatase pseudo closed-packed planes of oxygen are retained as rutile closed-packed planes, and a co-operative rearrangement of titanium and oxygen ions occurs within this configuration (Matsumoto *et al.*, 2001). The lowest temperature at which conversion of anatase to rutile takes place at a measurable rate is ca. 700°C, but this is not a transition temperature. The change is not reversible; ΔG for the change from anatase to rutile is always negative. The small differences in the Gibbs free energy (4–20 kJ/mole) between the three phases suggest that the metastable polymorphs are almost as stable as rutile at normal pressures and temperatures. If the particle sizes of the three crystalline phases are equal, anatase is most thermodynamically stable at sizes less than 11 nm, brookite is most stable between 11 and 35 nm, and rutile is most stable at sizes greater than 35 nm (Zhang, and Banfield, 2000).

Since both anatase and rutile are tetragonal, they are both anisotropic, and their physical properties, e.g. refractive index, vary according to the direction relative to the crystal axes. In most applications of these substances, the distinction between crystallographic direction is lost because of the random orientation of large numbers of small particles, and it is mean value of the property that is significant. A summary of the crystallographic properties of the three varieties is given in Table 3.1

Table 3.1 Crystallographic properties of anatase, brookite, and rutile. (Fujishima *et al.*, 1999)

Crystal structure	System	Unit cell	Density (kg/m ³)	Lattice constant (nm)		
				a	b	c
Anatase	Tetragonal	D _{4h} 19.4TiO ₂	3830	0.373	-	0.937
Rutile	Tetragonal	D _{4h} 12.3TiO ₂	4240	0.458	-	0.295
Brookite	Orthorhombic	D _{2h} 15.8TiO ₂	4170	0.543	0.916	0.513

Measurement of physical properties, in which the crystallographic directions are taken into account, may be made for both natural and synthetic rutile, natural anatase crystals, and natural brookite crystals. Measurements of the refractive index of titanium (IV) oxide must be made by using a crystal that is suitably orientated with respect to the crystallographic axis as a prism in a spectrometer. Crystals of suitable size of all three modifications occur naturally and have been studied. However, rutile is the only form that can be obtained in large artificial crystals from melts. The refractive index of rutile is 2.903. The dielectric constant of rutile varies with direction in the crystal and with any variation from the stoichiometric formula, TiO_2 ; an average value for rutile in powder form is 114. The dielectric constant of anatase powder is 48.

3.2.2 Preparation procedure of TiO_2 (O. Carp *et al.*, 2004)

TiO_2 can be prepared in the form of powder, crystals, or thin films. Both powders and films can be built up from crystallites ranging from a few nanometers to several micrometers.

3.2.2.1. Solution routes

For some applications, especially the synthesis of thin films, liquid-phase processing is one of the most convenient and utilized methods of synthesis. This method has the advantage of control over the stoichiometry, producing homogeneous materials, allowing formation of complex shapes, and preparation of composite materials. However, there are several disadvantages among which can (but need not) be: expensive precursors, long processing times, and the presence of carbon as an impurity. The most commonly used solution routes in the synthesis of TiO_2 are presented below.

1) Solvothermal methods

These methods employ chemical reactions in aqueous (hydrothermal method) or organic media (solvothermal method) such as methanol, 1,4 butanol, toluene under self-produced pressures at low temperatures (usually under 250 °C). Generally, but not always, a subsequent thermal treatment is required to crystallize the final material. The solvothermal treatment could be useful to control grain size, particle morphology, crystalline phase, and surface chemistry by regulating the solution composition, reaction temperature, pressure, solvent properties, additives, and ageing time.

2) Sol–gel methods

These methods are used for the synthesis of thin films, powders, and membranes. The sol-gel method has many advantages over other fabrication techniques such as purity, homogeneity, felicity, and flexibility in introducing dopants in large concentrations, stoichiometry control, ease of processing, control over the composition, and the ability to coat large and complex areas. This method involves the formation of a TiO₂ sol or gel or precipitation by hydrolysis and condensation (with polymer formation) of titanium alkoxides. To obtain a final product, the gel is heated. This heat treatment serves several purposes, i.e., to remove solvent, to decompose anions such as alkoxides or carbonates to give oxides, to rearrange of the structure of the solid, and to allow crystallization to occur.

3.2.2.2. Gas phase methods

For thin films, most synthesis routes are performed from the gas phase. These can be chemical or physical of nature. Most of these techniques can also synthesize powder, if a method to collect the produced particles is employed. The main techniques are:

1) Chemical vapour deposition (CVD)

CVD is a widely used versatile technique to coat large surface areas in a short span of time. In industry, this technique is often employed in a continuous process to produce ceramic and semiconductor films. Compounds, ranging from metals to composite oxides, are formed from a chemical reaction or decomposition of a precursor in the gas phase.

2) Spray pyrolysis deposition (SPD)

SPD is an aerosol deposition technique for thin films and powders related to CVD. It has been used for preparation of (mixed) oxide powders/films and uses mostly metal-organic compounds or metal salts as precursors. Spray pyrolysis of TiO_2 has merits such as simplicity, low costs, reproducibility, and the possibility of depositing large areas in a short time, while the films exhibit good electrical and optical properties.

3.2.3 Applications of titanium dioxide

Titanium dioxide is one of the most common materials in our daily life. Titanium dioxide has been widely used in a variety of paints, plastics, paper, inks, fibers, cosmetics, sunscreens, and foodstuffs. Naturally, the type of titanium dioxide that is used as a pigment is different from that used as a photocatalyst. The photocatalytic technology is becoming more and more attractive to industries today because environmental pollution has been recognized as a serious problem that needs to be addressed immediately. Various applications in which research and development activities involving titanium dioxide have been investigated, such as anti-fogging activity, anti-bacterial activity, anti-viral activity, fungicidal activity, anti-soiling activity, self-cleaning property and self-sterilizing property, deodorizing effect, photocatalytic air purification, cancer therapy, water treatment and water purification, decomposition of organic compounds.

3.3 Photocatalytic process (Fujishima *et al.*, 1999 and Linsebigler *et al.*, 1995)

The primary photocatalytic process occurs upon irradiation of a semiconductor. A semiconductor has an electronic band structure. The highest occupied energy band (valence band) and the lowest empty band (conduction band) are separated by a band gap. The magnitude of the energy of band gap between the electronically populated valence band and the largely vacant conduction band governs the extent of thermal population of the conduction band in its intrinsic state. The band gap defines the wavelength sensitivity of the semiconductor to irradiation (Fox and Dulay, 1993).

Absorption of a photon by semiconducting solids excites an electron (e^-) from the valence band to the conduction band if the photon energy, $h\nu$, equals or exceeds the band gap of the semiconductor/photocatalyst. Simultaneously, an electron vacancy or a positive charge called a hole (h^+) is also generated in the valence band (Figure 3.2). Ultraviolet (UV) or near-ultraviolet photons are typically required for this kind of reaction.

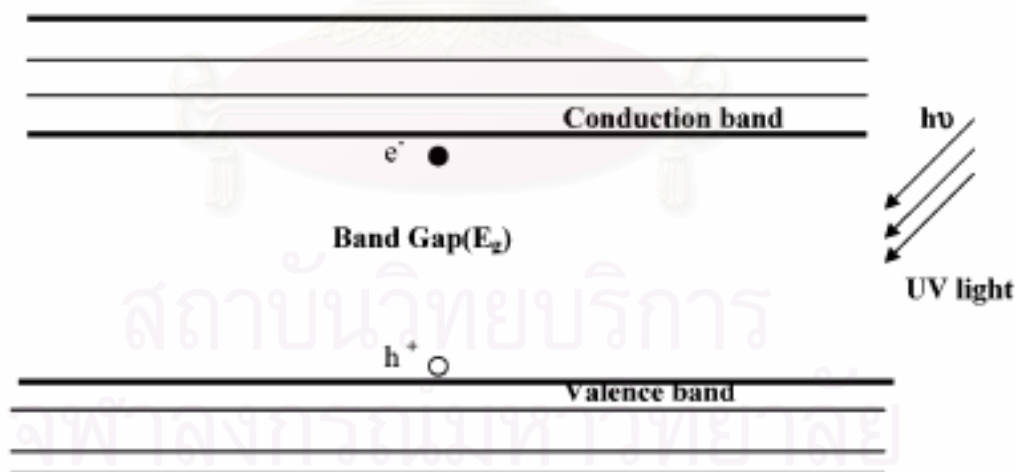


Figure 3.2 Band-gap diagram formation of holes (h^+) and electrons (e^-) upon UV irradiation of semiconductor surface.

The electron-hole pair (e^-h^+ pair) thus created migrates to the photocatalyst surface where it either recombines, producing thermal energy, or participates in redox reactions with the compounds adsorbed on the photocatalyst (see Figure 3.3). The lifetime of an e^-h^+ pair is a few nanoseconds, but this is still long enough for promoting redox reactions in the solution or gas phase in contact with the semiconductor.

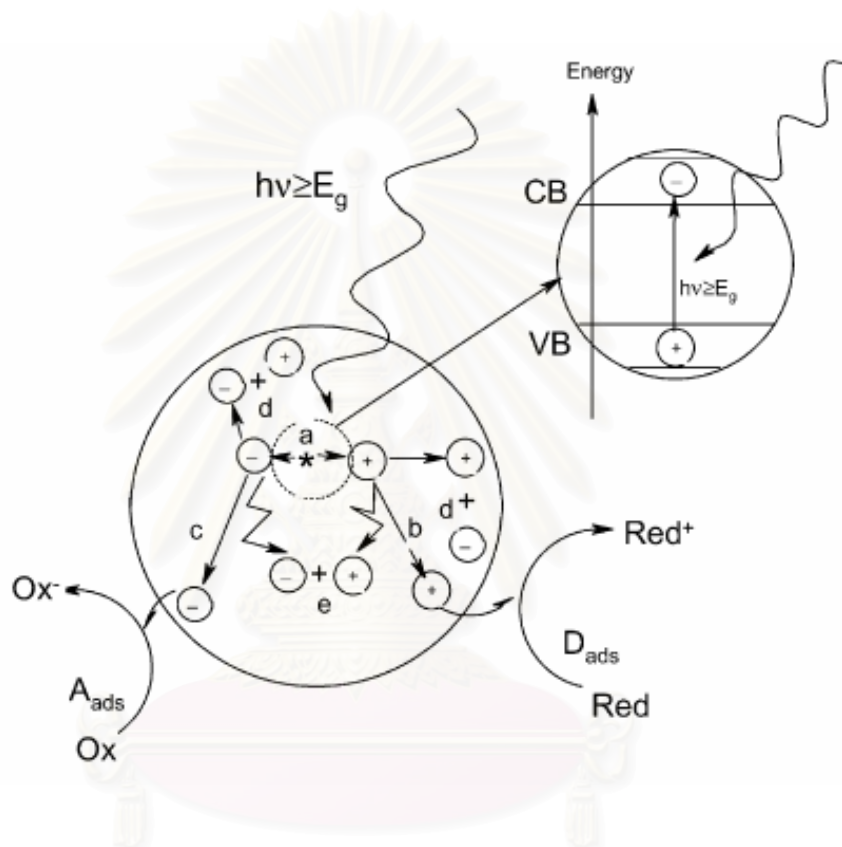


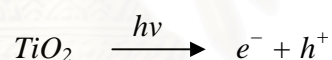
Figure 3.3 Main processes occurring on a semiconductor particle: (a) electron–hole generation; (b) oxidation of donor (D); (c) reduction of acceptor (A); (d) and (e) electron–hole recombination at surface and in bulk, respectively. (Fujishima *et al.*, 1999)

Generally, the hole oxidizes water to hydroxyl radicals (which subsequently initiate a chain of reactions leading to the oxidation of organics), or it can be combined with the electron from a donor species (D), depending on the mechanism of the photoreaction. Similarly, the electron can be donated to an electron acceptor (A) such as an oxygen molecule (leading to formation of superoxide radical) or a metal ion (with a redox potential more positive than the band gap of the photocatalyst). This metal ion can

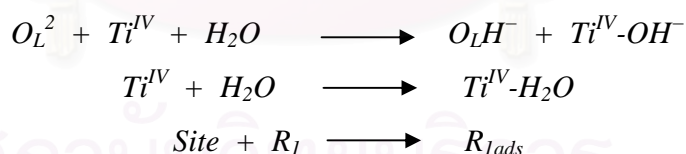
be reduced to its lower valence states and deposited on the surface of the catalyst. The electron-transfer process is more efficient if the species are preadsorbed on the surface (Linsebigler *et al.*, 1995).

In principle, a photocatalytic reaction may proceed on the surface of TiO₂ powders via several steps, namely (a) production of electron-hole pairs, photogenerated by exciting the semiconductor with light energy; (b) separation of electrons and holes by traps available on the TiO₂ surface; (c) a redox process induced by the separated electrons and holes with the adsorbates present on the surface; (d) desorption of the products and reconstruction of the surface. The example of photocatalytic reaction scheme for the degradation of organic water contaminants (Turchi and Ollis, 1990). The sequence of steps representing the proposed mechanisms is as follows

(i) Excitation of the catalyst by photon energy greater than the band gap, generating electrons and holes.

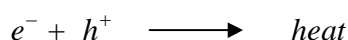


(ii) Adsorption on the catalyst surface and lattice oxygen (O_L²⁻)

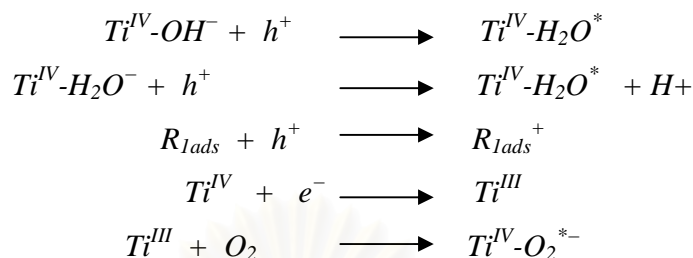


where R₁ represents an organic molecule, R_{1ads} represents an adsorbed organic molecule

(iii) Recombination of the e⁻-h⁺ pair, producing thermal energy



(iv) Trapping of the hole and electron



However, the detailed mechanism of the photocatalytic process on the TiO_2 surface is still not completely clear, particularly that concerning the initial steps involved in the reaction of reactive oxygen species and organic molecules.

3.4 CO-hydrogenation

The hydrogenation of carbon monoxide over a late transition metal catalyst to predominantly linear hydrocarbons and/or oxygenates has come to be called the Fischer–Tropsch synthesis (Anderson, 1984). Fischer-Tropsch synthesis (FTS) that discovered by Frans Fischer and Hans Tropsch over 77 years ago, as an alternate process, can convert the synthesis gas (H_2/CO) derived from carbon sources such as coal, peat, biomass and natural gas, into hydrocarbons and oxygenates. This process makes it possible to obtain high-purity transportation fuels from feedstocks other than crude oil, such as natural gas, charcoal, or biomass. These raw materials are first converted into syngas by partial oxidation or steam reforming processes.

This synthesis is basically the reductive polymerization (oligomerization) of carbon monoxide by hydrogen to form organic products containing mainly hydrocarbons and some oxygenated products in lesser amounts. By manipulation of the reaction conditions, the process may be designed to produce heavier saturated hydrocarbons or lower olefins or oxygenated hydrocarbons as we shall see in the following discussion.

Metals that have significant activity for Fischer-Tropsch synthesis include iron, cobalt, nickel and ruthenium. Iron has proved so far to be the best. It is superior to cobalt with respect to conversion rate, selectivity and flexibility. Nickel has disadvantage of producing appreciable amounts of methane. Ruthenium enhances the formation of high molecular weight alkanes and catalyzes polymerization to polymethane. Other group VIII metals are of low activity. Copper does not catalyze Fischer-Tropsch synthesis.

The catalyst is usually prepared by fusion or precipitation over a silica, alumina or kieselguhr support. Small amounts of promoters such as alkali metal or copper salts are included in the catalytic mixture. Copper is believed to facilitate the reduction of the catalyst, alkali metal salt, particularly K_2O enhance activity and olefins selectivity. The support increased the surface area of the catalyst metal thus extremely increasing in dispersion.

Sulfur compounds generally poison the catalyst and they must be removed from the synthesis gas feed stream. However, partial sulfur poisoning may have favorable effects. Thus, it has been found that deliberate slight sulfur poisoning of the iron/manganese catalyst enhances selectivity to short chain olefins.

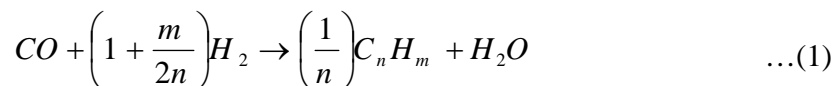
Three main types of reactors are currently in use in the Fischer-Tropsch processes: Fixed-bed, fluidized-bed and slurry bed reactors. Fixed-bed reactors are usually tubular tube, each tube having 50 mm ID and 12 m length. A single reactor may contain as many as 2000 such tubes. Fluidized-bed reactors provide for better heat transfer and continuous regeneration of the catalyst. The catalyst used in fluidized-bed reactors must have high physical stability. SASOL (in South Africa), uses fluidized-bed reactors 46 m high, 230 cm in diameter with reaction temperature of 320-360°C and pressure. In the slurry-bed reactors the feed gas is bubbled through a suspension of finely divided catalyst particles. It has the advantage of good temperature control thus providing greater flexibility of reaction conditions.

Each type of reactor is better suited for certain product composition. Fixed-bed reactors, for example, produce high boiling straight-chain hydrocarbons consisting, typically, of 33% gasoline hydrocarbons (C_5-C_{11}), 17% diesel and 40% heavy paraffins and higher waxes. The gasoline fraction is of low octane value and requires further treatment (isomerization or blending) before use. Fluidized-bed reactors are the best when lighter hydrocarbons are desired. A typical product composition is 72% lower molecular weight gasoline-range hydrocarbons rich in olefins and 14% oxygenated hydrocarbons. However, the product is low in diesel. Thus two or more different reactors may be operated in parallel to provide an integrated fuel plant.

The demands on selectivity of Fischer-Tropsch reactions are ever-increasing. In the earlier days of the process the concern was to improve selectivity with respect to better gasoline grade and/or diesel oil chemicals. With the realization of feasible route of converting synthesis gas to industrial intermediates, more stringent conditions are being imposed on the reaction parameters to make the process more selective.

Selectivity improvement is sought with respect to product properties such as chain length, chain branching, olefin content, alcohol content and methane content. Reaction conditions that particularly eliminate or minimize carbon deposition are desirable. In order to achieve and improve product selectivity the optimization of the following reaction parameters has been investigated: reaction temperature and pressure, H_2/CO ratio, conversion, space velocity, amount and type of promoters, nature of the catalyst, size of catalyst particles and mode of its deposition, type of support, and type of reactor.

The main reactions of FTS are



Equations (1) is the formation of hydrocarbons higher than C1, and the equation (2) is methanation. The water-gas shift reaction, which is undesirable for natural gas conversion, is shown in equation (3). The Boudouard reaction, which results in carbon deposition on the catalyst surface, is shown in equation (4).

The mechanism consists of surface steps in five categories: (1) the adsorption of reactants (H_2 and CO); (2) chain initiation; (3) chain propagation; (4) chain termination and desorption of products; (5) readsorption and secondary reaction of olefins. Depending upon the type of catalyst used, promoters, reaction conditions (pressure, temperature and H_2/CO ratios), and type of reactors, the distribution of the molecular weight of the hydrocarbon products can be noticeably varied.

With regards to the operating conditions, usually higher pressures will result in higher rates. Entrained bed reactors or slurry bubble column reactors are better than fixed-bed reactors for FTS since they can remove heat from this exothermic synthesis, allowing better temperature control.

The current main goal in using FTS is to obtain high molecular weight, straight chain hydrocarbons. However, methane and other light hydrocarbons are always present as less desirable products from the synthesis. Many attempts have been made to minimize these byproducts and increase the yield of long chain liquid hydrocarbons by improving

chain growth probability. A key element in improved Fischer–Tropsch processes is the development of active catalysts with high wax selectivity. Normally, catalysts used for this synthesis are group VIII metals. By nature, the hydrogenation activity increases in order of $\text{Fe} < \text{Co} < \text{Ni} < \text{Ru}$. Ru is the most active. Ni forms predominantly methane, while Co yields much higher ratios of paraffins to olefins and much less oxygenated products such as alcohols and aldehydes than Fe does.

3.4 Cobalt and Cobalt Oxides (Young 1960)

Cobalt, a transition series metallic element having atomic number 27, is similar to silver in appearance. The electronic structure of cobalt is $[\text{Ar}] 3d^7 4s^2$. At room temperature the crystalline structure of the α (or ϵ) form, is close-packed hexagonal (cph) and lattice parameters are $a = 0.2501$ nm and $c = 0.4066$ nm. Above approximately 417°C , a face-centered cubic (fcc) allotrope, the γ (or β) form, having a lattice parameter $a = 0.3544$ nm, becomes the stable crystalline form. Cobalt exists in the +2 or +3 valance states for the major of its compounds and complexes.

Cobalt has three well-known oxides:

Cobalt (II) oxide, CoO , is an olive green, cubic crystalline material. Cobalt (II) oxide is the final product formed when the carbonate or the other oxides are calcined to a sufficiently high temperature, preferably in a neutral or slightly reducing atmosphere. Pure cobalt (II) oxide is a difficult substance to prepare, since it readily takes up oxygen even at room temperature to re-form a higher oxide. Above about 850°C , cobalt (II) oxide form is the stable oxide. The product of commerce is usually dark gray and contains 75-78 wt % cobalt. Cobalt (II) oxide is soluble in water, ammonia solution, and organic solvents, but dissolves in strong mineral acids. It is used in glass decorating and coloring and is a precursor for the production of cobalt chemical.

Cobalt (III) oxide, Co_2O_3 , is form when cobalt compounds are heated at a low temperature in the presence of an excess of air. Some authorities told that cobalt (III) oxide exists only in the hydrate form. The lower hydrate may be made as a black power

by oxidizing neutral cobalt solutions with substances like sodium hypochlorite. Co_2O_3 or $\text{Co}_2\text{O}_3 \cdot \text{H}_2\text{O}$ is completely converted to Co_3O_4 at temperatures above 265°C . Co_3O_4 will absorb oxygen in a sufficient quantity to correspond to the higher oxide Co_2O_3 .

Cobalt oxide, Co_3O_4 , is formed when cobalt compounds, such as the carbonate or the hydrated sesquioxide, are heated in air at temperatures above approximately 265°C and not exceeding 800°C .

3.5 Co-based catalysts (Jongsomjit et al., 2004)

Co-based catalysts are known to be commercially attractive for FTS because of its high activity and selectivity for linear hydrocarbons, low water–gas shift activity, low deactivation rates, and comparatively low price. Disadvantages are the high costs of cobalt and low water–gas shift activity. Therefore, cobalt catalysts are viable for natural-gas-based Fischer–Tropsch processes for the production of middle distillates and high molecular-weight products.

The Co-based catalysts, synthesized in the form of a metal oxide, are subjected to an activation treatment to become active for FT synthesis. Cobalt catalysts are almost always reduced in H_2 at temperatures between 473 and 723 K. The Co active phase is generally deposited over an oxidic support, for example, SiO_2 , Al_2O_3 , ZrO_2 , CeO_2 or TiO_2 , which provides good mechanical strength and thermal stability under reaction conditions. According to the literature, the interaction of cobalt with titania is stronger than that with silica. Moreover, strong metal–support interaction has been found to affect the metal dispersion. The influence of various types of cobalt precursors used was also investigated. It was found that the use of organic precursors, such as cobalt (III) acetyl acetonate resulted in a significant increase of carbon monoxide conversion, compared with the reference catalyst made from cobalt nitrate.

CHAPTER IV

EXPERIMENTAL

4.1 Catalyst preparation

4.1.1 Synthesis of TiO₂

Nanocrystalline TiO₂ was prepared using the solvothermal method in the same manner as that of Payakgul *et al.* Titanium (IV) *n*-butoxide (purity 97 %, Aldrich) was used as the starting material. Approximately 15-25 g of titanium *n*-butoxide was suspended in 100 ml of toluene, in a test tube, which was then placed in a 300 ml autoclave. The same solvent was filled in the gap between the test tube and the autoclave wall. The autoclave was purged completely by nitrogen after that it was heated up to the desired temperature (300°C-320°C) with the rate of 2.5 K/min. The temperature of the autoclave was held constant at 573 K for 0.5-6 h and then cooled down to room temperature. The obtained TiO₂ was washed by acetone for several times and finally dried in air. The chemicals used in synthesis of TiO₂ are shown in Table 4.1

Table 4.1 Chemicals used in synthesis of TiO₂

Chemical	Supplier
Titanium (IV) <i>n</i> -butoxide (purity 97%)	Aldrich
Toluene	Aldrich
Acetone	Aldrich

4.1.2 Synthesis of metal-doped TiO₂

The Si- and Zr-doped TiO₂ were prepared by adding a small amount of TEOS (tetraethylorthosilicate, Aldrich) and zirconium (IV) *n*-butoxide (Aldrich) into the solution of 25g TNB (Aldrich) in 100 ml toluene, respectively. The molar ratios of Si/Ti and Zr/Ti were calculated at 0.002, 0.005, and 0.1. Then, set up the test tube in a 300 cm³ autoclave. The gap between the test tube and the autoclave wall was filled with 30 cm³ of the same solvent used in the test tube. The autoclave was purged completely by nitrogen before heating up to the desired temperature, in the range of 573 K at a rate of 2.5 K/min. Autogenously pressure during the reaction gradually increased as the temperature was raised. Once the prescribed temperature was reached, the temperature was held constant for 2 h. After the system was cooled down, the resulting powders were repeatedly washed with methanol and dried in air. The synthesized TiO₂ was calcined at 573 K with a heating rate of 10 K/min for 1 h and cooled down in air at room temperature or 77 K. All the samples were then air dried and stored in a desiccator. The chemicals used in synthesis of TiO₂ are shown in Table 4.2

Table 4.2 Chemicals used in of metal-doped TiO₂

Chemical	Supplier
Titanium (IV) <i>n</i> -butoxide (purity 97%)	Aldrich
Zirconium (IV) <i>n</i> -butoxide	Aldrich
Tetraethylorthosilicate	Aldrich
Toluene	Aldrich
Acetone	Aldrich

4.1.3 Quenching treatment

For quenching pre-treatment, the synthesized TiO₂ and metal-doped TiO₂ were dried in air atmosphere at 573 K with a heating rate of 10 K/min for 1 h and then it was taken out and immediately quenched in various quenching media. In this study, both liquid phase and gas phase media were used. For quenching in liquid phase media, liquid nitrogen at 77 K, water at room temperature and 373 K, 30 wt% hydrogen peroxide at room temperature and 373 K were selected. For quenching in gas phase media, air at room temperature and 77 K were selected. After the samples were quenched in the media for 30 min, all samples were dried in air at room temperature and stored in the desiccator.

4.1.4 Synthesis of Co/TiO₂ catalyst

The Co/TiO₂ catalyst procedures are as follows:

1. The previously quenched titania supports were impregnated with an aqueous solution of cobalt nitrate [Co(NO₃)₂·6H₂O] by incipient wetness technique. Using the water capacity measurement obtained previously for titania particles, a sufficient amount of the palladium precursor was added to obtain a 20% by weight of cobalt.
2. After an impregnation, the catalysts were dried at 383 K for 12 h.
3. The dried catalysts were calcined at 723 K for 4 h using a ramp rate of 1 K/min.
4. Finally, the catalysts were cooled down and stored in desiccators.

4.2 Catalyst Characterization

Various characterization techniques were used in this studied in order to clarify the catalyst structure and morphology and surface composition. The structure and morphology of quenched titania were studied using surface area measurements, X-ray diffractometer (XRD), Transmission electron microscope (TEM), Scanning electron microscopy (SEM), Temperature programmed desorption of carbon dioxide (CO₂-TPD), Electron spin resonance spectroscopy (ESR), and X-ray photoelectron spectroscopy

(XPS) and the details of each technique will be described in section 4.2.1. In the second part 4.2.2, the physical and chemical properties of Co/TiO₂ catalysts were investigated employing hydrogen pulse chemisorption, temperature-programmed reduction (TPR), Scanning electron microscopy and energy dispersive X-ray spectroscopy, and X-ray photoelectron spectroscopy (XPS).

4.2.1 TiO₂ photocatalyst

4.2.1.1 X-ray diffractometry (XRD)

The X-ray diffraction (XRD) patterns of powder were performed by SIEMENS D-5000 X-ray diffractometer at Center of Excellences on Catalysis and Catalytic Reaction Engineering, Chulalongkorn University. The experiments were carried out by using Ni-filtered CuK_α radiation ($\lambda = 1.54439 \text{ \AA}$). The spectra were scanned at a rate of $0.04^\circ \text{ min}^{-1}$ in the range $2\theta = 20\text{--}80^\circ$. The crystallite size was estimated from line broadening according to the Scherrer equation (see Appendix B) and $\alpha\text{-Al}_2\text{O}_3$ was used as standard.

4.2.1.2 Specific surface area measurement

The specific surface area was measured through nitrogen gas adsorption in a continuous flow method at liquid nitrogen temperature. The surface area was calculated as the Brunauer–Emmett–Teller (BET) single-point method. A mixture of nitrogen and helium was employed as the carrier gas using Micromeritics ChemiSorb 2750 Pulse Chemisorption System instrument. The samples were evacuated and dried at 150°C for 30 min before analysis.

4.2.1.3 Transmission electron microscope (TEM)

The morphology and size of primary particles of samples were observed by a JEOL TEM-200cx transmission electron microscope, operated at 100 kV at the Scientific and Technological Research Equipment Center, Chulalongkorn University (STREC).

4.2.1.4 Scanning electron microscopy (SEM)

The morphology and size of secondary particle of the samples were observed by Scanning electron microscopy (SEM). Model of SEM for experiments: JSM-5410LV at the Scientific and Technological Research Equipment Center, Chulalongkorn University (STREC).

4.2.1.5 Temperature programmed desorption of carbon dioxide (CO₂-TPD)

Temperature programmed desorption (TPD) using CO₂ as a probe molecule (CO₂-TPD) was performed to determine the Ti³⁺ site on surface titania. It was carried out using 0.5 g of a titania sample. Titania was dosed by 1% CO₂ in He for 1 h in liquid nitrogen and then desorped in a range of temperature from 123 to 253 K by level controlling. A Gow-Mac (Series 150 thermal conductivity detector) gas chromatography equipped with a thermal conductivity detector was used to analyze CO₂.

4.2.1.6 Electron spin resonance spectroscopy (ESR)

ESR measurements were carried out using JEOL JES-RE2X electron spin resonance spectrometer. It was performed to determine the amount of Ti³⁺ surface defect in mixed oxide catalysts. Recorded spectra were scanned and were converted to a g-value scale referring to a Mn²⁺ marker.

4.2.1.7 X-ray photoelectron spectroscopy (XPS)

XPS surface analysis was performed using a Kratos Amicus X-ray photoelectron spectroscopy. The XPS spectra were measured using the following conditions: Mg K_{α} X-ray source at current of 20 mA and 12 keV, resolution 0.1 eV/step, and pass energy 75 eV. The operating pressure was approximately 1×10^{-6} Pa. The surface of TiO_2 was in situ cleaned using an Ar ion gun sputtering for 30 seconds with 0.5 kV beam voltage and 50 mA emissions current. A wide-scan survey spectrum was collected for each sample in order to determine the elements present on the surface. Then, window spectra were recorded for the C 1s, O 1s, and the Ti $2p_{3/2}$ and Ti $2p_{1/2}$ photopeaks of each TiO_2 sample. All the binding energies were calibrated internally with the carbon C 1s photoemission peak at 285.0 eV. Photoemission peak areas were determined after smoothing and background subtraction using a linear routine. Deconvolution of complex spectra were done by fitting with Gaussian (70%)–Lorentzian (30%) shapes using a VISION 2 software equipped with the XPS system.

4.2.2 Supported metal catalyst

4.2.2.1 Scanning electron microscopy and energy dispersive X-ray spectroscopy

SEM and EDX were used to determine the catalyst morphologies and elemental distribution throughout the catalyst granules, respectively. The SEM of JEOL mode JSM-5800LV was applied. EDX was performed using Link Isis series 300 program.

4.2.2.2 Temperature-programmed reduction (TPR)

Temperature-programmed reduction (TPR) studies were performed in a U-shaped tubular quartz reactor with Micromeritics Pulse Chemisorb 2750 apparatus

equipped with a thermal conductivity detector (TCD). For the TPR experiments, 0.05 g of catalyst was loaded into the reactor. A cold trap was placed before the detector to remove water produced during the reaction. The samples were initially dried in an Ar flow at 150 °C for 30 min; once the TCD signal was stable, the gas stream was switched to 5% H₂/Ar, and the temperature was raised from 40 to 800 °C at a rate of 10 °C/min. H₂ consumption was measured by analyzing the effluent gas using a thermal conductivity detector, and calibration was done by reduction of Ag₂O powder.

4.2.2.3 Hydrogen pulse chemisorption

H₂-chemisorption was carried out by using a Micromeritics Pulse Chemisorb 2700 apparatus. Cobalt dispersion was determined by pulsing hydrogen over the freshly reduced catalyst. A defined amount of catalyst was filled in a quartz tube, incorporated in a temperature-controlled oven and connected to a thermal conductivity detector (TCD). The catalyst was reduced in a flow of hydrogen at 350 °C for 10 h. Afterwards, the sample was purged with helium at 400 °C for 1 h and finally cooled down to 100 °C. Hydrogen was pulsed at 100 °C over the reduced catalyst until the TCD signal was constant.

4.2.2.4 X-ray photoelectron spectroscopy (XPS)

XPS surface analysis was performed using a Kratos Amicus X-ray photoelectron spectroscopy. Window spectra were recorded for the C 1s, O 1s, Co 2p and the Ti 2p photopeaks of each Co/TiO₂ sample. Deconvolution of complex spectra were done by fitting with Gaussian-Lorentzian (70/30) shapes using a VISION 2 software equipped with the XPS system.

4.3 Reactivity measurements

4.3.1 Photocatalytic reaction

The apparatus and experimental procedures employed to evaluate the performance of various photocatalysts were described in this section.

4.3.1.1 Chemicals and reagents

The reactant gas used for this study was ethylene in air as supplied by Thai Industrial Gas Limited. The gas mixture contained 0.1 vol % ethylene in balance air. Total flow rate of gas in the experiments was 10 ml/min.

4.3.1.2 Instruments and apparatus

The schematic diagram of the gas phase photocatalytic oxidation of ethylene is shown in Figure 4.1. The part of instruments and apparatus are illustrated and described as follows:

1) The photoreactor

The photoreactor is horizontal quartz tube with an inside diameter of 1.0 cm (the length of the catalyst spread; 9 cm). The catalyst particles were spread along horizontal photoreactor between quartz glass wool layer. A 500 W high-pressure mercury lamp (Philips, HPL-N) was used as the light source (distance between the lamp and catalyst; 20 cm).

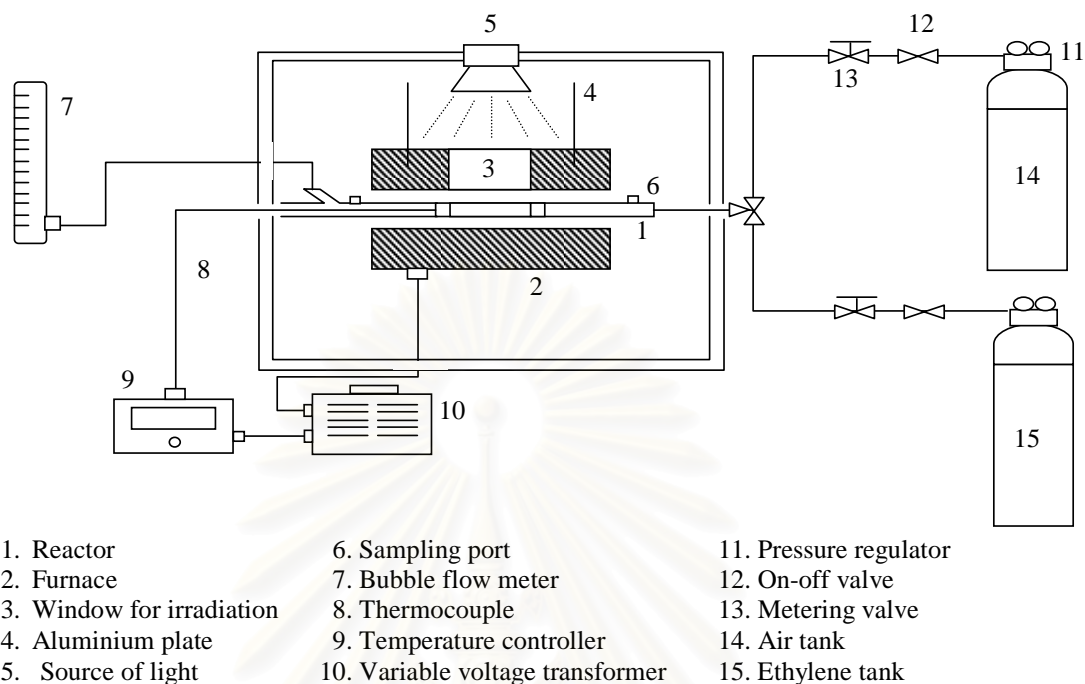


Figure 4.1 Photoreactor for experiment

2) Gas controlling system

The cylinder of air and 0.1% ethylene in air, equipped with a pressure regulator (1 bar), an on-off valve and fine metering valve used for adjusting the required values. The air containing ethylene in a concentration 1000 ppm was continuously supplied to the horizontal quartz at a constant flow rate.

3) Gas chromatograph

A gas chromatograph (SHIMADZU GC-14B) equipped with a flame ionization detector (FID) was used to analyzed feed and product. The operating conditions for GC and detector are summarized in Table 4.3

Table 4.3 Operating conditions for gas chromatograph for photocatalytic reaction

Gas Chromatograph	SHIMADZU GC-14B
Detector	FID
Column	VZ-10
Carrier gas	H ₂ (99.999%)
Carrier gas flow (ml/min)	30 cc/min
Column temperature	
- initial (°C)	70
- final (°C)	70
Injector temperature (°C)	100
Detector temperature (°C)	150
Current (mA)	-
Analysed gas	Hydrocarbon C ₁ -C ₄

4.3.1.3 Procedures

The photocatalytic activity was performed over 0.4 g of catalyst, which was packed in the reactor. The photoreactor was incorporated into the reactor system as shown in Figure 4.1. Prior to each experiment, the reactor was supplied with air at a flow rate of 15 ml/min. The photocatalyst was illuminated by ultraviolet light sources for one hour in order to remove any organic compounds that might remain from previous experiments from the surface of the catalyst. After one hour, the reactant, 0.1% (v/v) ethylene in air, was fed to the reactor at a flow rate of 10 ml/min. The temperature of the reactor under illumination was about 90°C, as measured using a K-type thermocouple. The flow rate of each gas was measured using a bubble flow meter. Reactor effluent samples were taken at 30 min intervals and analyzed by GC. The composition of hydrocarbons in the feed and product stream was analyzed by a Shimadzu GC14B (VZ-10) gas chromatograph equipped with a flame ionization detector. In all case, steady state was reached within 3 h.

4.3.2 CO-hydrogenation reaction

4.3.2.1 Material

The reactant gas used for the reaction study was the carbon monoxide in hydrogen feed stream as supplied by Thai Industrial Gas Limited (TIG). The gas mixture contained 9.73 vol% Co in H₂. The total flow rate was 30 ml/min with the H₂/CO ratio of 10/1. Ultra high purity hydrogen and high purity argon manufactured by Thai Industrial Gas Limited (TIG) were used for reduction and balanced flow rate.

4.3.2.2 Instruments and apparatus

Flow diagram of CO hydrogenation system is shown in Figure 4.2. The system consists of a reactor, an automatic temperature controller, an electrical furnace and a gas controlling system.

1) Reactor

The reactor was made from a stainless steel tube (O.D. 3/8"). Two sampling points were provided above and below the catalyst bed. Catalyst was placed between two quartz wool layers.

2) Automation Temperature Controller

This unit consisted of a magnetic switch connected to a variable voltage transformer and a solid state relay temperature controller model no. SS2425DZ connected to a thermocouple. Reactor temperature was measured at the bottom of the catalyst bed in the reactor. The temperature control set point is adjustable within the range of 0-800⁰C at the maximum voltage output of 220 volt.

3) Electrical Furnace

The furnace supplied heat to the reactor for CO hydrogenation. The reactor could be operated from temperature up to 800⁰C at the maximum voltage of 220 volt.

4) Gas Controlling System

Reactant for the system was each equipped with a pressure regulator and an on-off valve and the gas flow rates were adjusted by using metering valves.

5) Gas Chromatograph

The composition of hydrocarbons in the product stream was analyzed by a Shimadzu GC-14B (VZ-10) gas chromatograph equipped with a flame ionization detector. A Shimadzu GC-8A (molecular sieve 5A) gas chromatograph equipped with a thermal conductivity detector was used to analyze CO and H₂ in the feed and product streams. The operating conditions for each instrument are shown in the Table 4.4.

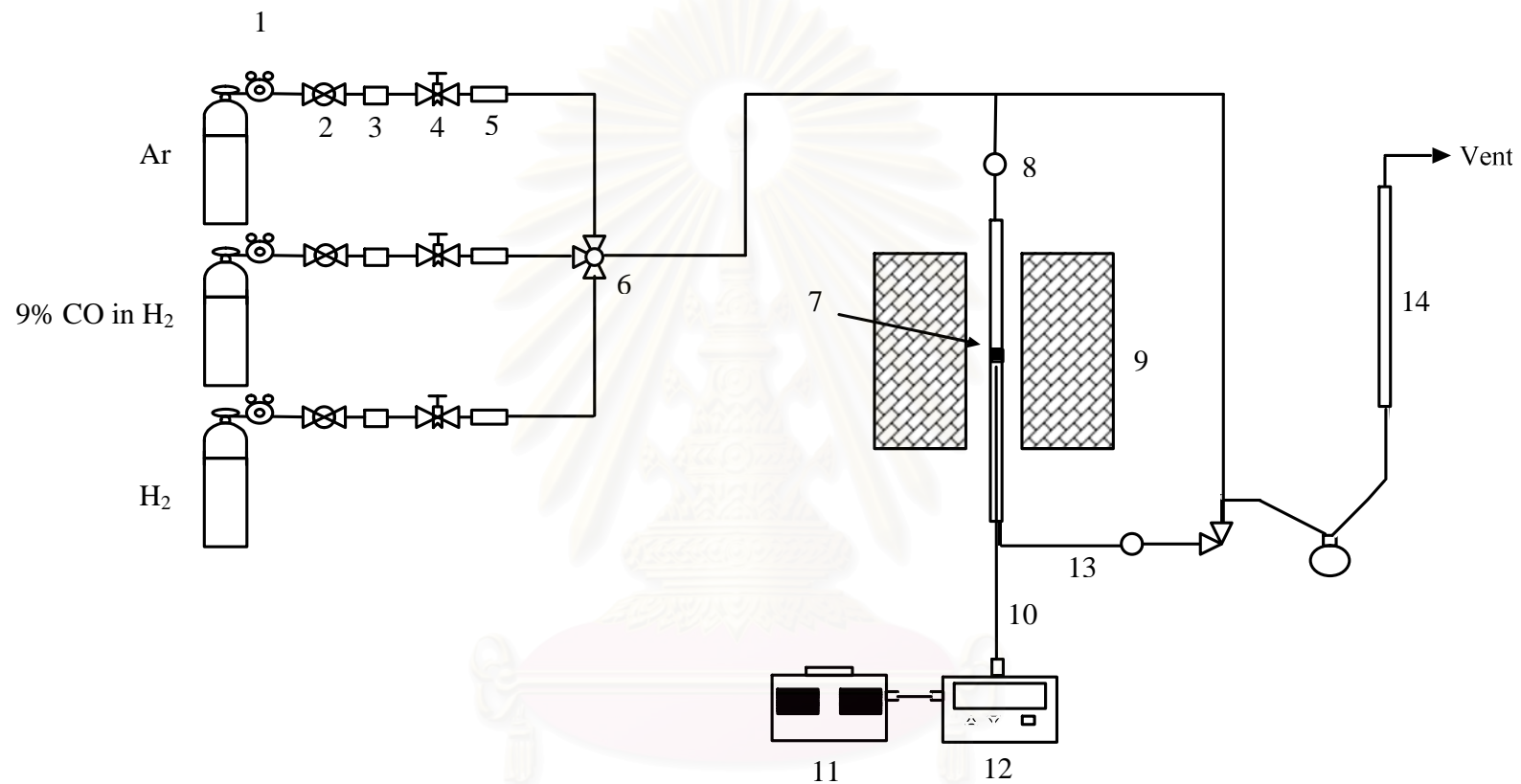
4.3.2.3 Procedures

CO hydrogenation was performed using 0.2 g of catalyst was packed in the middle of the stainless steel micro reactor, which located in the electrical furnace. The total flow rate was 30 ml/min with the H₂/CO ratio of 10/1. The catalyst sample was re-reduced *in situ* in flowing H₂ at 350 °C for 10 h prior to CO hydrogenation. CO hydrogenation was carried out at 220 °C and 1 atm total pressure. The product streams were analyzed by gas chromatography (GC). In all cases, steady-state was reached within 5 h. The effluent gases were sampled to analyse the concentration of hydrocarbon (C₁-C₄) using GC-14 B equipped with a VZ-10 column, whereas carbon monoxide concentration was analyzed by GC-8A equipped with a Molecular sieve 5A column.

Table 4.4 Operating condition for gas chromatograph for CO-hydrogenation

Gas Chromatograph	SHIMADZU GC-8A	SHIMADZU GC-14B
Detector	TCD	FID
Column	Molecular sieve 5A	VZ10
- Column material	SUS	-
- Length	2 m	-
- Outer diameter	4 mm	-
- Inner diameter	3 mm	-
- Mesh range	60/80	60/80
- Maximum temperature	350 ⁰ C	80 ⁰ C
Carrier gas	He (99.999%)	N ₂ (99.999%)
Carrier gas flow (ml/min)	30 ml./min	30 ml./min
Column temperature		
- initial (⁰ C)	60	70
- final (⁰ C)	60	70
Injector temperature (⁰ C)	100	100
Detector temperature (⁰ C)	100	150
Current (mA)	80	-
Analysed gas	Ar, CO, H ₂	Hydrocarbon C ₁ - C ₄

สถาบันวิทยบริการ
จุฬาลงกรณ์มหาวิทยาลัย



1. Pressure Regulator
 2. On-Off Valve
 3. Gas Filter
 4. Metering Valve
 5. Back Pressure

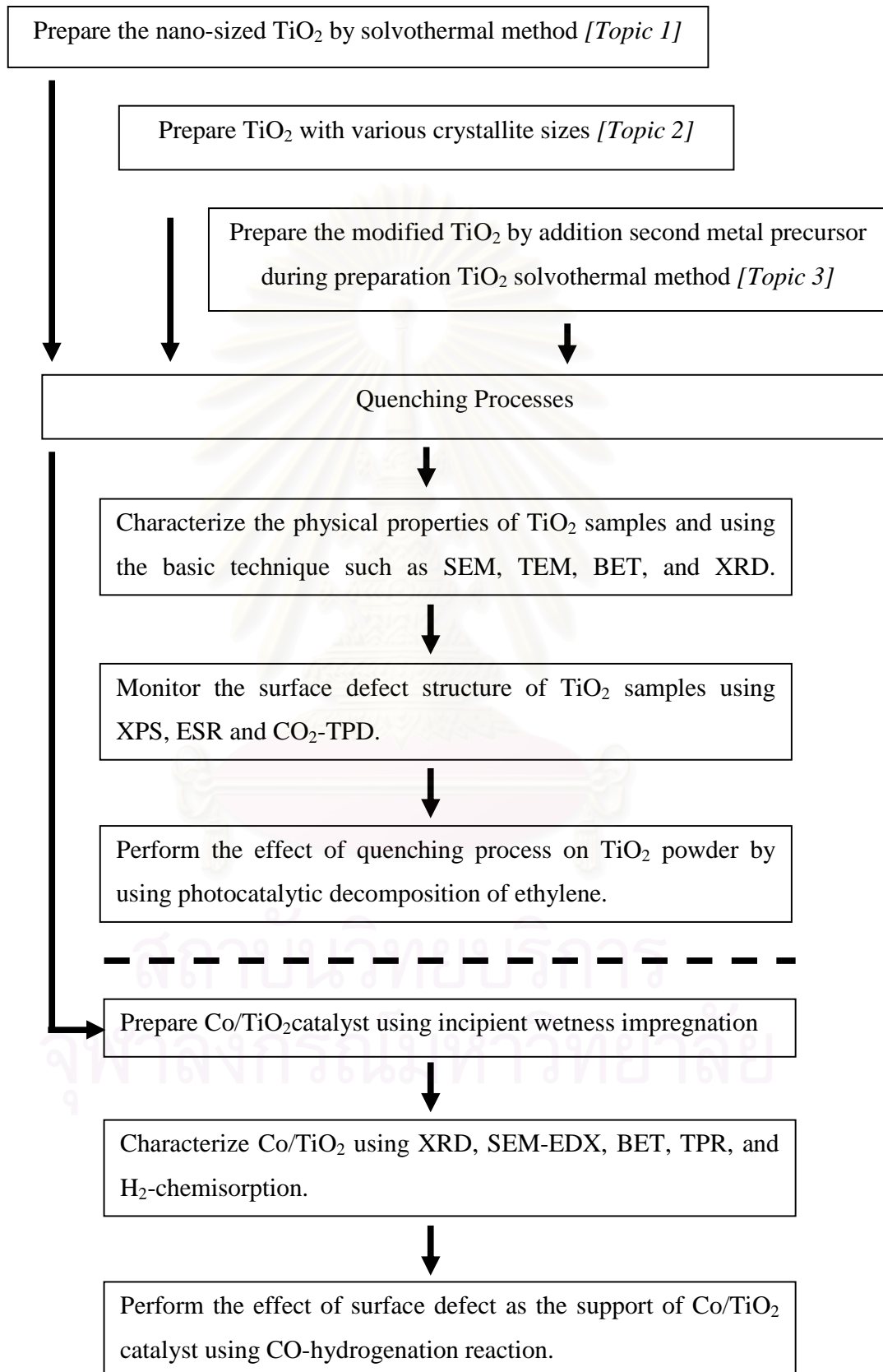
6. 3-way Valve
 7. Catalyst Bed
 8. Sampling point
 9. Furnace
 10. Thermocouple
 11. Variable Voltage Transformer
 12. Temperature Controller
 13. Heating Line
 14. Bubble Flow Meter

11. Variable Voltage Transformer
 12. Temperature Controller

8. Sampling point
 14. Bubble Flow Meter

Figure 4.2 Flow diagram of CO hydrogenation system

RESEARCH METHODOLOGY



CHAPTER V

RESULTS AND DISCUSSION

5.1. Titanium dioxide as photocatalyst

5.1.1 Effect of quenching medium on photocatalytic activity of nano-TiO₂ prepared by solvothermal method

5.1.1.1 Synthesis of Titanium (IV) oxide in toluene

Titanium (IV) oxide has been synthesized in toluene at various conditions (Solvothermal Method). Under inert organic solvent condition, thermal decomposition of TNB in toluene was occurred, yielding a $\equiv\text{Ti}-\text{O}^-$ anion. The nucleophilic attack of the titanate ion on another ion and crystallization was taken place, finally yielding the anatase titania. The mechanism of TNB in toluene can be depicted as shown in Figure 5.1.

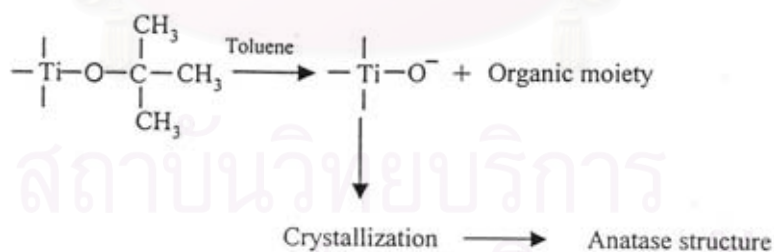


Figure 5.1 Mechanism of reaction in toluene for the titania product.

(Sornnarong Theinkeaw, 2000: 70)

5.1.1.2 Specific surface area and crystal structure

The BET surface areas of TiO₂ catalysts that were quenched at 300 °C for 1 hr were determined by nitrogen physisorption and were summarized in Table 5.1. The samples possessed reasonably high specific surface areas in the range of 87-112 m² g⁻¹. The XRD patterns of the TiO₂ samples quenched in different media (air, hydrogen peroxide, water, and liquid N₂ at different temperatures) were not significantly different (Figure 5.2); only the characteristic peaks of pure anatase phase TiO₂ were observed at $2\theta = 25.36^\circ, 37.82^\circ, 48.18^\circ$ (Watson *et al.*, 2003).

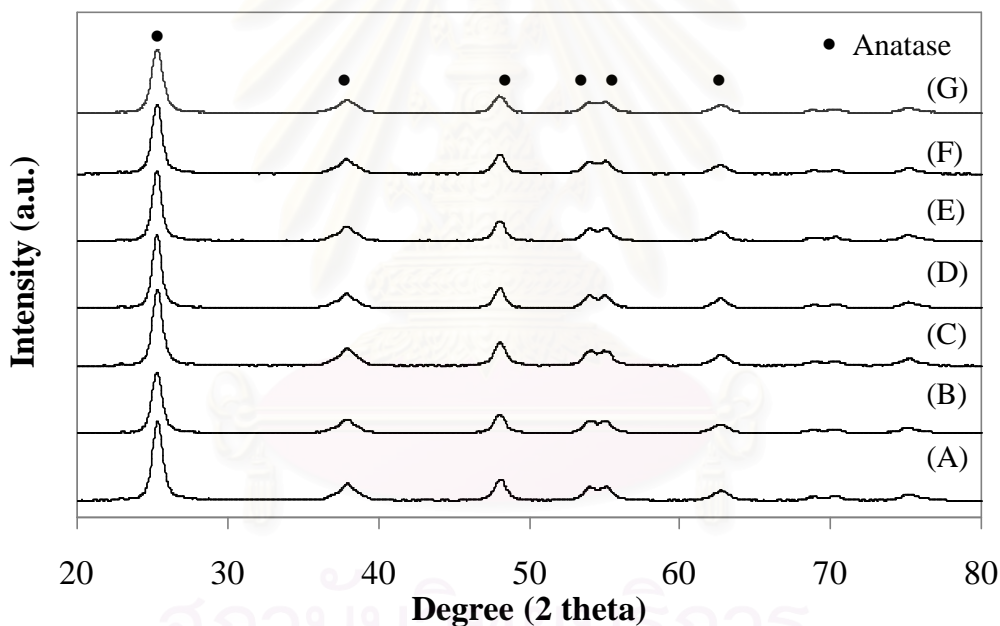


Figure 5.2 The XRD patterns of the TiO₂ obtained from quenching in various media; (A) liquid N₂, (B) H₂O at RT, (C) H₂O at 373 K, (D) 30%wt H₂O₂ at RT, (E) 30%wt H₂O₂ at 373 K, (F) air at RT and (G) air at 77 K.

As shown by XRD results, all the nano-TiO₂ samples prepared by the solvothermal method in this study were anatase phase TiO₂ with average crystallite size determined from the half-width of peaks using Scherrer's formula ($d = 0.9\lambda/\beta \cos \theta$) around 10-13 nm. The crystallite sizes and specific surface area of anatase titania were summarized in Table 5.1. Both the crystallite sizes and the specific surface areas indicated that the textural and bulk structural properties of TiO₂ catalysts were not significantly altered upon type of quenching media.

Table 5.1 Specific surface areas and crystallite sizes of titania under various quenching conditions

Sample	Quenching medium	Crystallite size ^a	
		(nm)	S_{BET} ^b (m ² /g)
A	Liquid N ₂	11	87
B	H ₂ O at RT	10	112
C	H ₂ O at 373 K	11	94
D	30wt% H ₂ O ₂ at RT	13	94
E	30wt% H ₂ O ₂ at 373 K	13	90
F	Air at RT	11	93
G	Air at 77 K	11	97

^a Determined using Scherrer's equation (applicable from 3 to 200 nm).

^b Determined using BET method.

5.1.1.3 Temperature programmed desorption of carbon dioxide (CO₂-TPD)

The characteristics of surface adsorption sites of the TiO₂ samples were studied by means of temperature program desorption of CO₂ from 143-273 K. The results are shown in Figure 5.3. All of the TiO₂ samples exhibited two main desorption peaks at 170 K and 200 K which can be assigned to CO₂ molecules bonded to different adsorption sites on the surface. The first peak at ca. 170 K was assigned to Ti⁴⁺ sites (perfect TiO₂ structure) and the second one at 200 K was assigned to Ti³⁺ sites or defect TiO₂ structure (Thompson *et al.*, 2003). The amounts of surface Ti³⁺ sites on the TiO₂ samples were observed from the areas under the Ti³⁺ TPD peaks and were found to be in the following order: air at 77 K > 30% H₂O₂ at RT > 30% H₂O₂ at 373 K > H₂O at RT > H₂O at 373 K > liquid N₂ > air at RT.

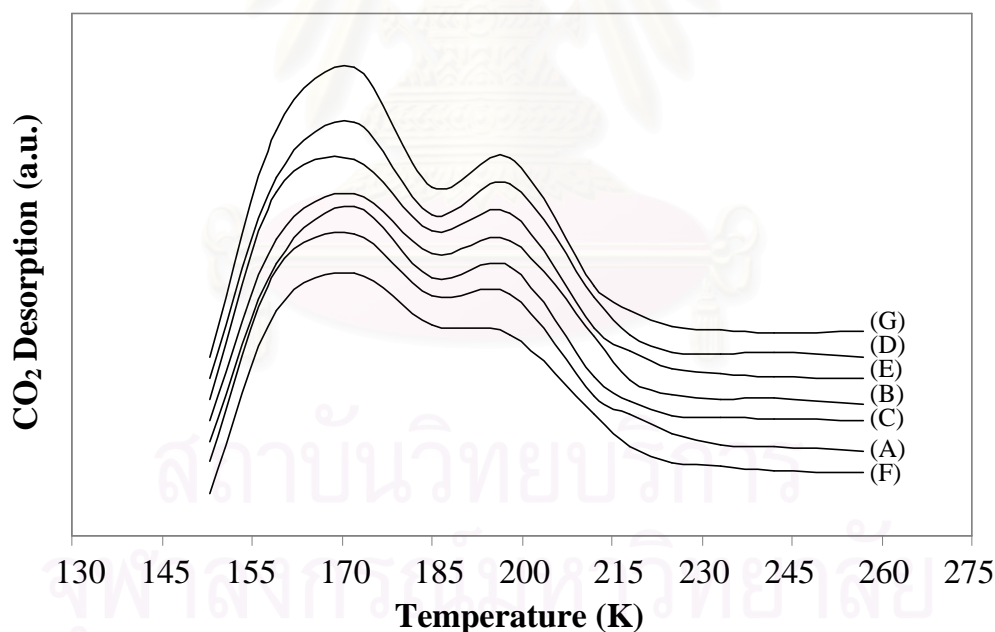


Figure 5.3 Thermal desorption spectra for CO₂ adsorbed on TiO₂ quenched in different media; (A) liquid N₂, (B) H₂O at RT, (C) H₂O at 373 K, (D) 30%wt H₂O₂ at RT, (E) 30%wt H₂O₂ at 373 K, (F) air at RT and (G) air at 77 K.

5.1.1.4 X-ray Photoelectron spectroscopic (XPS) measurements

The elements and their chemical states on surface of the TiO_2 samples after quenching treatment were also studied by XPS analysis. The typical XPS survey spectra of the TiO_2 powders after quenching treatment indicated that the powder was mainly composed of Ti and O elements with a small amount of C element (Figure 5.4).

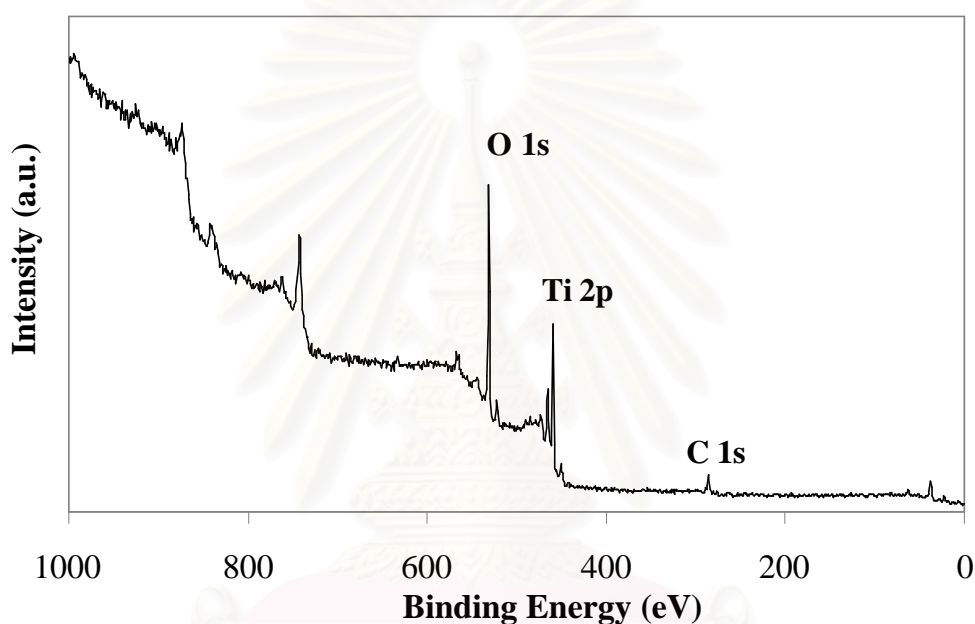


Figure 5.4 Overview X-ray photoelectron spectra in the case of TiO_2 sample quenched in 30%wt hydrogen peroxide at room temperature.

The shapes of the XPS spectra of Ti 2p and O 1s for all the TiO_2 samples are quite similar. For example, the high-resolution XPS spectra of Ti 2p recorded from the TiO_2 samples quenched in 30%wt H_2O_2 at room temperature are shown in Figure 5.5.

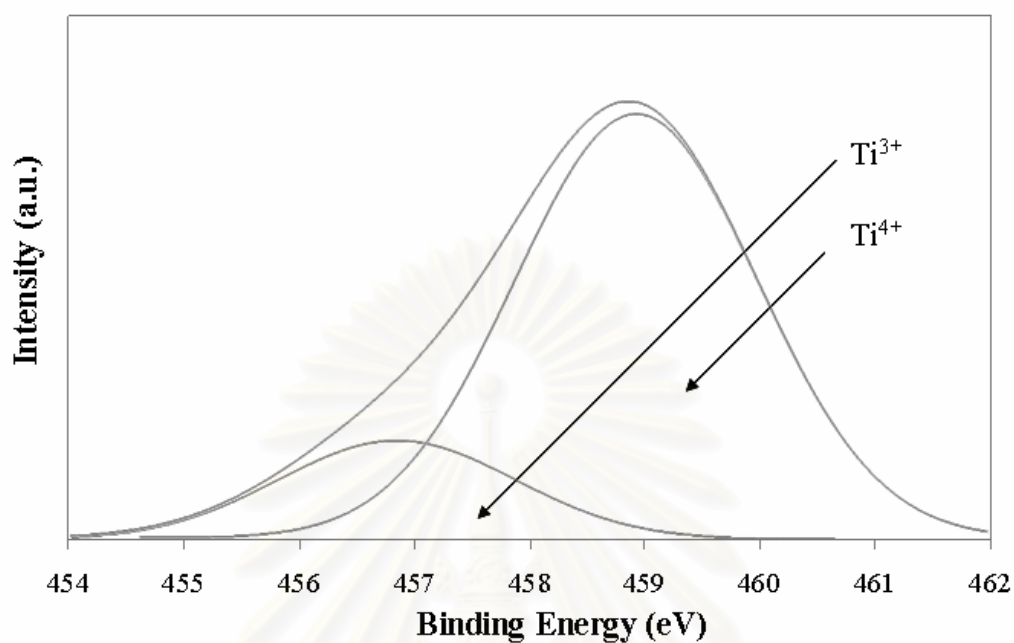


Figure 5.5 Ti 2p XPS spectra for TiO₂ sample quenched in 30%wt hydrogen peroxide at room temperature.

The Ti 2p spectrum can be fitted with Gaussian-Lorentzian functions into two spin-orbit components at binding energies 457.2, and 459.2 eV corresponding to Ti₂O₃ (Ti³⁺) and TiO₂ (Ti⁴⁺) fractions on the TiO₂ surface, respectively. The component binding energy values are in agreement with those reported in the literature (Kumar *et al.*, 2000). The XPS O 1s spectra of the TiO₂ sample quenched in hydrogen peroxide at room temperature is also presented in Figure 5.6.

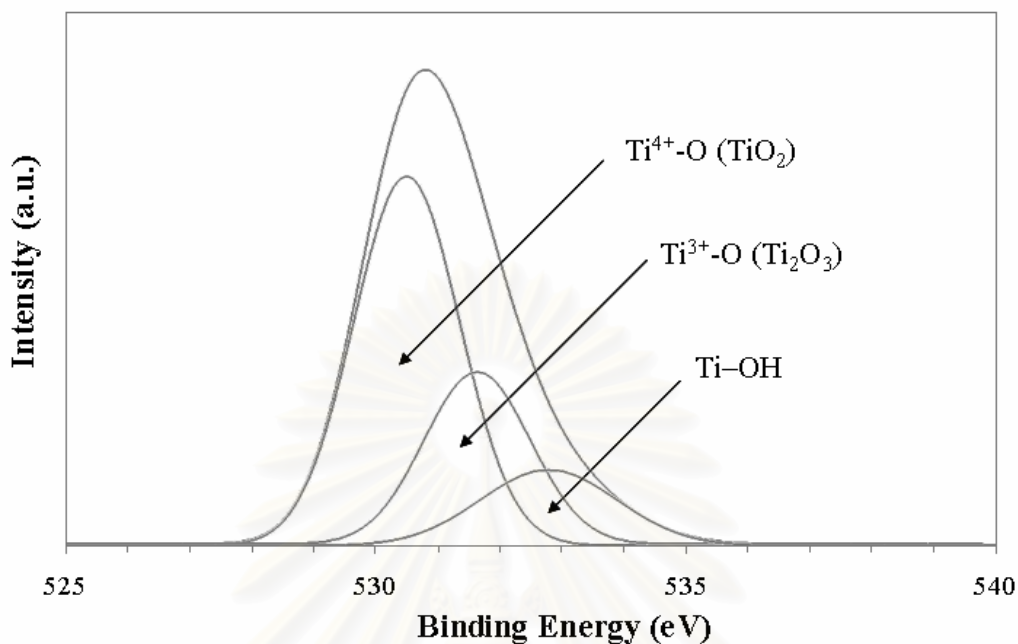


Figure 5.6 O 1s XPS spectra for TiO₂ sample quenched in 30% wt hydrogen peroxide at room temperature.

The O 1s peak is often believed to be composed of 3–5 different oxygen species such as Ti–O bonds in TiO₂ and Ti₂O₃, hydroxyl groups, C–O bonds, and adsorbed H₂O. It is shown that the O 1s peak is asymmetric suggesting that at least three peaks related to three different chemical states of oxygen are present (Pouilleau *et al.*, 1997). The binding energies of each individual components are 530.8 (Ti⁴⁺–O), 531.8 (Ti³⁺–O) and 533.3 eV (O–H). It was found that the amount of surface Ti³⁺ sites increased in a similar trend as those observed from CO₂-TPD results. The TiO₂ quenched in different media thus possessed different surface properties especially in terms of the amount of Ti³⁺ defect sites on TiO₂ surface.

5.1.1.5 Photocatalytic activity of the nano-TiO₂ quenched in different media

Photocatalytic decomposition of ethylene was conducted to assess the photocatalytic activity of the TiO₂ samples quenched in various media. The plots of ethylene conversion as a function of reaction time for all the samples are shown in Figure 5.7. Photocatalytic activity of the nano-sized TiO₂ quenched in different media is evidently different. It is likely that quenching process can modify surface properties of the TiO₂ samples i.e., enhancing the amount of surface defects (Ti³⁺) so that higher photocatalytic activity was obtained.

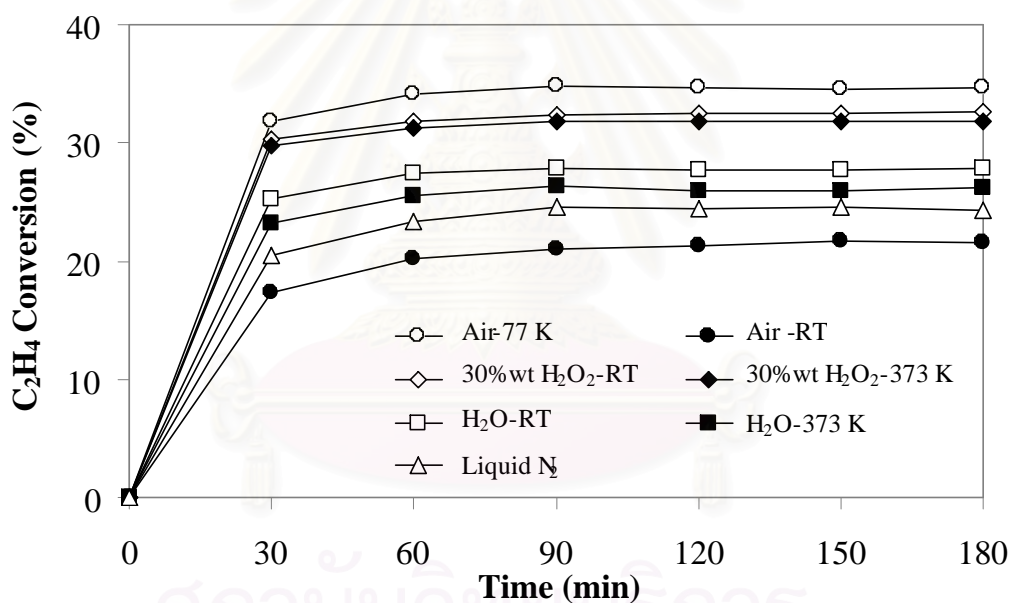


Figure 5.7 Results of photocatalytic testing comparing the activities of different TiO₂ samples.

The relationship between the amount of Ti^{3+} surface defect on the TiO_2 samples quenched in different media and ethylene conversion are illustrated in Figure 5.8. The surface Ti^{3+} defect sites on TiO_2 photocatalysts has been found to play an important role determining their photocatalytic activity since they can act as photoelectron trapping sites.

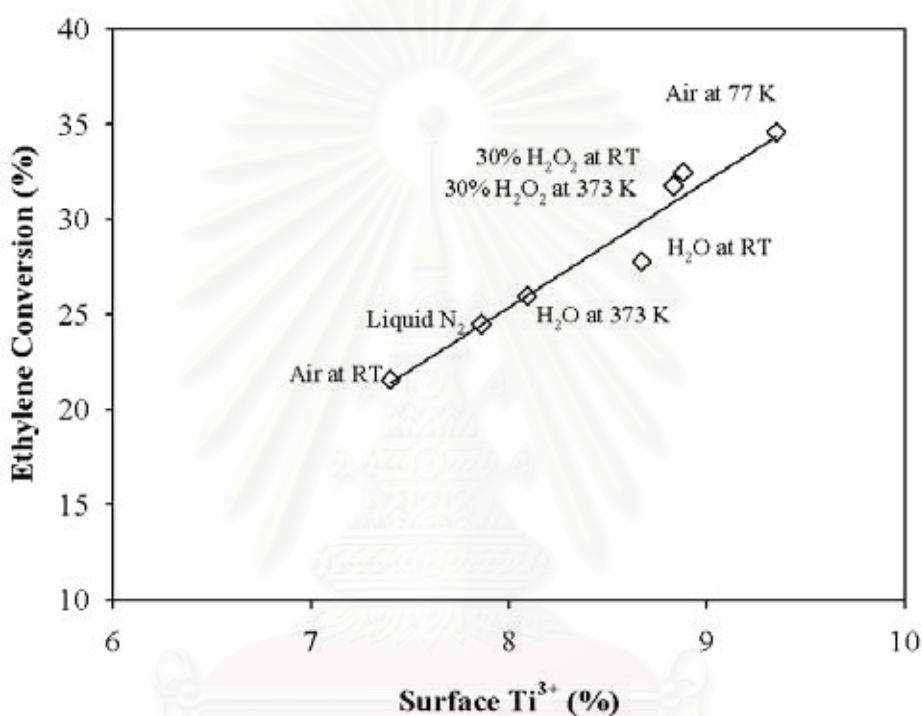


Figure 5.8 Ethylene conversions as a function of surface Ti^{3+} on the TiO_2 samples quenched in different media.

In photocatalysis, light irradiation of TiO_2 powder with a photon energy larger than the band-gap energy produces electrons (e^-) and holes (h^+) in the conduction band and the valence band, respectively. These electrons and holes are thought to have the respective abilities to reduce and oxidize chemical species adsorbed on the surface of TiO_2 particles. For a photocatalyst to be most efficient, different interfacial electron processes involving e^- and h^+ must compete effectively with the major deactivation processes involving e^-h^+ recombination. Park *et al.* (1999) has reported that modification of TiO_2 surface by increasing the amount of Ti^{3+} surface defects can

increase the photocatalytic activity of TiO₂. It is suggested that the photoelectrons were trapped by the surface defect (Ti³⁺) leading to inhibition of the e⁻-h⁺ recombination. In addition, Yu *et al.* (2002) proposed that the doped F atoms convert Ti⁴⁺ to Ti³⁺ by charge compensation and that the presence of a certain amount of Ti³⁺ reduces the electron-hole recombination rate and thus enhances the photocatalytic activity.

Recently, Xiao-Quan *et al.* (1999) reported that the trapping site of photogenerated holes or the surface OH is also an important factor affecting photocatalytic reaction besides the surface Ti³⁺. The nano-crystalline TiO₂ particles showed better photocatalytic activities when Ti³⁺/OH ratios on the TiO₂ surface were close to 1. In this study, Ti³⁺/OH ratios of the nano-TiO₂ quenched in various media were calculated based on the XPS results and are given in Table 5.2.

Table 5.2 The amount of Ti³⁺ surface defects of TiO₂ catalysts from XPS measurements

Sample	Quenching medium	Surface Ti ³⁺ (%) ^a	Surface OH (%) ^a	Ratio Ti ³⁺ /OH	Ethylene Conversion (%) ^b
A	Liquid N ₂	7.9	10.91	0.72	24.5
B	H ₂ O at RT	8.7	10.96	0.79	27.8
C	H ₂ O at 373 K	8.1	10.46	0.77	26.0
D	30wt% H ₂ O ₂ at RT	8.9	9.79	0.91	32.5
E	30wt% H ₂ O ₂ at 373 K	8.8	10.31	0.86	31.8
F	Air at RT	7.4	10.43	0.71	21.6
G	Air at 77 K	9.4	10.06	0.93	34.6

^a Determined using XPS.

^b Photocatalytic reaction was carried out at 313–328 K, 1 bar, and 0.1% ethylene in air.

It was also found that the TiO₂ quenched in air at 77 K (sample G) with Ti³⁺/OH ratio = 0.93 (closest to 1 among the various samples) exhibited the highest photocatalytic activity. Thus, it is clearly shown from this study that quenching condition and medium during post-synthesis treatment strongly affect photocatalytic activity of the nano-TiO₂. Considering the TiO₂ samples quenched in the same type of quenching media (i.e., in H₂O, 30% H₂O₂, or air), it was found that TiO₂ samples quenched at lower temperature exhibited higher photocatalytic activity than those quenched in high temperature ones. For example, TiO₂ quenched in air at 77 K showed higher ethylene conversion than the one quenched in air at room temperature. These results can probably be explained in terms of the thermal shock effect. The large difference in temperature between media and TiO₂ surface may lead to modification of the surface properties i.e., increasing the amount of Ti³⁺ defects on the TiO₂ surface. Additionally, it is noted that for the used of liquid phase media, the TiO₂ sample quenched in the media containing more -OH group in molecules exhibited higher photocatalytic activity.

5.1.2. Dependence of quenching process on the photocatalytic activity of solvothermal-derived TiO₂ with various crystallite sizes

In this topic, the effect of quenching on surface defect and photocatalytic activity of the solvothermal-derived nanocrystalline TiO₂ with average crystallite sizes between 9-13 nm was extensively studied.

5.1.2.1 Textural properties of the TiO₂ photocatalysts

Physical properties of the various TiO₂ such as the BET surface areas and the average TiO₂ crystallite sizes after quenching in different media are shown in Table 5.3. Due to the different preparation conditions, the TiO₂ samples possessed different crystallite sizes and specific surface areas. The average crystallite size of TiO₂ samples increased from 9 to 13 nm as the BET surface area of the TiO₂ samples decreased from ca. 95 to 65 m²/g. Quenching treatments, however, did not significantly alter the specific

surface area and the average crystallite size of the TiO₂. The anatase TiO₂ crystalline phase was preserved after quenching. All the TiO₂ samples consisted of only pure anatase phase TiO₂ (major XRD peaks at 25.36, 37.82, and 48.18° 2θ). XRD patterns of the TiO₂ with various crystallite sizes after quenching in air at room temperature are shown in Figure 5.9.

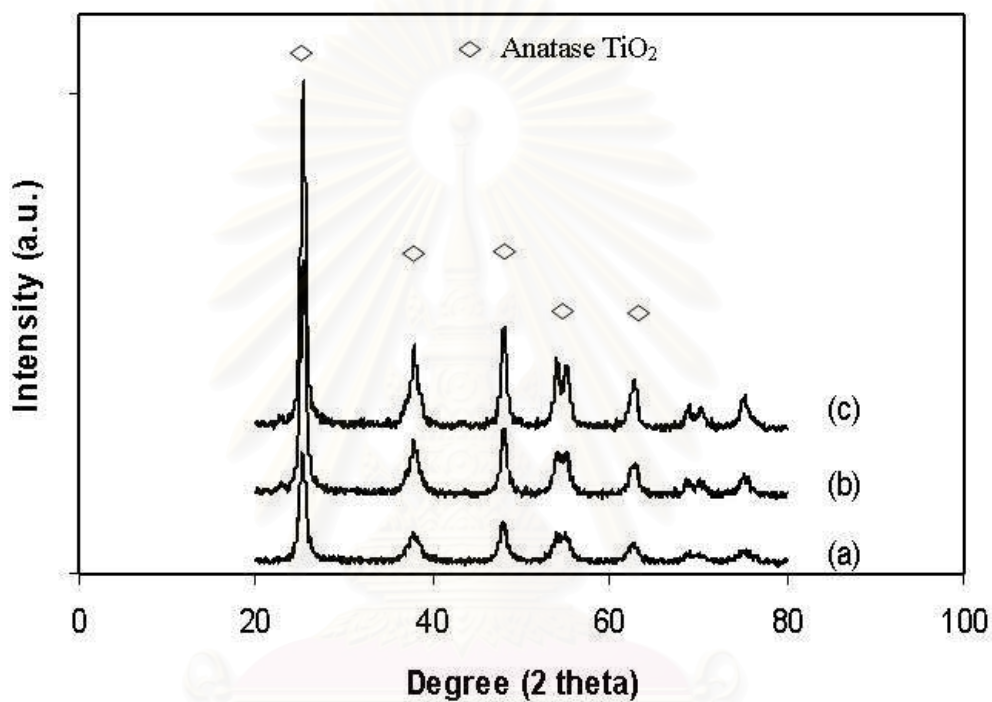


Figure 5.9 The XRD patterns of the various TiO₂ samples after quenching in air at room temperature: (a) 9 nm, (b) 11 nm, (c) 13 nm.

Table 5.3

Phase compositions and structural properties of the TiO₂ synthesized by solvothermal method after quenching in various media

Synthesis Conditions	Quenching medium	Crystallite size (nm)	S _{BET} (m ² /g)	Sample Nomenclature
TNB 15 g	Air at 373 K	8.6	96	9A
Toluene 100 ml	Air at RT*	9.4	94	9B
Temp. 573 K	H ₂ O at 373 K	9.0	99	9C
Holding Time 0.5 h	H ₂ O at RT	8.9	104	9D
	30wt% H ₂ O ₂ at 373 K	10.0	92	9E
	30wt% H ₂ O ₂ at RT	10.5	91	9F
TNB 25 g	Air at 373 K	9.6	85	11A
Toluene 100 ml	Air at RT	10.6	93	11B
Temp. 573 K	H ₂ O at 373 K	10.4	95	11C
Holding Time 2 h	H ₂ O at RT	10.5	112	11D
	30wt% H ₂ O ₂ at 373 K	13.2	90	11E
	30wt% H ₂ O ₂ at RT	13.3	94	11F
TNB 15 g	Air at 373 K	10.4	60	13A
Toluene 100 ml	Air at RT	13.4	67	13B
Temp. 593 K	H ₂ O at 373 K	13.4	67	13C
Holding Time 6 h	H ₂ O at RT	13.2	69	13D
	30wt% H ₂ O ₂ at 373 K	14.6	61	13E
	30wt% H ₂ O ₂ at RT	14.7	63	13F

* RT = Room temperature

The crystallite sizes of the TiO_2 from XRD are in good agreement with those observed from the TEM micrographs of the samples (Figure 5.10).

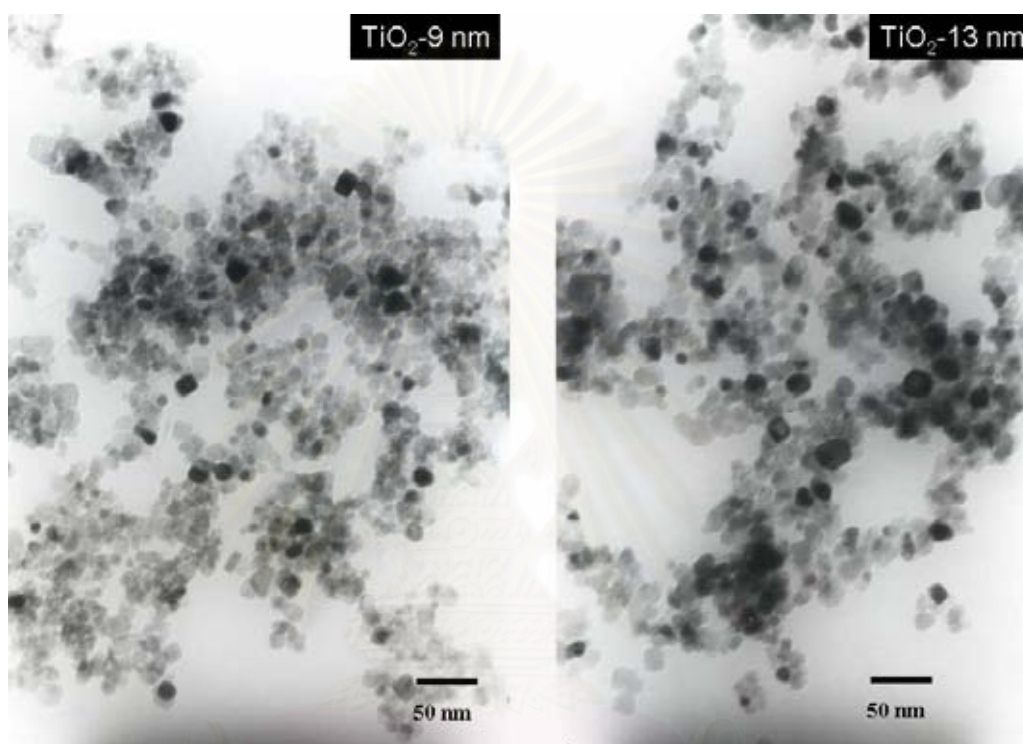


Figure 5.10 TEM micrographs of TiO_2 -9 nm and TiO_2 -13 nm (non-quenched)

5.1.2.2 Temperature programmed desorption of carbon dioxide (CO_2 -TPD)

The surface structure of TiO_2 was characterized by temperature programmed desorption of CO_2 . All of the TiO_2 samples exhibited two main desorption peaks at temperatures ca. 145 K and 170 K which could be attributed to adsorption of CO_2 on two different structures of TiO_2 surface. For example, the CO_2 -TPD profiles of TiO_2 samples with average crystallite size of 11 nm after quenching in various media are shown in Figure 5.11.

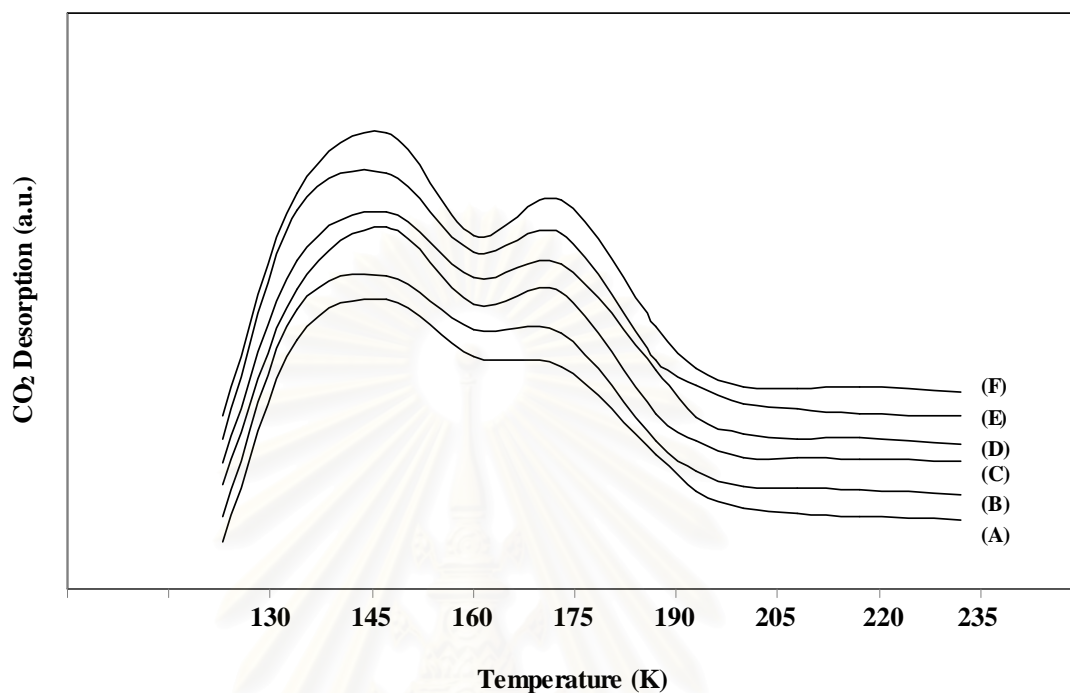


Figure 5.11 CO₂ temperature programmed desorption results of the TiO₂ 11 nm quenched in different media; (A) Air at 373 K, (B) Air at RT, (C) H₂O at 373 K, (D) H₂O at RT, (E) 30% wt H₂O₂ at 373 K, (F) 30% wt H₂O₂ at RT (RT = room temperature)

(* This figure is modified from figure 5.3)

The desorption peak at ca. 145 K was attributed to CO₂ molecules bounding to regular five-coordinate Ti⁴⁺ site which was considered as the perfected TiO₂ structure. The second peak at ca. 170 K has been considered as desorption of CO₂ molecules bounding to Ti³⁺ defect sites of TiO₂. Based on the CO₂-TPD results, it was found that for a given TiO₂ crystallite size, the peak areas for CO₂ desorption at ca. 170 K (representing the amount of Ti³⁺ defective sites) depended on the type of quenching media employed in the following order: air 373 K < air RT < H₂O 373 K < H₂O RT < H₂O₂ 373 K < H₂O₂ RT. It is known that quenching treatment of a metal can create nucleation of dislocations, surface defect, and concentration of stress on the metal surface.

The results in this study have shown that quenching process can be applied as a post-synthesis treatment for controlling the amount of surface defects on nanocrystalline TiO₂. The Ti³⁺/Ti⁴⁺ ratios calculated from CO₂-TPD results of the various quenched TiO₂ samples and the non-quenched one are illustrated in Figure 5.12.

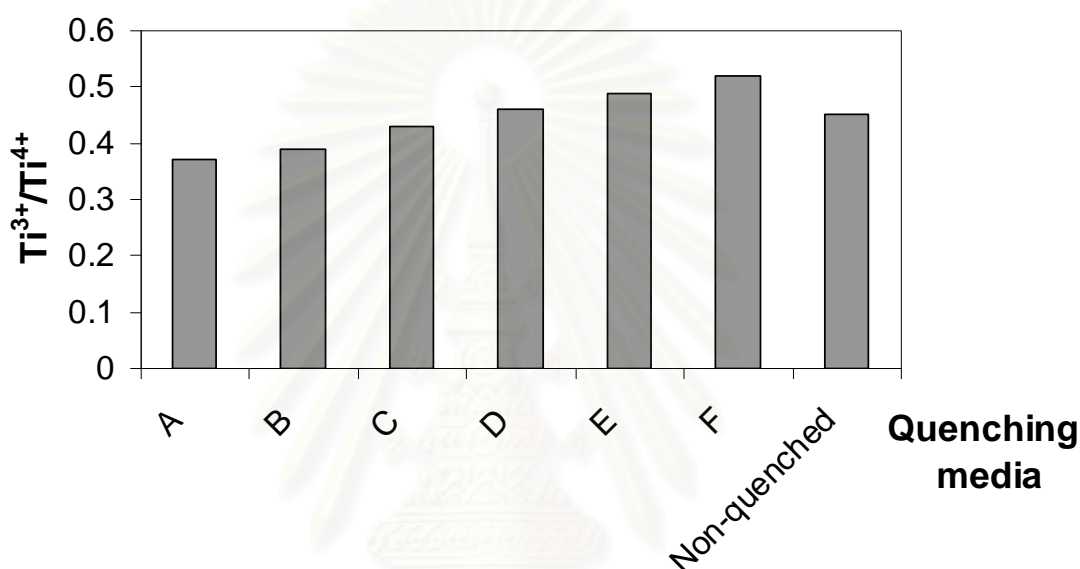


Figure 5.12 Ti³⁺/Ti⁴⁺ calculated from CO₂-TPD results of the TiO₂-11 nm quenched in different media: (A) Air at 373 K, (B) Air at RT, (C) H₂O at 373 K, (D) H₂O at RT, (E) 30wt% H₂O₂ at 373 K, (F) 30wt% H₂O₂ at RT (RT = room temperature)

It was found that the non-quenched sample also possessed significant amount of Ti³⁺ in a similar degree to that quenched in H₂O at room temperature. However, when compared the TiO₂ sample quenched in 30%wt H₂O₂ and H₂O, it is noticed that the TiO₂ sample quenched in liquid phase media that contained more -OH group in molecules exhibited higher Ti³⁺/Ti⁴⁺ and higher photocatalytic activity.

5.1.2.3 Photocatalytic activity of the nano-TiO₂ quenched in different media

Photocatalytic activities of the TiO₂ samples with various crystallite sizes after quenching in different media were evaluated in the decomposition of ethylene in gas-phase and the results are shown in Figure 5.13. Ethylene conversions at steady-state (after 180 min of run) for the quenched TiO₂ samples with various crystallite sizes were ranged from ca. 20-37% while that of TiO₂ Degussa P25 under similar reaction conditions gave ca. 30% ethylene conversion. It was found that for a given TiO₂ crystallite size, ethylene conversions were strongly dependent on the quenching media and were found to be in the order: 30%wt H₂O₂ RT > 30%wt H₂O₂ 373 K > H₂O RT > H₂O 373 K > air RT > air 373 K. Such results were in good agreement with the amount of Ti³⁺ surface defect on the TiO₂ samples in which those with higher amounts of Ti³⁺ surface defect exhibited higher photocatalytic activities for ethylene decomposition. For a similar quenching medium, the TiO₂ quenched at low temperature resulted in larger amount of Ti³⁺ and exhibited higher photocatalytic activity compared to those quenched at high temperature. This can probably be explained by a thermal shock effect that a large difference in temperature of the TiO₂ surface and quenching medium can create more surface defects. However, compared to the TiO₂ sample that was slowly cooled down after calcination (the non-quenched sample), only the smaller crystallite size TiO₂ (TiO₂-9 nm) that quenched in 30%wt H₂O₂ exhibited higher photocatalytic activities. The effect of quenching was less pronounced on the larger TiO₂ crystallite size and the non-quenched samples showed higher activities.

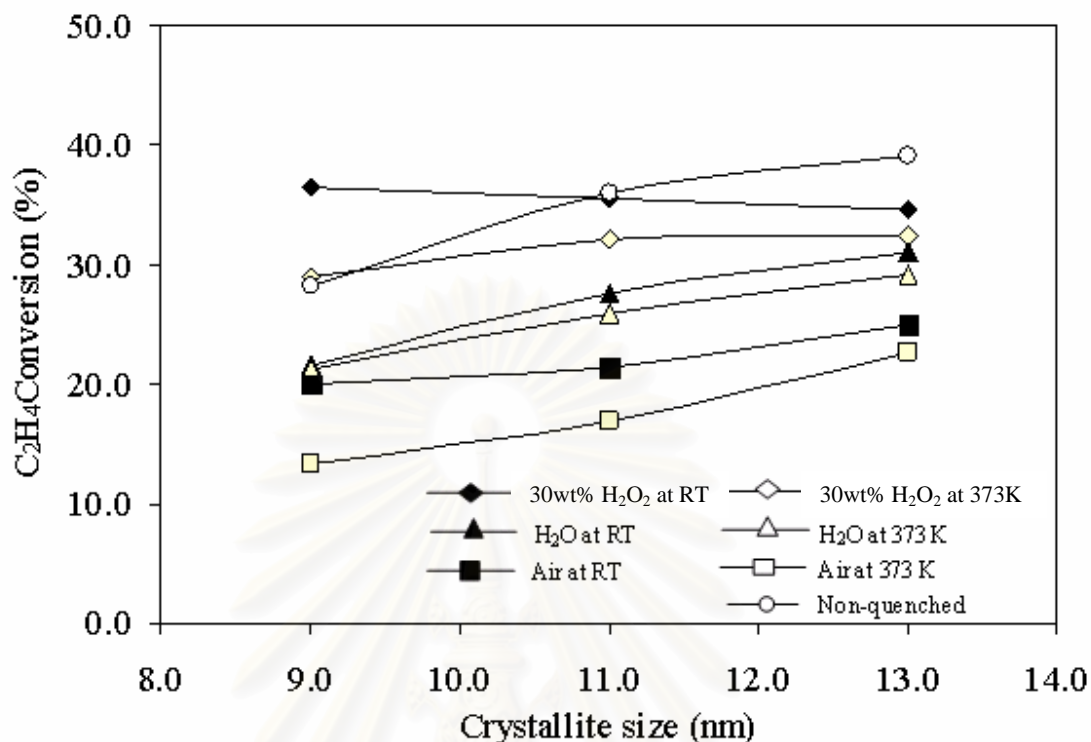


Figure 5.13 Results of the photocatalytic activities of TiO₂ samples quenched in different media.

5.1.3 Effect of Si and Zr addition on the surface defect and photocatalytic activity of the solvothermal-derived TiO₂

5.1.3.1 Textural properties of the TiO₂ photocatalysts

X-ray diffraction patterns of the base TiO₂ and the metal-doped TiO₂ samples with metal/titanium molar ratio 0.1 are shown in Figure 5.14. All the samples exhibited the XRD patterns of only pure anatase phase TiO₂ without any contamination of other phases. However, the peak intensities of anatase TiO₂ decreased with the increase of the second metal content due probably to formation of amorphous phases. No diffraction lines of zirconia or silica were observed suggesting that all the Zr and Si were incorporated into the anatase TiO₂ structure or the amount of metal doping is too low (Iwamoto *et al.*, 2000 and Inoue *et al.*, 2000). The average crystallite sizes of TiO₂

samples were determined from the full width at half maximum of the XRD peak at $2\theta = 25.36^\circ$ using Scherrer's equation. As shown in Table 5.4, addition of a small amount of Si or Zr to TiO_2 powder, the average crystallite size of TiO_2 decreased (from 11.0 nm to 9.0 nm). It is likely that second metal-doping suppressed crystal growth of TiO_2 thus smaller crystallite sizes were obtained (Hirano et al., 2000). According to the BET analysis, it can be observed that the Si- and Zr-doped TiO_2 samples have larger BET surface area than pure TiO_2 . The results were in accordance to those reported previously for Zr- and Si-doped TiO_2 with higher second metal contents (Jung et al., 1999 and Wiwattanapongpan et al., 2007).

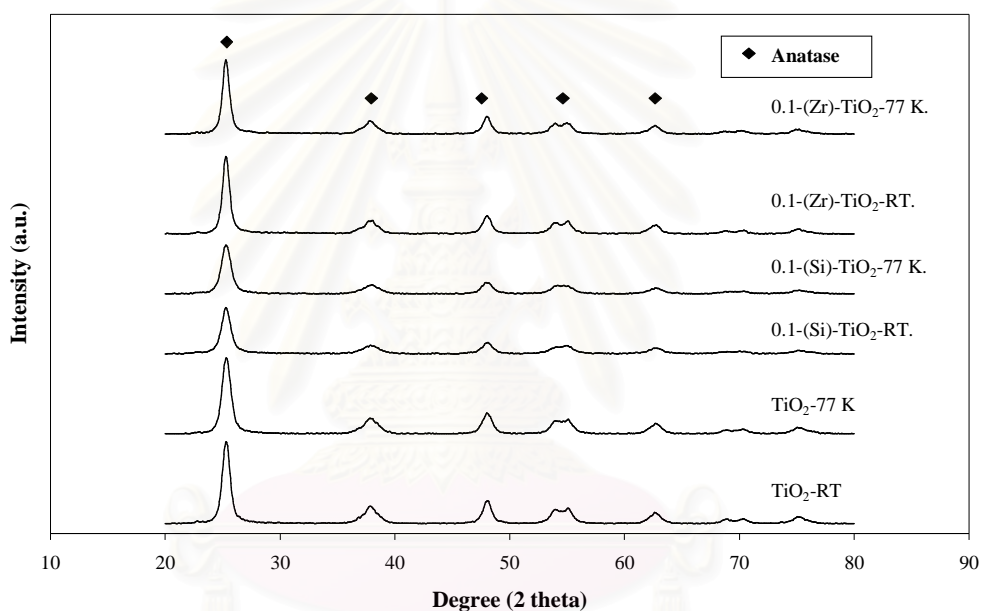


Figure 5.14 X-ray diffraction patterns of pure TiO_2 and metal doped- TiO_2

It is believed that the process of annealing or calcination has shown to result in a variety of surface defects, strains, and reconstructions of materials. So, the variation of cooling temperature was applied as a post-synthesis treatment with the aims to create more defects on the TiO_2 surface and as a consequence, improve their photocatalytic activities. Moreover, the post-synthesis treatment in cooling temperature did not significantly alter the specific surface area and the average crystallite size of the TiO_2 (see Table 5.4).

Table 5.4 Physical properties and activities of Si- and Zr-doped TiO₂ samples synthesized by solvothermal method

Sample nomenclature	Crystallite size ^a (nm)	BET surface area ^b (m ² /g)	Intensity of ESR/BET	Ethylene Conversion ^c (%)
TiO ₂ -RT	10.6	93	47	21.5
TiO ₂ -77 K	10.6	97	257	34.6
0.002-(Si)-TiO ₂ -RT.	9.0	159	77	23.5
0.002-(Si)-TiO ₂ -77 K	9.0	156	199	31.5
0.005-(Si)-TiO ₂ -RT.	8.9	133	144	27.9
0.005-(Si)-TiO ₂ -77 K	8.6	136	213	32.4
0.1-(Si)-TiO ₂ -RT.	9.0	133	56	22.1
0.1-(Si)-TiO ₂ -77 K	8.4	136	62	22.5
0.002-(Zr)-TiO ₂ -RT.	9.5	95	111	25.7
0.002-(Zr)-TiO ₂ -77 K	9.7	99	225	33.2
0.005-(Zr)-TiO ₂ -RT.	7.7	101	245	34.5
0.005-(Zr)-TiO ₂ -77 K	7.8	106	322	39.5
0.1-(Zr)-TiO ₂ -RT.	8.2	104	57	22.2
0.1-(Zr)-TiO ₂ -77 K	8.4	105	79	23.5

^a Determined using Scherrer's equation

^b Determined using BET method.

^c Photocatalytic reaction was carried out at 313–328 K, 1 bar, and 0.1% ethylene in air.

5.1.3.2 Electron spin resonance spectroscopy (ESR) study

It is known that the surface Ti^{3+} defect sites (oxygen vacancies) are the sites that oxygen adsorption occurs as well as that the photo-generated electrons are trapped (Diebold, 2003), so they are effective sites for interface electrons transferring. Relationship between the amount of Ti^{3+} defects on TiO_2 surface and their photocatalytic activities has been reported by many authors. In this study, the number of defective sites of TiO_2 was determined using electron spin resonance spectroscopy technique and the results are shown in Figure 5.15.

From figure 5.15, all the TiO_2 samples exhibited similar ESR spectra in which mainly one signal at the g value of 1.996 were observed. According to Nakaoka *et al.* (1997), this peak was attributed to the Ti^{3+} site on TiO_2 . It is clearly seen that the Zr-doped TiO_2 exhibited higher intensity of the ESR signals than the Si-doped ones. The intensity of ESR spectra per surface area of the TiO_2 is given in Table 5.4. The results indicate that Zr-doped TiO_2 possessed higher concentration of Ti^{3+} defective sites than Si-doped TiO_2 .

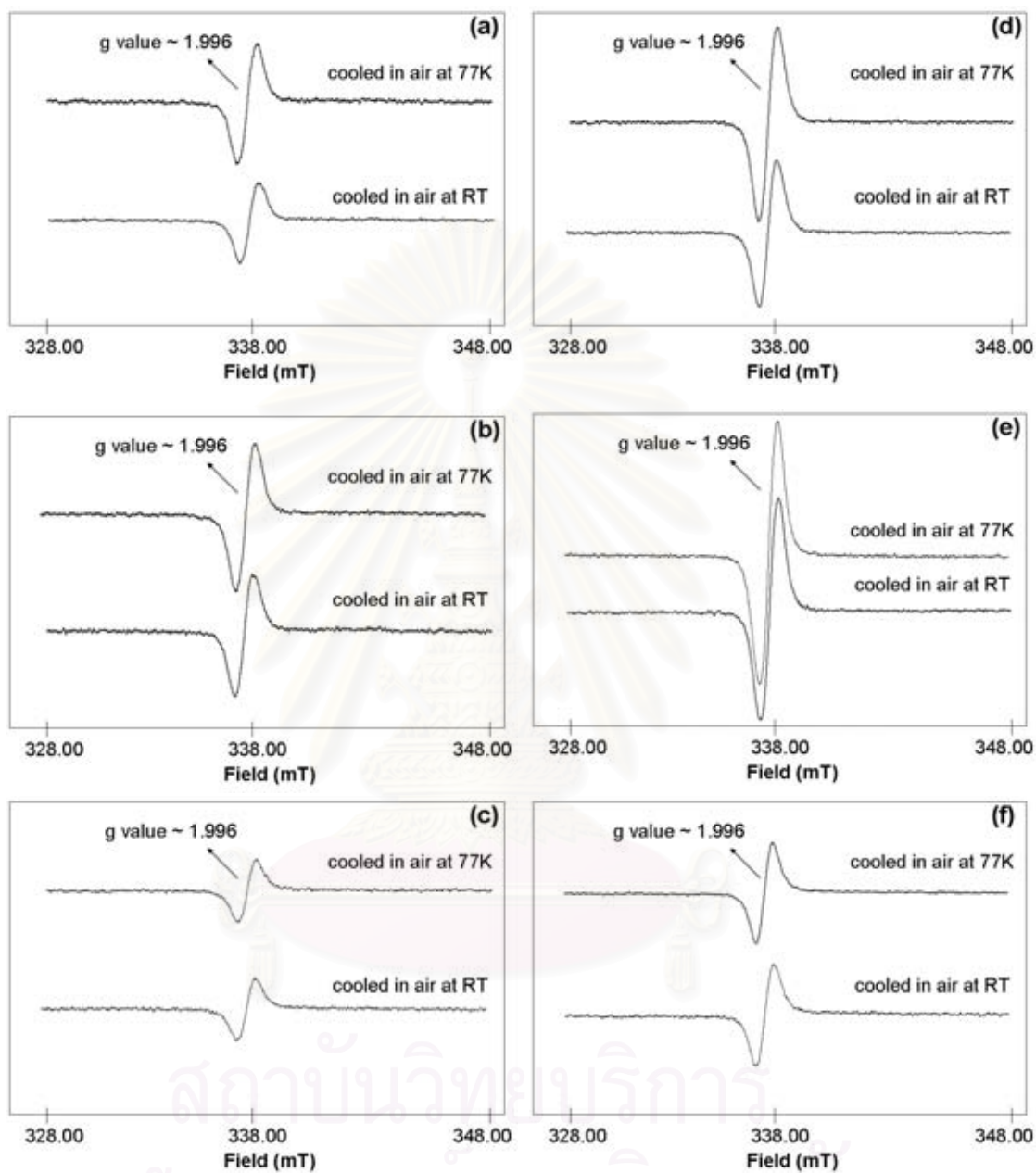


Figure 5.15

ESR spectra of (a) 0.002 Si-doped TiO_2 , (b) 0.005 Si-doped TiO_2 , (c) 0.1 Si-doped TiO_2 , (d) 0.002 Zr-doped TiO_2 , (e) 0.005 Zr-doped TiO_2 , (f) 0.1 Zr-doped TiO_2

5.1.3.3 X-ray photoelectron spectroscopy (XPS) study

It is well-known that XPS is a surface probe detecting electrons that are generated from a depth of a few nanometers on the surface of the sample. The elemental composition and their chemical states on the surface of metal-doped TiO₂ samples that were subjected to two different cooling temperatures were studied by XPS analysis. The binding energy values and the full width at half maximum (FWHM) values of Zr 3d, O 1s, Si 2p and Ti 2p photoelectron peaks as determined by XPS of the various TiO₂ samples are summarized in Table 5.5. The binding energies for Si 2p and Zr 3d levels are in agreement with those reported for pure SiO₂ (Bosman *et al.*, 1996) and ZrO₂ (Bastl *et al.*, 2002) at ca.103.0 and 183.5 eV, respectively. No significant variation has been observed for these elements over the metal-doped TiO₂ samples. However, the binding energy of the Ti 2p band for the metal-doped samples was found to be lower than that of the pure TiO₂.

Table 5.5XPS binding energies (eV) and FWHM (eV) values of Si- and Zr-doped TiO₂ catalysts

Sample nomenclature	Ti 2p		O 1s		Zr 3d		Si 2p	
	BE	FWHM	BE	FWHM	BE	FWHM	BE	FWHM
TiO ₂ -RT	459.3	1.7	530.8	1.5	-	-	-	-
TiO ₂ -77 K	459.2	1.7	530.6	1.4	-	-	-	-
0.002-(Si)-TiO ₂ -RT.	458.8	1.4	530.1	1.5	-	-	102.1	2.0
0.002-(Si)-TiO ₂ -77 K	458.9	1.4	530.2	1.5	-	-	102.0	1.9
0.005-(Si)-TiO ₂ -RT.	458.3	1.4	530.1	1.5	-	-	102.1	2.1
0.005-(Si)-TiO ₂ -77 K	458.4	1.4	530.2	1.5	-	-	102.1	2.3
0.1-(Si)-TiO ₂ -RT.	458.5	1.5	530.2	1.6	-	-	102.3	2.2
0.1-(Si)-TiO ₂ -77 K	458.6	1.5	530.3	1.6	-	-	102.4	2.1
0.002-(Zr)-TiO ₂ -RT.	458.5	1.4	530.2	1.5	182.1	1.8	-	-
0.002-(Zr)-TiO ₂ -77 K	458.3	1.4	530.1	1.6	182.0	2.0	-	-
0.005-(Zr)-TiO ₂ -RT.	458.3	1.5	530.3	1.4	182.1	1.9	-	-
0.005-(Zr)-TiO ₂ -77 K	458.6	1.4	530.3	1.6	182.4	1.8	-	-
0.1-(Zr)-TiO ₂ -RT.	458.2	1.4	530.1	1.5	182.3	2.2	-	-
0.1-(Zr)-TiO ₂ -77 K	458.4	1.4	530.3	1.5	182.1	2.1	-	-

For better comparison, the XPS bands of Ti 2p for Si- and Zr-doped TiO₂ are shown in Figure 5.16. Normally, The Ti 2p XPS spectra of TiO₂ sample show two shoulder peaks at lower binding energy (Ti 2p_{3/2}) and higher binding energy (Ti 2p_{1/2}), respectively (Mukhopadhyay and Garofalini, 1990). From Figure 5.16, the binding energy of Ti 2p electrons was found to be lower than the value normally published for Ti⁴⁺ ions in TiO₂ (459.2 eV) (Kumar *et al.*, 2000). The observed shift towards lower binding energies can be attributed to the presence of surface Ti³⁺ ions and/or presence of oxygen vacancies around Ti⁴⁺ ions. So, it is feasible that the introduction of second metals produces different types of Ti cation (Ti³⁺, Ti²⁺, etc.), resulting in different photocatalytic performance.

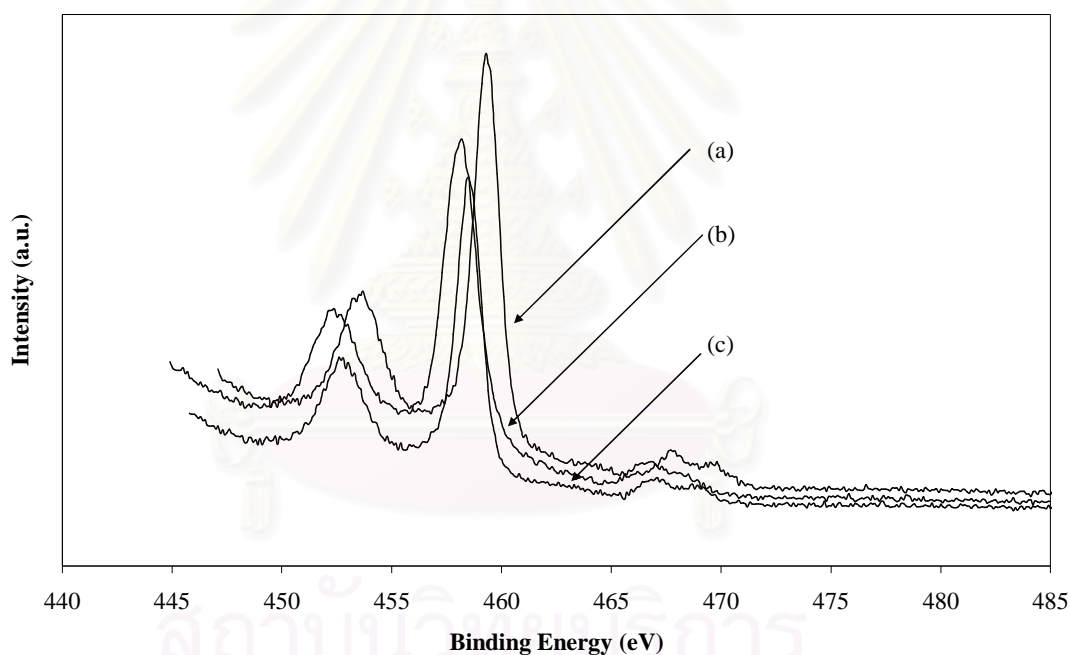


Figure 5.16 Ti 2p XPS spectra of various TiO₂ samples: (a) TiO₂-RT, (b) 0.1-(Zr)-TiO₂-RT, (c) 0.1-(Si)-TiO₂-RT.

5.1.3.4 Photocatalytic activity test

The photocatalytic activity of the TiO₂ and metal-doped TiO₂ samples was tested for the photocatalytic decomposition of ethylene in gas-phase under UV illumination. Under these conditions, the only products detected by gas chromatography were CO₂ and H₂O. The mechanism of photocatalytic decomposition of ethylene has been reported by many researchers (Yamazaki et al., 1999 and Sirisuk et al., 1999). The mechanism is believed to involve absorption of an UV photo by TiO₂ to produce an electron-hole pair. Both hole and electron play an important role on creating the reaction intermediate, which react further and form CO₂ as the final product.

Photocatalytic activities of the TiO₂ samples with different proportions of Si/Ti and Zr/Ti were evaluated in the decomposition of ethylene in gas-phase and the results are shown in Table 5.4. It was founded that the photocatalytic activity of the metal-doped TiO₂ cooled down in different cooling temperature is evidently different. The ethylene conversion results showed that the metal-doped TiO₂ at lower amounts of metal (Si/Ti and Zr/Ti < 0.005) exhibit a higher photocatalytic activity than pure titania. Ethylene conversions at steady-state for the metal-doped TiO₂ samples after cooling at room temperature were ranged from ca. 22-39% while pure TiO₂ sample under similar reaction conditions gave ca. 21% ethylene conversion. In addition, the photocatalytic activity of metal-doped TiO₂ depended on the cooling temperature applied after calcination. It was found that metal-doped TiO₂ samples cooled at lower temperature exhibited higher photocatalytic activity than those cooled in high temperature ones. For example, the ethylene conversion of 0.005 Zr-doped TiO₂ was 34.5% and 39.5% for the sample cooled down at room temperature and at 77 K, respectively. From Table 5.4, Si-doped TiO₂ samples are more efficient photocatalysts than pure TiO₂. The increase in photocatalytic efficiency has been attributed to the improved adsorption and concentration of the reactants near the active centers. At the same time, silica acts as the carrier of titania and helps to obtain a large surface area as well as suitable porous structure. Moreover, Zr-doped TiO₂ samples exhibit more photocatalytic activity than pure TiO₂. Due to the Zr-doping possibly suppresses the recombination of electrons and

positive holes by their trapping (Lukáč *et al.*, 2007).

Additionally, the results in this study show that for a similar metal content, the Zr-doped TiO₂ exhibited higher photocatalytic activity than the Si-doped ones. However, one may notice that the Si-doped TiO₂ had larger BET surface areas than the Zr-doped ones and in general, anatase TiO₂ nanoparticles with higher specific surface area typically exhibit higher photocatalytic activity. The increase of surface area means the increase of the number of active sites on which the electron acceptor and donor are adsorbed and participate in the photocatalytic reaction. Since the Zr-doped TiO₂ samples possessed more Ti³⁺ defective sites on the surface than the Si-doped ones and showed higher photocatalytic activity, it is suggested that the amount of Ti³⁺ sites on TiO₂ play an important role for enhancing photocatalytic activity of the TiO₂. More Ti³⁺ states may cause more oxygen defects, and O₂ is more easily adsorbed on TiO₂ surface.

5.2 Titanium dioxide as catalyst support

5.2.1 Catalytic behaviors of quenched TiO₂-supported cobalt Fischer–Tropsch catalysts for carbon monoxide hydrogenation

This section is an attempt to apply the TiO₂ sample after quenching in air RT, water at RT, and water at 373 K are used as catalyst support. The effect of defective structures in titania on the catalytic performance of the titania supported cobalt in CO hydrogenation was investigated.

5.2.1.1 Characteristics of catalyst

The crystallite sizes of titania calculated from the XRD line broadening using the Scherrer's equation and the BET surface areas are reported in Table 5.6. The average crystallite sizes of the titania were approximately 10–11 nm. The BET surface areas of the nanocrystalline titania were found to be 94–112 m²/g.

Table 5.6 Crystallite sizes and BET surface areas of quenched titania support

Sample	Quenching medium	Crystallite size ^a (nm)	S_{BET} ^b (m ² /g)
A	Air at RT	11	93
B	H ₂ O at RT	10	112
C	H ₂ O at 373 K	11	94

The BET surface areas of the various Co/TiO₂ catalysts and the H₂ chemisorption results are reported in Table 5.7. After loading 20 wt% Co, the BET surface areas of the titania supported cobalt catalysts were slightly less than that of the original titania supports suggesting that cobalt was deposited in some of the pores of titania.

Static H₂ chemisorption on the reduced cobalt catalyst samples was used to determine the number of reduced Co metal surface atoms. This is usually related to the overall activity of the catalyst during CO hydrogenation. Based on the CO₂-TPD and ESR results in previous discussion, the amounts of surface Ti³⁺ sites on the TiO₂ samples were in the following order: H₂O at RT > H₂O at 373 K > air at RT. It was found that the number of reduced cobalt metal surface atoms increased with the amount of defect present in the titania supports.

Table 5.7 Characteristics of various Co/TiO₂ catalysts

Samples	BET surface area (m ² /g)	H ₂ chemisorption x10 ¹⁷ (molecule H ₂ /g cat.)
20%Co/TiO ₂ -Air at RT	48.5	4.2
20%Co/TiO ₂ -H ₂ O at RT	50.3	6.3
20%Co/TiO ₂ -H ₂ O at 373K	48.8	5.1

XRD patterns of TiO_2 supports and Co/TiO_2 catalysts are shown in Figure 5.17. It was found that XRD patterns of TiO_2 showed strong diffraction peaks at 26° , 37° , 48° , 55° , 62° , 69° , 71° and 75° indicating the TiO_2 in its anatase form. All of Co/TiO_2 catalysts exhibited XRD peaks at 31° , 36° , and 65° , which were assigned to presence of Co_3O_4 (Jongsomjit et al., 2004).

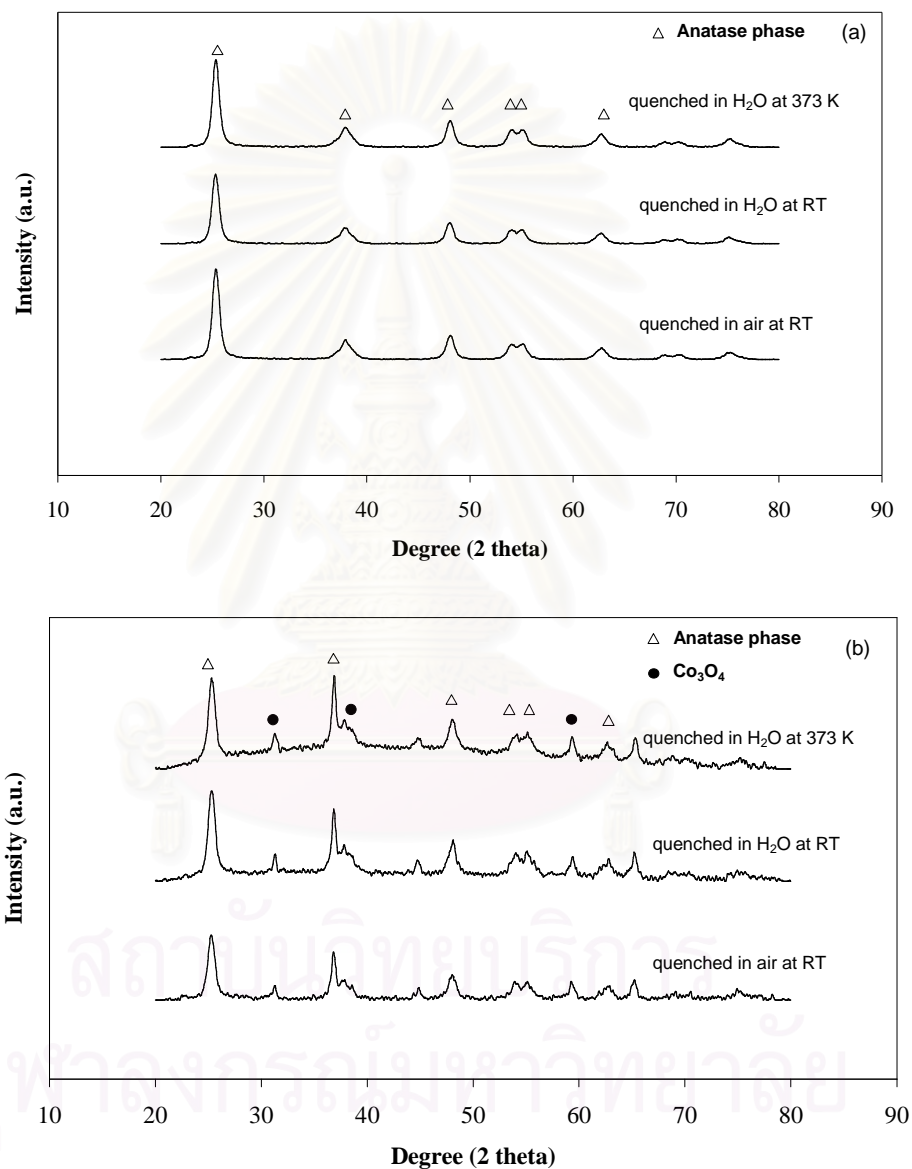


Figure 5.17 XRD patterns of sample pretreated under various quenching conditions; (a) TiO_2 supports and (b) Co/TiO_2 catalysts

SEM and EDX were performed to study the morphologies and elemental distribution of the catalyst samples, respectively. The typical SEM micrograph along with the EDX mapping (for Co, Ti, and O) are illustrated in Figure 5.18 a), b) and c) for Co/TiO₂ quenching air, water, and water at 373K, respectively. The external surface of catalyst granule is shown in all figures and the light or white patches (the term “patches” is used to refer the entities rich in cobalt supported on the catalyst granules) on the catalyst granule surface represent high concentration of cobalt oxide species on the surface. It can be seen that the cobalt oxide species were dispersed and distributed (shown on mapping) all over the catalyst granule in all samples regardless of the quenched titania supports.

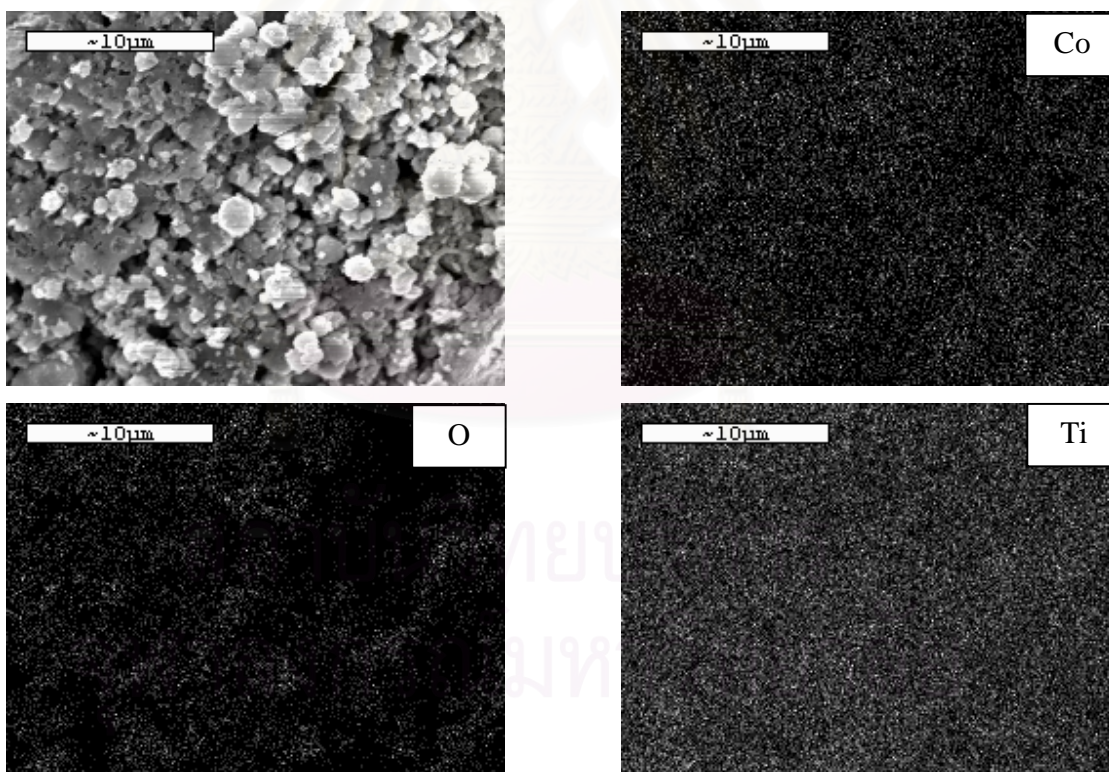


Figure 5.18 a) SEM micrograph and EDX mapping of Co/TiO₂ quenched in air.

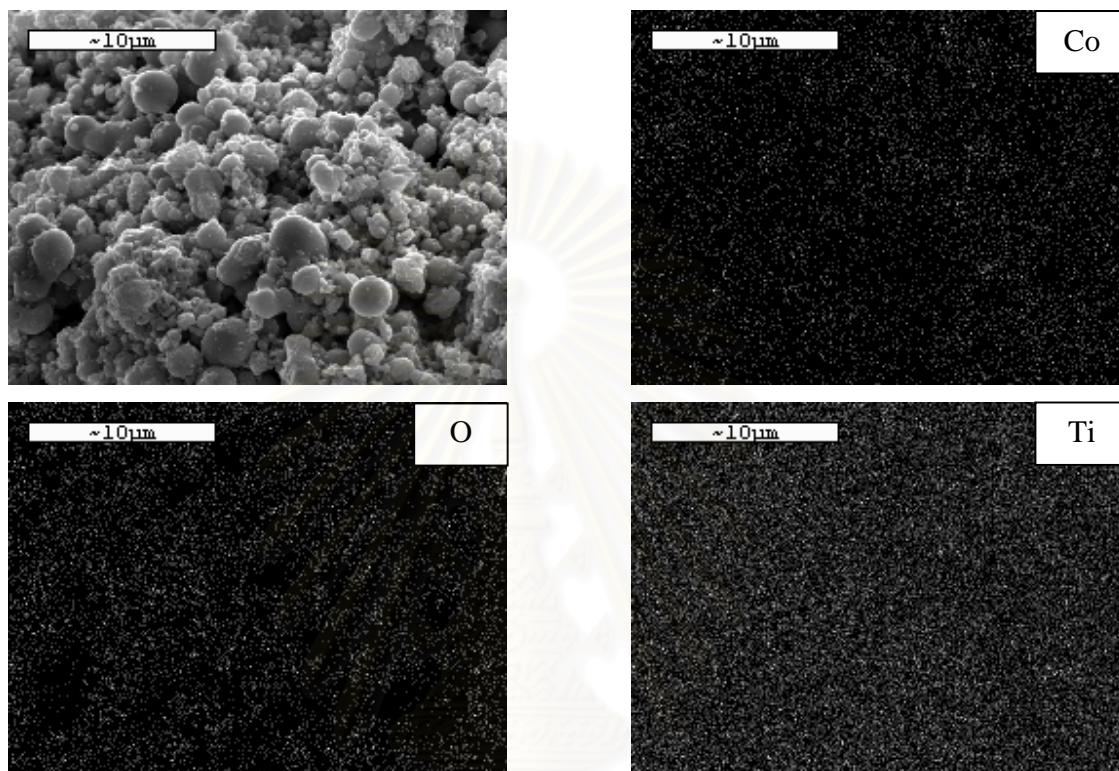


Figure 5.18 b) SEM micrograph and EDX mapping of Co/TiO₂ quenched in water at room temperature.

สถาบันวิทยบริการ
จุฬาลงกรณ์มหาวิทยาลัย

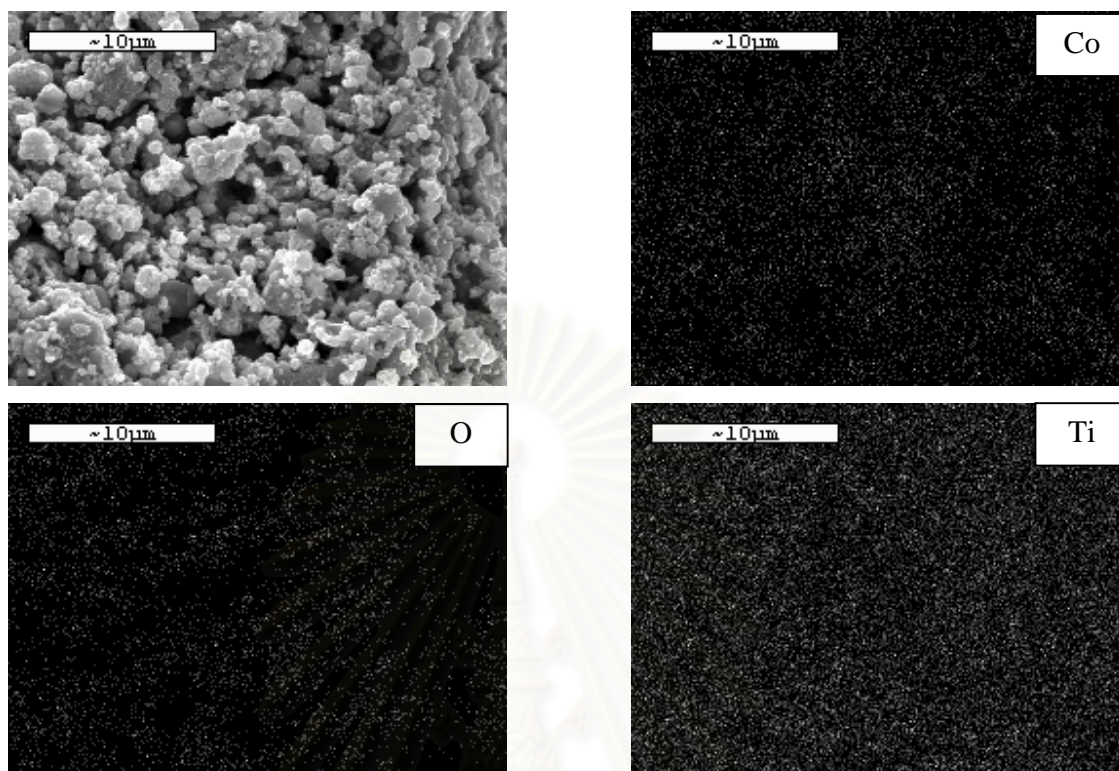


Figure 5.18 c) SEM micrograph and EDX mapping of Co/TiO₂ quenched in water at 373K

สถาบันวิทยบริการ
จุฬาลงกรณ์มหาวิทยาลัย

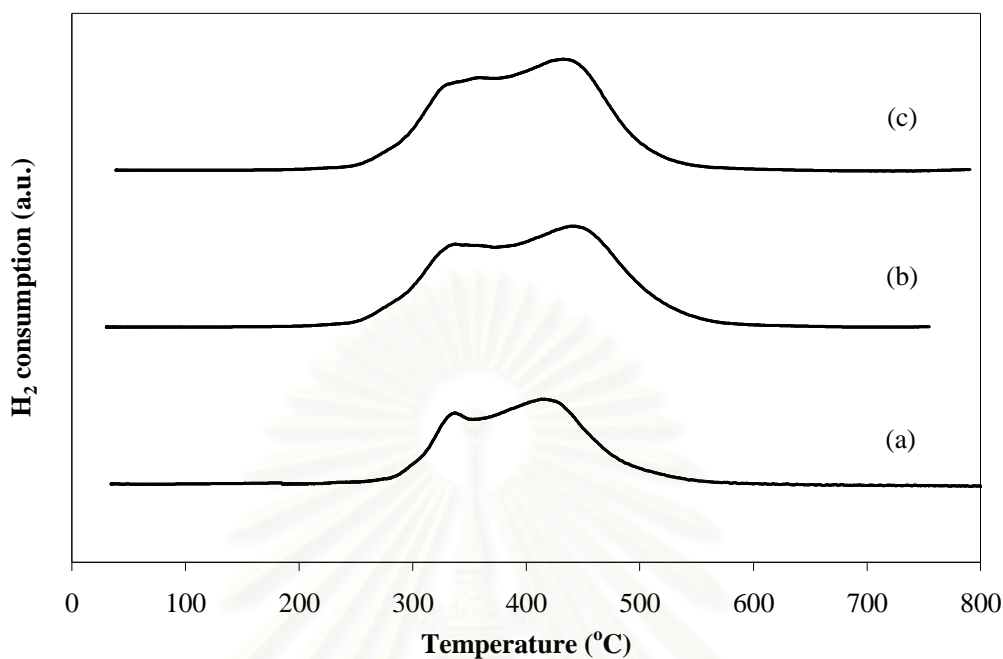


Figure 5.19 Temperature-programmed reduction of the catalyst samples (a) 20%Co/TiO₂-Air; (b) 20%Co/TiO₂-H₂O; (c) 20%Co/TiO₂-H₂O at 373K

TPR was performed in order to determine the reduction behaviors of samples. The TPR profiles for all catalyst samples are shown in Figure 5.19. Reduction of cobalt in the oxide form, Co₃O₄ or Co₂O₃, to Co₀ involves a two-step reduction: first reduction of Co₃O₄ to CoO and then the subsequent reduction of CoO to Co₀ (Jongsomjit et al., 2004). TPR profiles for all cobalt catalysts were also similar exhibiting two reduction peak. The first peak located at ca. 300–350 °C and second peak located at ca. 350-500 °C

5.2.1.2 Catalytic properties

In order to determine the effect of quenching process on the catalytic properties of Co/TiO₂, CO hydrogenation (H₂/CO=10/1) was performed to determine the overall activity and product selectivity of the samples. Hydrogenation of CO was carried out at 220 °C and 1 atm. A flow rate of H₂/CO/He=20/2/8 cc/min in a fixed-bed flow reactor was used. Results obtained from the reaction study are shown in Table 5.8. As expected, the CO hydrogenation rates increased by 15-33% for the Co supported on quenched titania. Based on the H₂ chemisorption results, the overall activities and TOF, it was found that the quenching treatment of titania support exhibited a positive influence on catalytic activity for CO hydrogenation reaction. The product selectivities were not significantly differently, since all the catalysts showed methane selectivities ca. 95-98%. Considering the selectivity of product, it showed that the selectivity to methane essentially decreased for quenching of titania support in the water.

Table 5.8 Reaction study during CO hydrogenation of catalyst samples pretreated under various quenching conditions

Sample	Reaction rate ^a (x10 ² gCH ₂ /gcat.h)	Production selectivity		TOF ^b (s ⁻¹)
		C ₁	C ₂ -C ₅	
20%Co/TiO ₂ -Air at RT	14.9	98.18	1.82	2.1
20%Co/TiO ₂ -H ₂ O at RT	33.0	95.77	4.23	3.1
20%Co/TiO ₂ -H ₂ O at 373K	25.3	95.65	4.35	2.9

^a Error ±5%. Rate of -CH₂- formed as same as moles of CO converted represented the repeating unit of all hydrocarbon chains in product stream.

^b TOF =
$$\frac{\text{Rate of CO hydrogenation (molecules of CO/ g catalyst. Sec)}}{2 \times \text{Hydrogenation chemisorption (molecules/ g catalyst)}}$$

CHAPTER VI

CONCLUSIONS AND RECOMMENDATIONS

6.1 Conclusions

This research was divided into two parts. The first part involved the characterization and utilization of titania as photocatalyst. The second part involved Co/TiO₂ catalyst

6.1.1 Titanium dioxide as photocatalyst

- **Effect of quenching medium on photocatalytic activity of nano-TiO₂ prepared by solvothermal method**

The surface properties as well as photocatalytic activities of the solvothermal-derived nano-TiO₂ can be modified by quenching process post-synthesis treatment whilst the average crystallite size and BET surface area of the samples were essentially similar. It was found that quenching process especially the use of low temperature medium can create a thermal shock effect that as a consequence resulting in more surface Ti³⁺ defects on the TiO₂ sample and hence higher photocatalytic activity.

- **Dependence of quenching process on the photocatalytic activity of solvothermal-derived TiO₂ with various crystallite sizes**

The surface properties and photocatalytic activities of nano-sized TiO₂ powders synthesized by solvothermal method with various crystallite sizes (9-13 nm) were significantly influenced by quenching media and quenching conditions. For the use of similar quenching media, the TiO₂ quenched in a low temperature medium has shown to result in more Ti³⁺ surface defects on the TiO₂ surface and consequently higher photocatalytic activity that those quenched in a high temperature one. The amount of Ti³⁺

and photocatalytic activity of the quenched samples depended on the type of quenching medium in the order: $\text{H}_2\text{O}_2 > \text{H}_2\text{O} > \text{air}$. Compared to the non-quenched sample (the one slowly cooled down after calcination), quenching in 30wt% H_2O_2 has shown to result in higher Ti^{3+} and photocatalytic activity of the TiO_2 with small crystallite size (9 nm). There was less effect of quenching on larger crystallite size TiO_2 .

- **Effect of Si and Zr addition on the surface defect and photocatalytic activity of the solvothermal-derived TiO_2**

The Si- and Zr-doped TiO_2 with Si/Ti and Zr/Ti molar ratios ranging from 0.002-0.1% were prepared via the solvothermal method using titanium n-butoxide as the titanium precursor and toluene as the solvent. It was found that selection of a suitable second metal doping can enhance photocatalytic activity of the TiO_2 . Based on ESR and XPS analyses, the improved photocatalytic activity of the TiO_2 is suggested to be due to the presence of Ti^{3+} defect sites on the surface of TiO_2 . Moreover, a post-synthesis treatment by cooling in air at 77 K effectively enhanced the amount of Ti^{3+} and photocatalytic activity of the TiO_2 and the metal-doped TiO_2 .

6.1.2 Titanium dioxide as catalyst support

- **Catalytic behaviors of quenched TiO_2 -supported cobalt catalysts for carbon monoxide hydrogenation**

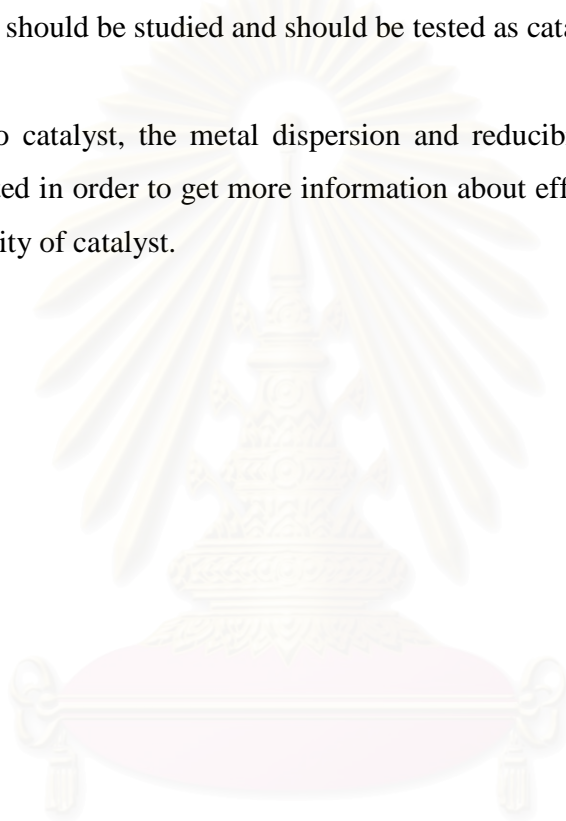
The impact of various quenched TiO_2 -supported cobalt catalysts on their catalytic behaviors was discussed. It was found that the quenching treatment seemed to have positive effect on activities for CO hydrogenation upon the amount of surface defect present in titania supports. The increased activities had to be attributed to the more number of reduced cobalt metal surface atoms for catalyzing the reaction.

6.2 Recommendations for future studies

From the previous conclusions, the following recommendations for future studies are proposed.

1. Quenching of titania by others quenching media, e.g. acid-base solution, oil, or polymer solution should be studied and should be tested as catalyst and catalyst support.

2. For Co catalyst, the metal dispersion and reducibility of samples should be further investigated in order to get more information about effect of quenching processes on catalytic activity of catalyst.



สถาบันวิทยบริการ
จุฬาลงกรณ์มหาวิทยาลัย

REFERENCES

- Anderson, R.B. The Fischer–Tropsch Synthesis, first ed., Academic Press, Orlando, 1984.
- Amama, P.B., Itoh, K., Murabayashi, M. Gas-phase photocatalytic degradation of trichloroethylene on pretreated TiO₂, Appl. Catal. B: Environ. 37 (2002): 321–330.
- Amiridis, M.D., Duevel, R.V., Wachs, I.E. The effect of metal oxide additives on the activity of V₂O₅/TiO₂ catalysts for the selective catalytic reduction of nitric oxide by ammonia. Appl. Catal. B: Environ. 20 (1999): 111-122.
- Bastl, Z., Senkevich, A.I., Spirovova, I., Vrtilkova, V. Angle-resolved core-level spectroscopy of Zr1Nb alloy oxidation by oxygen, water and hydrogen peroxide. Surf. Interface Anal. 34 (2002): 477-480.
- Blanco, J., Alvarez, E., Knapp, C. Control dioxin emissions from combustion processes Chemical Engineering. 106 (1997): 149-150
- Blount, M.C. and Falconer, J.L. Characterization of Adsorbed Species on TiO₂ after Photocatalytic Oxidation of Toluene. J. Catal. 200 (2001): 21-33.
- Bosman, H.J.M., Pijpers, A.P., Jaspers, A.W.M.A. An X-Ray Photoelectron Spectroscopy Study of the Acidity of SiO₂–ZrO₂ Mixed Oxides. J. Catal. 161 (1996): 551-559.
- Boyer, H. E., Quenching and Control of Distortion.ASM International, Ohio, 1988.
- Busca, G. And Larrubia, M.A. An FT-IR study of the conversion of 2-chloropropane, o-dichlorobenzene and dibenzofuran on V₂O₅-MoO₃-TiO₂ SCR-DeNO_x catalysts. Appl.Catal.B:Environ. 39 (2002): 343-352.
- Carp, O., Huisman, C.L., Reller, A. Photoinduced reactivity of titanium dioxide. Prog. Solid State Chem. 32 (2004): 33–177.
- Cheng, P., Zheng, M., Jin, Y., Huang Q., Gu, M. Preparation and characterization of silica-doped titania photocatalyst through sol–gel method. Mater. Lett. 57 (2003): 2989-2994.

- Chun, S.W., Jang, J.Y., Park, D.W., Woo, H.C., Chung, J.S. Selective oxidation of H₂S to elemental sulfur over TiO₂/SiO₂ catalysts. Appl. Catal. B: Environ. 16 (1998): 235-243
- Corma, A., Martínez, A., Martínez, C. The effect of sulfation conditions and activation temperature of sulfate-doped ZrO₂, TiO₂ and SnO₂ catalysts during isobutane/2-butene alkylation. Appl. Catal. A: Gen. 144 (1996): 249–268.
- Diebold, U. The surface science of titanium dioxide. Surf. Sci. Rep. 48 (2003): 53-229.
- Ohtani, B., Ogawa, Y., Nishimoto, S.-i. Photocatalytic Activity of Amorphous-Anatase Mixture of Titanium(IV) Oxide Particles Suspended in Aqueous Solutions. J. Phys. Chem. B. 101 (1997): 3746-3752.
- Fan, L., Ichikuni, N., Shimazu, S., Uematsu, T. Preparation of Au/TiO₂ catalysts by suspension spray reaction method and their catalytic property for CO oxidation. Appl. Catal. A: Gen. 246 (2003): 87-95.
- Fox, M. A. and Dulay, M. T. Heterogeneous Photocatalysis. Chem. Rev. 93 (1993): 341 – 357.
- Fujishima, A., Hashimoto, K., Watanabe, T. TiO₂ Photocatalysis Fundamental and Applications. 1st ed. Tokyo: BKC, 1999.
- Hirano, M., Nakahara, C., Ota, K., Inagaki, M. Direct Formation of Zirconia-Doped Titania with Stable Anatase-Type Structure by Thermal Hydrolysis. J. Am. Ceram. Soc. 85, 5 (2002): 1333 – 1335.
- Hirano, M., Nakahara, C., Ota, K., Tanaike, O., Inagaki, M. Photoactivity and phase stability of ZrO₂-doped anatase-type TiO₂ directly formed as nanometer-sized particles by hydrolysis under hydrothermal conditions. J. Solid State Chem. 170 (2003): 39–47.
- Henderson, M.A. An HREELS and TPD study of water on TiO₂ (110): the extent of molecular versus dissociative adsorption. Surf. Sci. 355 (1996): 151–166.
- Hoffmann, M.R., Martin, S.T., Choi, W., Bahnemann, D.W. Environmental Applications of Semiconductor Photocatalysis. Chem. Rev. 95 (1995): 69- 96.
- Hu, S. and Apple, T.M. ¹⁵N NMR Study of the Adsorption of NO and NH₃ on Titania-Supported Vanadia Catalysts. J. Catal. 158 (1996): 199-204.

- Inoue, M., Sato, K., Nakamura, T., Inui, T. Glycothermal synthesis of zirconia–rare earth oxide solid solutions. Chem. Lett. 65 (2000): 79-83.
- Iwamoto, S., Tanakulrungsank, W., Inoue, M., Kagawa, K., Prasertthdam, P. Synthesis of large-surface area silica-modified titania ultrafine particles by the glycothermal method. J. Mater. Sci. Lett. 19 (2000): 1439-1443.
- Jongsomjit, B., Sakdamnusun, C., Goodwin, J.G., Prasertthdam, P. Co-support compound formation in titania-supported cobalt catalyst. Cata. Lett. 94 (2004): 209-215.
- Jung, K.Y. and Park, S.B. Enhanced Photocatalytic of Silica-Embedded Titania Particles Prepared by Sol-Gel Process for the Decomposition of Trichloroethylene. Appl. Catal. B: Environ. 25 (1999): 249-256.
- Kaluža, L., Gulková, D., Vít, Z., Zdražil M. Effect of support type on the magnitude of synergism and promotion in CoMo sulphide hydrodesulphurisation catalyst. Appl Catal A: Gen. 324 (2007): 30-35.
- Kamat, P. V. and Dimitrijevic, N. M. Colloidal Semiconductors as Photocatalysts for Solar Energy Conversion. Sol. Energy 44 (1990): 83-98.
- Kim, C.-S., Moon, B. K., Park, J.-H., Chung, S.T., Son, S.-M. Synthesis of nanocrystalline TiO₂ in toluene by a solvothermal route. J. Cryst. Growth. 254 (2003): 405-410.
- Kominami, H., Kohno, M., Takada, Y., Inoue, M., Inui, T., Kera, Hydrothermal of Titanium Alkoxide in Organic Solvent at High Temperatures: A New Synthetic Method for Nanosized, Thermally Stable Titanium (IV) Oxide. Ind. Eng. Chem. Res. 38 (1999): 3925-3931.
- Kumar, P.M., Badrinarayanan, S., Sastry, M. Nanocrystalline TiO₂ studied by optical, FTIR and X-ray photoelectron spectroscopy: correlation to presence of surface states. Thin Sol. Films. 358 (2000): 122–130.
- Larson, S. A. and Falconer, J. L. Characterization of TiO₂ Photocatalysts Used in Trichloroethene Oxidation. Appl. Catal. B: Environ. 4 (1994): 325 – 342.
- Li, J., Jacobs, G., Das, T., Davis, B.H. Fischer–Tropsch synthesis: effect of water on the catalytic properties of a ruthenium promoted Co/TiO₂ catalyst. Appl Catal A: Gen. 233 (2002): 255-262.

- Linsebigler, A.L., Lu, G., Yates Jr, J.T. Photocatalysis on TiO₂ surfaces: principles, mechanisms, and selected results. Chem. Rev. 95 (1995): 735–758.
- Liu, H., Ma, H.T., Li, X.Z., Li, W.Z., Wu, M., Bao, X.H. The enhancement of TiO₂ photocatalytic activity by hydrogen thermal treatment. Chemosphere. 50 (2003): 39–46.
- Lukáč, J., Klementová, M., Bezdička, P., Bakardjieva, S., Šubrt, J., Szatmáry, L., Bastl, Z., Jirkovský, J. Influence of Zr as TiO₂ doping ion on photocatalytic degradation of 4-chlorophenol. Appl. Catal. B: Environ. 74 (2007): 83-91
- Maira, A.J., Yeung, K.L., Lee, C.Y., Yue, P.L., Chan, C.K. Size effects in gas-phase photo-oxidation of trichloroethylene using nanometer-sized TiO₂ catalysts. J. Catal. 192 (2000): 185-196.
- Marinas, J.M., Colmenares, J.C., Aramendía, M.A., Marinas, A., Urbano, F.J. Synthesis, characterization and photocatalytic activity of different metal-doped titania systems. Appl. Catal. A: Gen. 306 (2006): 120-127
- Matsuda, S.; Kato, A. Titanium Oxide Based Catalysts-a Review. Appl. Catal. 8 (1983): 149.
- Matsumoto, Y., Murakami, M., Shono, T., Hasegawa, T., Fukumura, T., Kawasaki, M., Ahmet, P., Chikyow, T., Koshihara, S.-Y., Koinuma, H. Room-temperature ferromagnetism in transparent transition metal-doped titanium dioxide. Science. 291 (2001): 854-856.
- Morrison Jr., P.W., Raghavan, R., Timpone, A.J., Artelt, C.P., Pratsinis, S.E. In Situ Fourier Transform Infrared Characterization of the Effect of Electrical Fields on the Flame Synthesis of TiO₂ Particles. Chem. Mater. 9 (1997): 2702-2708.
- Mukhopadhyay, S. and Garofalini, S. Surface studies of TiO₂-SiO₂ glasses by X-ray photoelectron spectroscopy. J. Non-Cryst. Solids. 126 (1990): 202-208.
- Nakaoka, Y., Nosaka, Y. ESR Investigation into the effects of heat treatment and crystal structure on radicals produced over irradiated TiO₂ powder. J.Photochem. Photobiol. A: Chem. 110 (1997): 299.
- Park, D.-R., Zhang, J., Ikeue, K., Yamashita, H., Anpo, M. Photocatalytic oxidation of ethylene to CO₂ and H₂O on ultrafine powdered TiO₂ photocatalysts in the presence of O₂ and H₂O. J. Catal. 185 (1999): 114–119.

- Payakgul, W., Mekasuwandumrong, O., Pavarajarn, V., Praserttham, P. Effects of reaction medium on the synthesis of TiO₂ nanocrystals by thermal decomposition of titanium(IV) *n*-butoxide. Ceram. Int. 31 (2005): 391–397.
- Pouilleau, J., Devilliers, D., Groult, H., Marcus, P. Surface study of a titanium based ceramic electrode material by X-ray photoelectron spectroscopy. J. Mater. Sci. 32 (1997): 5645–5651.
- Rusu, C.N. and Yates Jr., J.T. Defect sites on TiO₂ (110) Detection by O₂ photodesorption. Langmuir. 13 (1997): 4311-4316.
- Sandoval, A., Gómez-Cortés, A., Zanella, R., Díaz, G., Saniger, J.M. Gold nanoparticles: Support effects for the WGS reaction. J. Mol. Catal. A-Chem. 278 (2007): 200-208.
- Sirisuk, A., Hill, C.G., Anderson, M.A. Photocatalytic degradation of ethylene over thin films of titania supported on glass rings. Catal. Today. 54 (1999): 159-164
- Sornnarong Theinkeaw. Synthesis of Large-Surface Area Silica Modified Titanium (IV) Oxide Ultra Fine Particles. Master's thesis, Department of Chemical Engineering, Graduated School, Chulalongkorn University, 2000.
- Serpone, N. Relative photonic efficiencies and quantum yields in heterogeneous photocatalysis. J. Photochem. Photobiol. A: Chem. 104 (1997): 1-12.
- Shklover, V., Nazeeruddin, M.-K., Zakeeruddin, S.M., Barbé, C., Kay, A., Haibach, T., Steurer, W., Hermann, R., Nissen, H.-U., Grätzel, M. Structure of Nanocrystalline TiO₂ Powders and Precursor to Their Highly Efficient Photosensitizer. Chem. Mater. 9 (1997): 430-439.
- Thompson, T.L., Diwald, O., Yates Jr., J.T. CO₂ as a probe for monitoring the surface defects on TiO₂ (110)-temperature-programmed desorption. J. Phys. Chem. B. 107 (2003): 11700–11704.
- Torimoto, T., Fox III, R.J., Fox, M.A. Photoelectrochemical doping of TiO₂ particles and the effect of charge carrier density on the photocatalytic activity of microporous semiconductor electrode films. J. Electrochem. Soc. 143 (1996): 3712-3717.
- Turchi, C. S., Ollis, D. F. Mixed Reactant Photocatalysis: Intermediates and Mutual Rate Inhibition. J. Catal. 119 (1990): 483-487.

- Watson, S.S., Beydoun, D., Scott, J.A., Amal, R. The effect of preparation method on the photoactivity of crystalline titanium dioxide particles. Chem. Eng. J. 95 (2003): 213–220.
- Wiwattanapongpan, J., Mekasuwandumrong, O., Chaisuk, C., Praserttham, P. Effect of dopants on the properties of metal-doped zirconia prepared by the glycothermal method. Ceram. Int. 33, (2007): 1469-1473.
- Xu, N.P., Shi, Z.F., Fan, Y.Q., Dong, J.H., Shi, J., Hu, M.Z.C. Effects of particle size of TiO₂ on photocatalytic degradation of methylene blue in aqueous suspensions, Ind. Eng. Chem. Res 38 (1999): 373–379.
- Yamazaki, S., Tanaka, S., Tsukamoto, H. Kinetic studies of oxidation of ethylene over a TiO₂ photocatalyst. J. Photochem. Photobiol. A: Chem. 121 (1999): 55–61.
- Young, R.S. COBALT: Its Chemistry, Metallurgy, and Uses. New York: Reinhold Publishing Corporation, 1960.
- Yu, J.C., Yu, J., Ho, W., Jiang, Z., Zhang, L. Effects of F-doping on the photocatalytic activity and microstructures of nanocrystalline TiO₂ powders. Chem. Mater. 14 (2002): 3808–3816.
- Zaharescu, M., Crisan, M., Simionescu, L., Crisan, D., Gartner, M. TiO₂-Based Porous Materials obtained from Gels, in Different Experimental Conditions. J. Sol-Gel Sci. 8 (1997): 249-253.
- Zhang, H., Banfield, J.F. Understanding polymorphic phase transformation behavior during growth of nanocrystalline aggregates: Insights from TiO₂. J. Phys. Chem. B. 104 (2000): 3481-3487.



APPENDICES

สถาบันวิทยบริการ
จุฬาลงกรณ์มหาวิทยาลัย

APPENDIX A

CALCULATION FOR CATALYST PREPARATION

Preparation of TiO₂ nanocrystal via solvothermal method are shown as follows

- Reagent:
- Titanium (IV) *n*-butoxide Molecular weight = 340.96
 - Zirconium (IV) *n*-butoxide Molecular weight = 383.7
 - Tetraethylorthosilicate Molecular weight = 208.33

Calculation for the preparation of metal-doped TiO₂ via solvothermal method

Zr-doped TiO₂

$$\text{Zr/Ti} = 0.002$$

Titanium (IV) *n*-butoxide 25 g were used for preparation catalyst.

Titanium (IV) *n*-butoxide 25 g consisted of titanium equal to:

$$\begin{aligned} \text{Titanium} &= \frac{25}{340.96} \times (47.88) \text{ g} \\ &= 3.51 \text{ g} \\ &= \frac{1.9815}{47.88} \text{ mol} \\ &= 0.07344 \text{ mol} \end{aligned}$$

For Zr/Ti = 0.002, 0.07344 mole of titanium

$$\begin{aligned} \text{Zirconium required} &= 0.07344 \times 0.002 \text{ mol} \\ &= 0.00015 \text{ mol} \\ &= 0.00015 \times 91.22 \text{ g} \\ &= 0.0136 \text{ g} \end{aligned}$$

Zirconium 0.0136 g was prepared from zirconium (IV) *n*-butoxide

$$= \frac{0.0136}{91.22} \times 383.7 \text{ g} = 0.057 \text{ g}$$

Si-doped TiO₂

$$\text{Si/Ti} = 0.002$$

Titanium (IV) n-butoxide 25 g were used for preparation catalyst.

Titanium (IV) n-butoxide 25 g consisted of titanium equal to:

$$\begin{aligned} \text{Titanium} &= \frac{25}{340.96} \times (47.88) \text{ g} \\ &= 3.51 \text{ g} \\ &= \frac{1.9815}{47.88} \text{ mol} \\ &= 0.07344 \text{ mol} \end{aligned}$$

For Si/Ti = 0.002, 0.07344 mole of titanium

$$\begin{aligned} \text{Silica required} &= 0.07344 \times 0.002 \text{ mol} \\ &= 0.00015 \text{ mol} \\ &= 0.00015 \times 28.08 \text{ g} \\ &= 0.0042 \text{ g} \end{aligned}$$

Silica 0.0136 g was prepared from tetraethylorthosilicate

$$= \frac{0.0042}{28.08} \times 208.33 \text{ g} = 0.031 \text{ g}$$

Calculation for the preparation of cobalt loading catalyst (20%Co/ TiO₂)

Base on 100 g of atalyst used, the composition of the catalyst will be as follow:

$$\begin{aligned} \text{Cobalt} &= 20 \text{ g} \\ \text{TiO}_2 &= 100-20 = 80 \text{ g} \end{aligned}$$

For 5 g of TiO₂

$$\text{Cobalt required} = 5 \times (20/80) = 1.25 \text{ g}$$

Cobalt 1.25 g was prepared from (Co(NO₃)₂×6H₂O) and molecular weight of Co is 58.59

$$\begin{aligned} \text{Co(NO}_3)_2 \times 6\text{H}_2\text{O} &= [\text{MW of Co(NO}_3)_2 \times 6\text{H}_2\text{O} \times \text{cobalt required}] / \text{MW of Co} \\ &= (290.93/58.93) \times 1.25 = 6.17 \text{ g} \end{aligned}$$

APPENDIX B

CALCULATION OF THE CRYSTALLITE SIZE

Calculation of the crystallite size by Debye-Scherrer equation

The crystallite size was calculated from the width at half-height of the diffraction peak of XRD pattern using the Debye-Scherrer equation.

From Scherrer equation:

$$D = \frac{K\lambda}{\beta \cos \theta} \quad (\text{A.1})$$

- where
- D = Crystallite size, Å
 - K = Crystallite-shape factor = 0.9
 - λ = X-ray wavelength, 1.5418 Å for CuK α
 - θ = Observed peak angle, degree
 - β = X-ray diffraction broadening, radian

The X-ray diffraction broadening (β) is the pure width of a powder diffraction, free of all broadening due to the experimental equipment. Standard α -alumina is used to observe the instrumental broadening since its crystallite size is larger than 2000 Å. The X-ray diffraction broadening (β) can be obtained by using Warren's formula.

From Warren's formula:

$$\beta^2 = B_M^2 - B_S^2 \quad (\text{A.2})$$

$$\beta = \sqrt{B_M^2 - B_S^2}$$

- Where
- B_M = The measured peak width in radians at half peak height.
 - B_S = The corresponding width of a standard material.

Example: Calculation of the crystallite size of titania

$$\begin{aligned} \text{The half-height width of 101 diffraction peak} &= 0.93125^\circ \\ &= 0.01625 \text{ radian} \end{aligned}$$

$$\text{The corresponding half-height width of peak of } \alpha\text{-alumina} = 0.004 \text{ radian}$$

$$\begin{aligned} \text{The pure width} &= \sqrt{B_M^2 - B_S^2} \\ &= \sqrt{0.01625^2 - 0.004^2} \\ &= 0.01577 \text{ radian} \end{aligned}$$

$$\beta = 0.01577 \text{ radian}$$

$$2\theta = 25.56^\circ$$

$$\theta = 12.78^\circ$$

$$\lambda = 1.5418 \text{ \AA}$$

$$\begin{aligned} \text{The crystallite size} &= \frac{0.9 \times 1.5418}{0.01577 \cos 12.78} = 90.15 \text{ \AA} \\ &= 9 \text{ nm} \end{aligned}$$

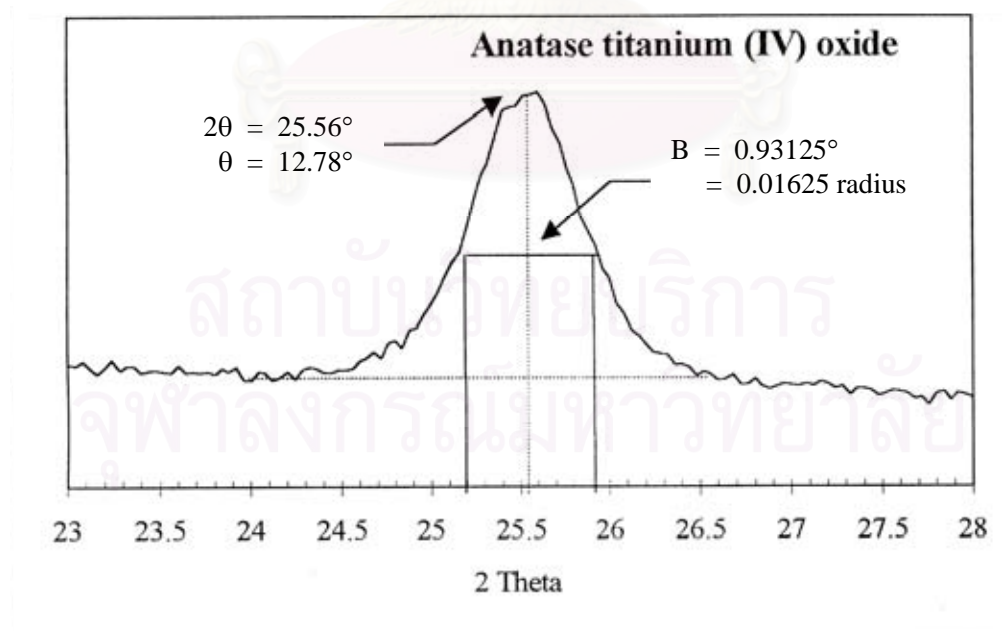


Figure A.1 The 101 diffraction peak of titania for calculation of the crystallite size

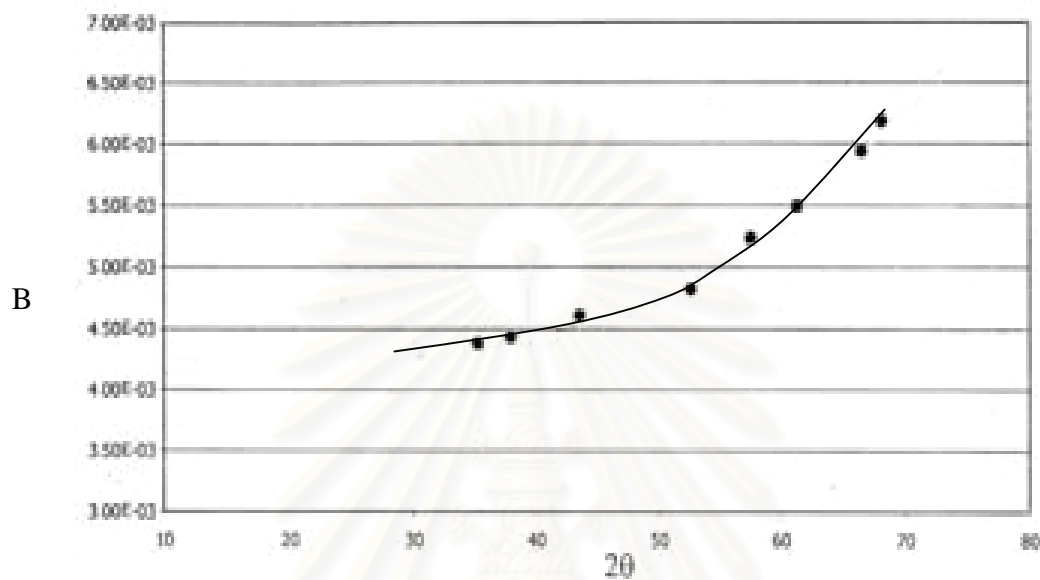


Figure A.2 The plot indicating the value of line broadening due to the equipment. The data were obtained by using α -alumina as standard.

สถาบันวิทยบริการ
จุฬาลงกรณ์มหาวิทยาลัย

APPENDIX C

CALCULATION FOR TOTAL H₂ CHEMISSORPTION

Calculation of the total H₂ chemisorption and metal dispersion of the catalyst, a stoichiometry of H/Co = 1, measured by H₂ chemisorption is as follows:

Let the weight of catalyst used	=	W	g
Integral area of H ₂ peak after adsorption	=	A	unit
Integral area of 45 μ l of standard H ₂ peak	=	B	unit
Amounts of H ₂ adsorbed on catalyst	=	B-A	unit
Volume of H ₂ adsorbed on catalyst	=	$45 \times [(B - A) / B]$	μ l
Volume of 1 mole of H ₂ at 100°C	=	28.038	μ l
Mole of H ₂ adsorbed on catalyst	=	$[(B - A) / B] \times [45 / 28.038]$	μ mole

$$\begin{aligned} \text{Total H}_2 \text{ chemisorption} &= [(B - A) / B] \times [45 / 28.038] \times [1 / W] \mu\text{mole/g of catalyst} \\ &= N \mu\text{mole/g of catalyst} \end{aligned}$$

สถาบันวิทยบริการ
จุฬาลงกรณ์มหาวิทยาลัย

APPENDIX D

THE OPERATING CONDITIONS OF GAS CHROMATOGRAPHY AND CALIBRATION CURVES

For Photocatalytic Reaction

The composition of hydrocarbons in the product stream was analyzed by a Shimadzu GC14B gas chromatograph equipped with a flame ionization detector. The operating conditions for each instrument are shown in the Table D.1.

Table D.1 The operating condition for gas chromatograph.

Gas Chromagroph	SHIMADZU GC-14B
Detector	FID
Column	VZ10
Carrier gas	H ₂ (99.999%)
Carrier gas flow (ml/min)	30 cc/min
Column temperature	
- initial (°C)	70
- final (°C)	70
Injector temperature (°C)	100
Detector temperature (°C)	150
Current (mA)	-
Analysed gas	Hydrocarbon C ₁ -C ₄

The calibration curves for calculation of composition of reactant in photocatalytic reaction. The reactant is ethylene.

The VZ10 column are used with a gas chromatography equipped with a flame ionization detector, Shimadzu modal 14B, to analyze the concentration of products including of ethylene.

Mole of reagent in y-axis and area reported by gas chromatography in x-axis are exhibited in the curves. The calibration curves of ethylene is illustrated in the following figure.

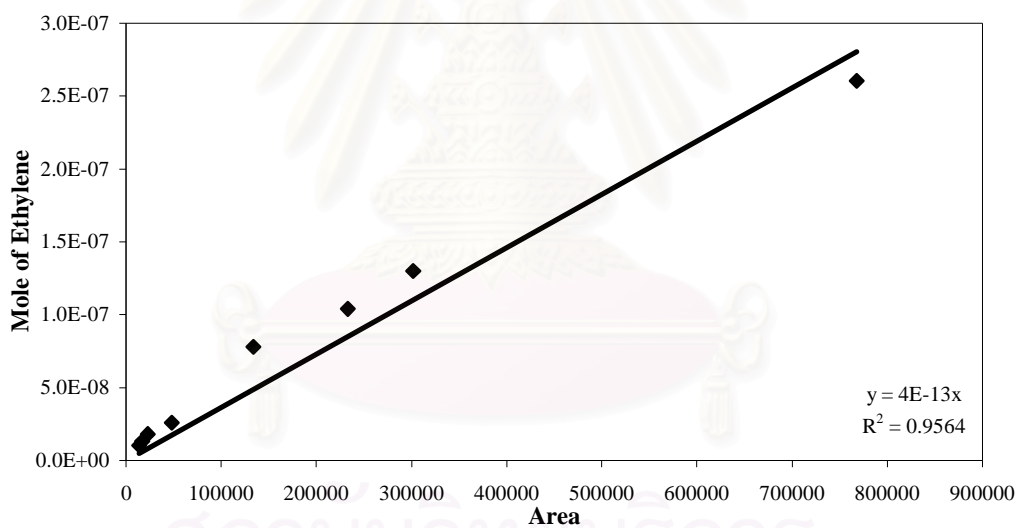


Figure D.1 The calibration curve of ethylene.

For CO Hydrogenation Reaction

This appendix showed the calibration curves for calculation of composition of reactant and products in CO hydrogenation reaction. The reactant is CO and the main product is methane. The other products are linear hydrocarbons of heavier molecular weight that are C₂-C₄ such as ethane, ethylene, propane, propylene and butane.

The thermal conductivity detector, gas chromatography Shimadzu model 8A was used to analyze the concentration of CO by using Molecular sieve 5A column.

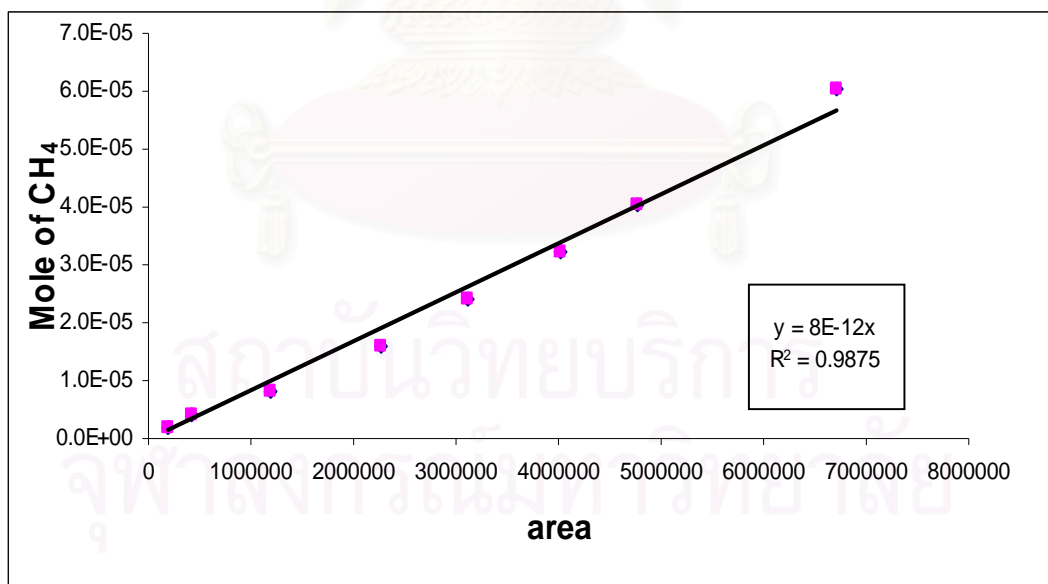
The VZ10 column are used with a gas chromatography equipped with a flame ionization detector, Shimadzu model 14B, to analyze the concentration of products including of methane, ethane, ethylene, propane, propylene and butane. Conditions uses in both GC are illustrated in Table D.2.

Mole of reagent in y-axis and area reported by gas chromatography in x-axis are exhibited in the curves. The calibration curves of CO, methane, ethane, ethylene, propane, propylene and butane are illustrated in the following figures.

สถาบันวิทยบริการ
จุฬาลงกรณ์มหาวิทยาลัย

Table D.2 Conditions use in Shimadzu modal GC-8A and GC-14B.

Parameters	Condition	
	Shimadzu GC-8A	Shimadzu GC-14B
Width	5	5
Slope	50	50
Drift	0	0
Min. area	10	10
T.DBL	0	0
Stop time	50	60
Atten	0	0
Speed	2	2
Method	41	41
Format	1	1
SPL.WT	100	100
IS.WT	1	1

**Figure D.2** The calibration curve of methane.

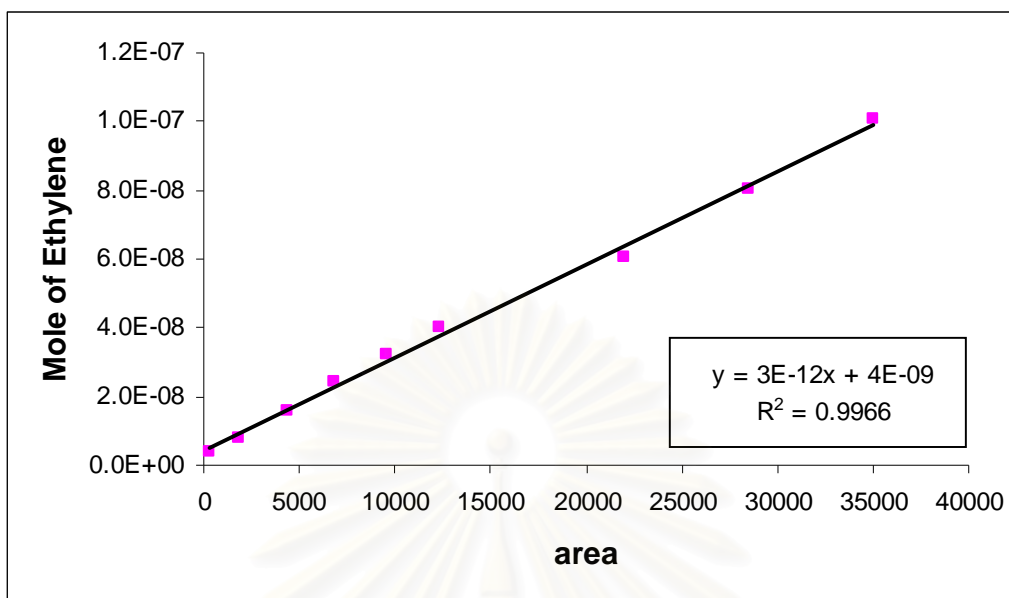


Figure D.3 The calibration curve of ethylene.

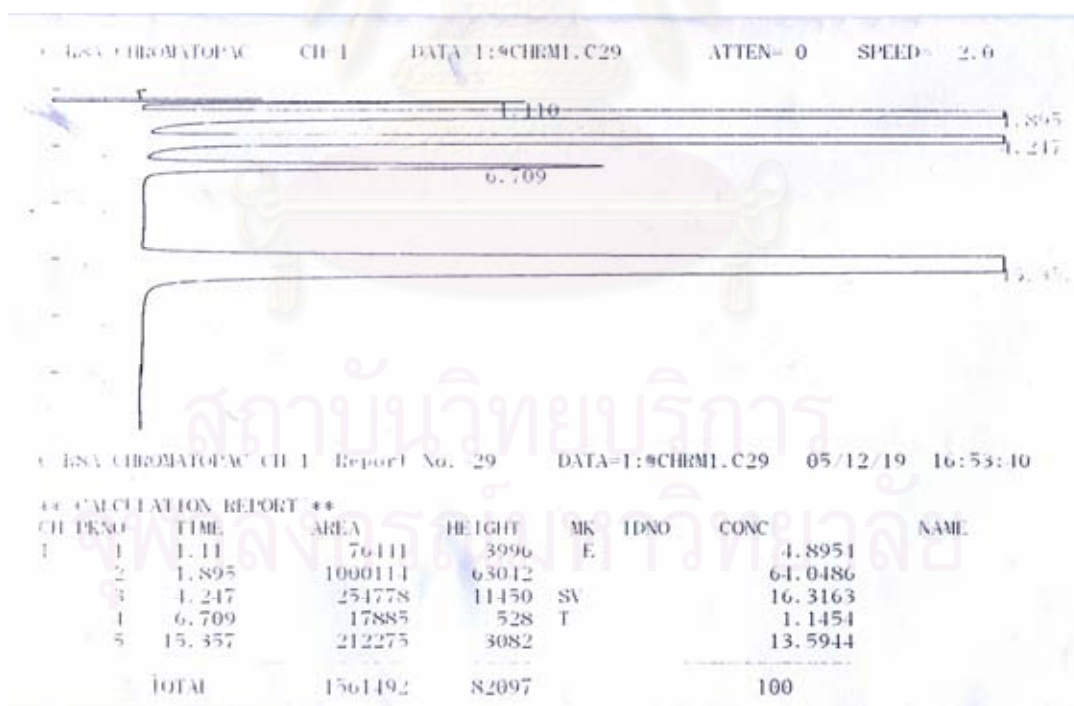


Figure D.4 The chromatograms of catalyst sample from thermal conductivity detector, gas chromatography Shimadzu model 8A (Molecular sieve 5A column).

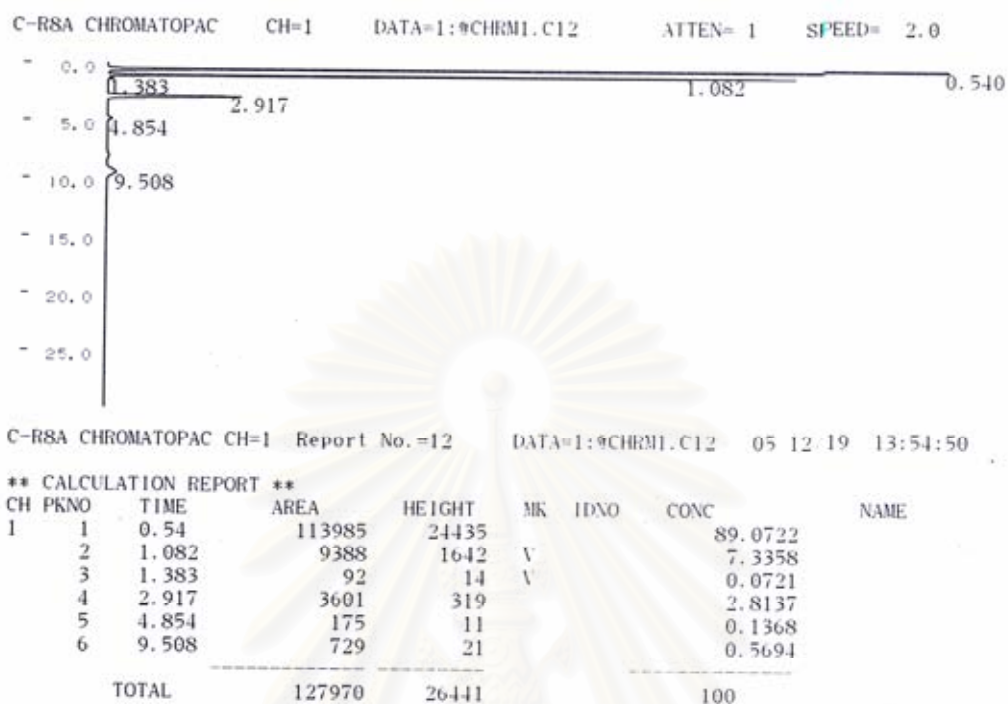


Figure D.5 The chromatograms of catalyst sample from flame ionization detector, gas chromatography Shimadzu model 14B (VZ10 column).

สถาบันวิทยบริการ
จุฬาลงกรณ์มหาวิทยาลัย

APPENDIX E

CALCULATION OF CO CONVERSION REACTION RATE AND SELECTIVITY

The catalyst performance for the CO hydrogenation was evaluated in term of activity for CO conversion, reaction rate and selectivity.

CO conversion is defined as moles of CO converted with respect to CO in feed:

$$\text{CO conversion (\%)} = \frac{100 \times [\text{mole of CO in feed} - \text{mole of CO in product}]}{\text{mole of CO in feed}} \quad (\text{i})$$

Reaction rate was calculated from CO conversion that is as follows:

Let the weight of catalyst used	=	W	g
Flow rate of CO	=	2	cc/min
Reaction time	=	60	min
Weight of CH ₂	=	14	g
Volume of 1 mole of gas at 1 atm	=	22400	cc

$$\text{Reaction rate (g CH}_2\text{/g of catalyst/h)} = \frac{[\% \text{ conversion of CO}/100] \times 60 \times 14 \times 2}{W \times 22400} \quad (\text{ii})$$

Selectivity of product is defined as mole of product (B) formed with respect to mole of CO converted:

$$\text{Selectivity of B (\%)} = 100 \times [\text{mole of B formed} / \text{mole of total products}] \quad (\text{iii})$$

Where B is product, mole of B can be measured employing the calibration curve of products such as methane, ethane, ethylene, propane, propylene and butane

$$\text{mole of CH}_4 = (\text{area of CH}_4 \text{ peak from integrator plpt on GC-14B}) \times 8 \times 10^{12} \quad (\text{iv})$$

APPENDIX F

LIST OF PUBLICATIONS

- **Proceeding**

1. Piyawat Supphasrirongjaroen, Piyasan Praserthdam and Joongjai Panpranot, "Surface Modification of Nano-Sized TiO₂ by Quenching Processes for Enhancement of Photocatalytic Activity", Proceeding of the 13th Regional Symposium on Chemical Engineering "Advances in Chemical and Biomolecular Engineering", Singapore, 3-5 December, 2006.

2. Piyawat Supphasrirongjaroen, Piyasan Praserthdam "Effect of quenching medium on photocatalytic activity of nano-sized TiO₂ synthesized by solvothermal method", Poster presentation of the 17th International Congress of Chemical and Process Engineering (CHISA 2006), Prague, Czech Republic, 27-31 August, 2006.

- **International Papers**

1. Supphasrirongjaroen, P., Praserthdam, P., Panpranot J., Na-Ranong, D., Mekasuwandumrong, O. Effect of quenching medium on photocatalytic activity of nano-TiO₂ prepared by solvothermal method Chem.Eng. J. 138 (2008) 622-627

2. Supphasrirongjaroen, P., Kongsuebchart, W., Panpranot, J., Mekasuwandumrong, O., Satayaprasert, C., Praserthdam, P. Dependence of Quenching Process on the Photocatalytic Activity of Solvothermal-Derived TiO₂ with Various Crystallite Sizes. Ind. Eng. Chem. Res. 47 (2008) 693-697.



Effect of quenching medium on photocatalytic activity of nano-TiO₂ prepared by solvothermal method

Piyawat Supphasirongjaroen^a, Piyasan Praserttham^{a,*}, Joongjai Panpranot^a, Duangkamol Na-Ranong^b, Okorn Mekasuwandumrong^c

^a Center of Excellence on Catalysis and Catalytic Reaction Engineering, Department of Chemical Engineering, Faculty of Engineering, Chulalongkorn University, Bangkok 10330, Thailand

^b Department of Chemical Engineering, Faculty of Engineering, King Mongkut's Institute of Technology Ladkrabang, Bangkok 10520, Thailand

^c Department of Chemical Engineering, Faculty of Engineering and Industrial Technology, Silpakorn University, Nakhonphatom 73000, Thailand

Received 19 April 2007; received in revised form 17 September 2007; accepted 21 September 2007

Abstract

Pure anatase nano-TiO₂ powders were synthesized by solvothermal method using titanium butoxide as the precursor and were subjected to a rapid quenching in various media such as H₂O, H₂O₂, air, and liquid N₂ as a post-synthesis treatment. By creating a thermal shock effect, quenching process has shown to be an easy novel route for modifying surface defects of the nano-TiO₂ and its photocatalytic activity. In this study, the TiO₂ sample quenched in air at 77 K contained the highest amount of Ti³⁺ surface defect with the highest Ti³⁺/OH and was found to exhibit the highest photocatalytic activity for ethylene decomposition.

© 2007 Elsevier B.V. All rights reserved.

Keywords: Titanium dioxide; TiO₂; Photocatalyst; Solvothermal; Ethylene decomposition; Quenching; Defects

1. Introduction

Nanoparticle TiO₂ semiconductor is a very useful material and has been employed in various fields such as solar cells, photocatalytic splitting of water for green-energy hydrogen production, selective synthesis of organic compounds, air purification, removal of organic and inorganic pollutants, and photokilling of pathogenic organisms [1–4]. In general, when TiO₂ nanoparticles adsorb light (wavelength smaller than 385 nm), the valence band electron jumps through the band gap to the conduction band, leaving a positive hole in valence band, and generating an electron–hole pair. These pairs are able to initiate redox reactions to destroy the organic species adsorbed on the TiO₂ surfaces. The photocatalytic activity of TiO₂ strongly depends on preparation methods and post-treatment conditions since they have a decisive influence on crystal phase and size,

specific surface area, pore–wall structure, as well as the surface properties, particularly surface defect, of the TiO₂ [5,6].

Various techniques have been reported for the preparation of nano-TiO₂ such as solvothermal method [7–10], precipitation method [11], sol–gel method [12–14], chemical vapor deposition [15], and thermal decomposition of alkoxide [16]. The sol–gel method is an easy method but the precipitated powders obtained are amorphous in nature and further heat treatment is required for crystallization. Solvothermal method is an alternative route for direct (one-step) synthesis of pure anatase nano-TiO₂. Particle morphology, crystalline phase, and surface chemistry of the solvothermal-derived TiO₂ can be controlled by regulating precursor composition, reaction temperature, pressure, solvent property, and aging time.

In order to improve the photocatalytic activity of TiO₂ under UV light region, different methods have been studied such as ion implantation [17], doping with transition metals [18,19], the use of two semiconductors composite [20], sulfation [21,22], reduction with hydrogen [23], halogenation, [24] and the creation of surface defect [25]. However, most of the improvement meth-

* Corresponding author. Tel.: +66 2 218 6766; fax: +66 2 218 6769.
E-mail address: piyasan.p@chula.ac.th (P. Praserttham).

ods reported in the literature are time-consuming, high cost, and rather complicated.

In this study, quenching process has been applied as a post-synthesis treatment for enhancement of photocatalytic activity of nano-TiO₂ synthesized by solvothermal method. Quenching is defined as the mechanism of “rapid cooling” of material (cooling from a relatively high temperature to a fairly low temperature in a short period of time). The process of annealing or quenching has shown to result in a variety of surface defects, strains, and reconstructions of materials [26]. The effects of quenching medium (liquid N₂, H₂O, H₂O₂, and air) and quenching temperature on physicochemical properties of the nano-TiO₂ synthesized by solvothermal method were investigated in details using X-ray diffraction (XRD), X-ray photoelectron spectroscopy (XPS), N₂ physisorption, and CO₂ temperature programmed desorption. The photocatalytic activity of the TiO₂ nanoparticles was evaluated in the gas-phase decomposition of ethylene under UV irradiation.

2. Experimental

2.1. Preparation of nano-TiO₂

Nanocrystalline TiO₂ was prepared using the solvothermal method in the same manner as that of Payakgul et al. [27]. Titanium(IV) *n*-butoxide (purity 97%, Aldrich) was used as the starting material. Approximately 25 g of titanium *n*-butoxide was suspended in 100 ml of toluene, in a test tube, which was then placed in a 300 ml autoclave. The same solvent was filled in the gap between the test tube and the autoclave wall. The autoclave was purged completely by nitrogen after that it was heated up to the desired temperature at 573 K with the rate of 2.5 K/min. The temperature of the autoclave was held constant at 573 K for 2 h and then cooled down to room temperature. The obtained TiO₂ was washed by methanol for several times and finally dried in air.

2.2. Quenching treatment

Prior to quenching, the synthesized TiO₂ was dried in air atmosphere at 573 K with a heating rate of 10 K/min for 1 h and then it was taken out and immediately quenched in various quenching media. In this study, both liquid phase and gas-phase media were used. For quenching in liquid phase media, liquid nitrogen at 77 K (sample A), water at room temperature and 373 K (samples B and C), and hydrogen peroxide (30% wt, Merck) at room temperature and 373 K (samples D and E) were selected. For quenching in gas-phase media, air at room temperature and 77 K (samples F and G) were used. After the samples were quenched in selected media for 30 min, all samples were dried in air at room temperature and stored in a desiccator.

2.3. Catalyst characterization

The Brunauer–Emmett–Teller (BET) surface area (S_{BET}) was determined by nitrogen adsorption at 77 K in a Micromeritics Chemisorb 2750 automated system. All the samples were dried

at 150 °C for 30 min in a 30% N₂-helium flow prior to measurements. The X-ray diffraction (XRD) patterns of TiO₂ were recorded with an X-ray diffractometer (SIEMENS, D-5000) using Cu K α radiation with a Ni filter in the 2θ range from 20° to 80° with a scanning rate of 0.04°/min. The powder was contained in a flat holder. The average anatase crystallite diameter d_{Scherrer} was determined from half-height width of the 101 diffraction peak of anatase using the Scherrer equation. Temperature programmed desorption using CO₂ as a probe molecule (CO₂-TPD) was performed in order to determine the Ti³⁺ defective sites existing on the surface of TiO₂ particle [28]. Approximately 0.05 g of a TiO₂ sample was dosed by 1 vol.% CO₂ in helium for 1 h and then desorbed from 143 to 273 K with the rate of 21.5 K/min. The XPS measurement was carried out using an AMICUS photoelectron spectrometer equipped with an Mg K α X-ray as a primary excitation and KRATOS VISION2 software. XPS elemental spectra were acquired with 0.1 eV energy step at a pass energy of 75 kV. All the binding energies were referenced to the C 1s peak at 285 eV of the surface adventitious carbon. TEM images were obtained using the JEOL JEM 2010 transmission electron microscope that employed a LaB₆ electron gun in the voltage range of 80–200 kV with an optical point to point resolution of 0.23 nm.

2.4. Photocatalytic activity measurement

Photocatalytic decomposition of ethylene (C₂H₄) was used to as a model reaction to examine the photocatalytic activity of the synthesized TiO₂. Ethylene is harmful to all like forms, in order to keep enough food fresh in the CELSS (Controlled Ecological Life Support Systems), it is necessary to remove ethylene, which is released from plants. The complete photocatalytic oxidation of ethylene with oxygen into carbon dioxide and water has been achieved on ultrafine powdered TiO₂ photocatalysts [29]. All the experiments were carried out using horizontal quartz fixed bed reactor (i.d. 9 mm, length 60 cm). The weight of the catalyst was kept constant at 0.4 g. In order to avoid light penetration from outside, the reactor was placed in a closed stainless box at top of which a 500 W mercury lamp (Philips, HPL-N) was provided, emitting in the UV light region. Before exposure to the pollutant of interest, the photocatalyst sample is briefly cleaned by simultaneous exposure to UV and flowing air for 60 min [30]. Then, high purity grade air containing 0.1 vol.% ethylene was continuously fed at a constant flow rate with GHSV of 120 h⁻¹. The outlet gas was sampled every 30 min. Product compositions were analyzed using a SHIMADZU GC-14B gas chromatograph equipped with the flame ionized detector and a VZ-10 column, until the reaction reached steady-state.

3. Results and discussion

3.1. Characteristics of the nano-sized TiO₂

The properties of the solvothermal-derived nano-TiO₂ quenched in different media are given in Table 1. As shown by XRD results, all the nano-TiO₂ samples prepared by the solvothermal method in this study were anatase phase TiO₂ with

Table 1
Effects of quenching treatment on the physical properties and activities of TiO₂ samples synthesized by solvothermal method

Sample	Quenching medium	Crystallite size ^a (nm)	Specific surface area ^b (m ² /g)	Surface Ti ³⁺ (%)	Surface OH ⁻ (%)	Ratio Ti ³⁺ /OH	Ethylene conversion ^d (%)
A	Liquid N ₂	11	87	7.86	10.91	0.72	24.5
B	H ₂ O at RT	10	112	8.67	10.96	0.79	27.8
C	H ₂ O at 373 K	11	94	8.09	10.46	0.77	26.0
D	30% wt H ₂ O ₂ at RT	13	94	8.88	9.79	0.91	32.5
E	30% wt H ₂ O ₂ at 373 K	13	90	8.83	10.31	0.86	31.8
F	Air at RT	11	93	7.40	10.43	0.71	21.6
G	Air at 77 K	11	97	9.35	10.06	0.93	34.6

^a Determined using Scherrer's equation (applicable from 3 to 200 nm).

^b Determined using BET method.

^c Determined using XPS.

^d Photocatalytic reaction was carried out at 313–328 K, 1 bar, and 0.1% ethylene in air.

average crystallite size determined from the half-width of peaks using Scherrer's formula ($d = 0.9\lambda/\beta \cos \theta$) around 10–13 nm. The XRD patterns of the TiO₂ samples quenched in different media (air, hydrogen peroxide, water, and liquid N₂ at different temperatures) were not significantly different (Fig. 1); only the characteristic peaks of pure anatase phase TiO₂ were observed at $2\theta = 25.36^\circ$, 37.82° , 48.18° [31]. The specific surface areas of the TiO₂ samples were found to be 87–112 m²/g.

Fig. 2 shows transmission electron micrographs (TEM) and high resolution electron micrographs (HRTEM) for the as-prepared TiO₂ powders. The as-prepared powders consist of crystalline particles with primarily spheroidal shape with the size around 8–15 nm. The crystallite size calculated by Scherrer equation (11 nm) was in good agreement with size of the primary particle observed by TEM. It is revealed that each primary particle was a single crystal TiO₂.

The characteristics of surface adsorption sites of the TiO₂ samples were studied by means of temperature program desorption of CO₂ from 143 to 273 K. The results are shown in Fig. 3. All of the TiO₂ samples exhibited two main desorption peaks at 170 and 200 K which can be assigned to CO₂ molecules bonded to different adsorption sites on the surface. The first peak at ca. 170 K was assigned to Ti⁴⁺ sites (perfect TiO₂ structure) and the second one at 200 K was assigned to Ti³⁺ sites or defect TiO₂ structure [28]. The amounts of surface Ti³⁺

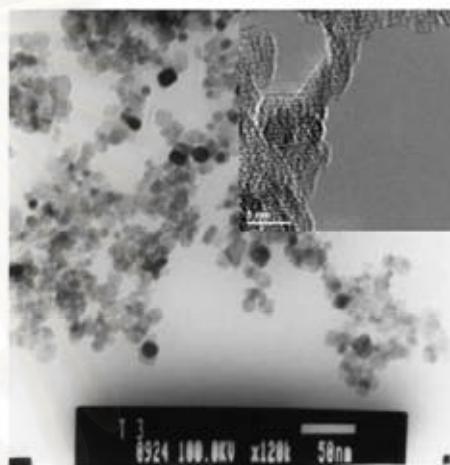


Fig. 2. TEM images of as-prepared TiO₂.

sites on the TiO₂ samples were observed from the areas under the Ti³⁺ TPD peaks and were found to be in the following order: air at 77 K > 30% H₂O₂ at RT > 30% H₂O₂ at 373 K > H₂O at RT > H₂O at 373 K > liquid N₂ > air at RT.

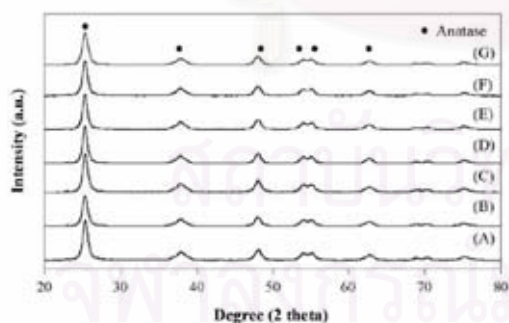


Fig. 1. The XRD patterns of the TiO₂ obtained from quenching in various media: (A) liquid N₂, (B) H₂O at RT, (C) H₂O at 373 K, (D) 30% H₂O₂ at RT, (E) 30% H₂O₂ at 373 K, (F) air at RT, and (G) air at 77 K.

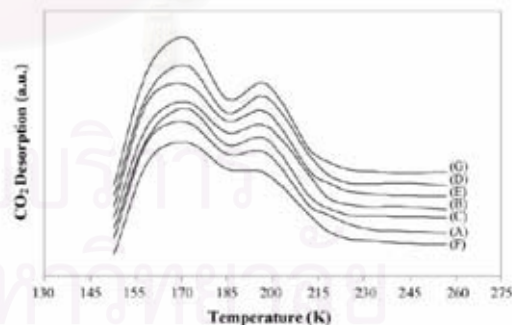


Fig. 3. Thermal desorption spectra for CO₂ adsorbed on TiO₂ quenched in different media: (A) liquid N₂, (B) H₂O at RT, (C) H₂O at 373 K, (D) 30% H₂O₂ at RT, (E) 30% H₂O₂ at 373 K (F) air at RT, and (G) air at 77 K.

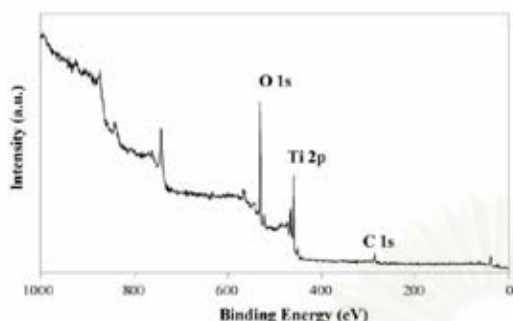


Fig. 4. Overview X-ray photoelectron spectra in the case of TiO_2 sample quenched in 30% hydrogen peroxide at room temperature.

The elements and their chemical states on surface of the TiO_2 samples after quenching treatment were also studied by XPS analysis. The typical XPS survey spectra of the TiO_2 powders after quenching treatment indicated that the powder was mainly composed of Ti and O elements with a small amount of C element (Fig. 4). The shapes of the XPS spectra of Ti 2p and O 1s for all the TiO_2 samples are quite similar. For example, the high-resolution XPS spectra of Ti 2p recorded from the TiO_2 samples quenched in H_2O_2 at room temperature are shown in Fig. 5. The Ti 2p spectrum can be fitted with Gaussian–Lorentzian functions into two spin–orbit components at binding energies 457.2 and 459.2 eV corresponding to Ti_2O_3 (Ti^{3+}) and TiO_2 (Ti^{4+}) fractions on the TiO_2 surface, respectively. The component binding energy values are in agreement with those reported in the literature [32]. The XPS O 1s spectra of the TiO_2 sample quenched in hydrogen peroxide at room temperature is also presented in Fig. 6. The O 1s peak is often believed to be composed of 3–5 different oxygen species such as Ti–O bonds in TiO_2 and Ti_2O_3 , hydroxyl groups, C–O bonds, and adsorbed H_2O . It is shown that the O 1s peak is asymmetric suggesting that at least three peaks related to three different chemical states of oxygen are present. The binding energies of each individual components are 530.8 (Ti^{4+} -O), 531.8 (Ti^{3+} -O), and 533.3 eV (O–H) [33,34]. It was found that the amount of surface Ti^{3+} sites increased in a sim-

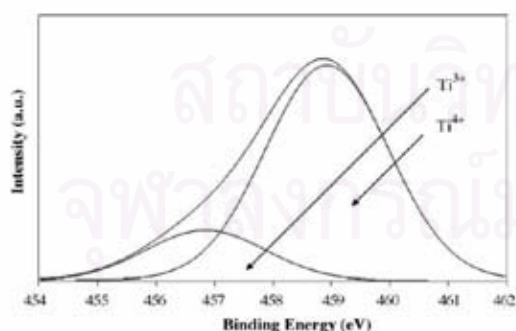


Fig. 5. Ti 2p XPS spectra for TiO_2 sample quenched in 30% wt hydrogen peroxide at room temperature.

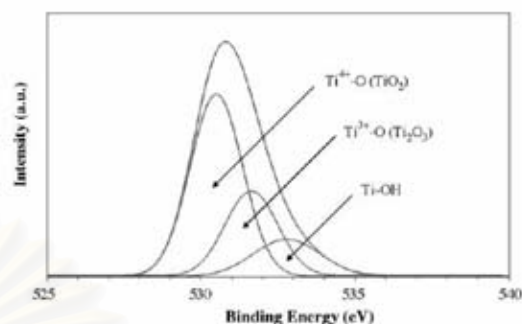


Fig. 6. O 1s XPS spectra for TiO_2 sample quenched in 30% wt hydrogen peroxide at room temperature.

ilar trend as those observed from CO_2 -TPD results. The TiO_2 quenched in different media thus possessed different surface properties especially in terms of the amount of Ti^{3+} defect sites on TiO_2 surface.

3.2. Photocatalytic activity of the nano- TiO_2 quenched in different media

Photocatalytic decomposition of ethylene was conducted to assess the photocatalytic activity of the TiO_2 samples quenched in various media. The amounts of adsorbed ethylene on the catalyst surface before degradation experiments were quite similar among the various catalysts as confirmed by ethylene-chemisorption and temperature programmed desorption experiments (results not shown). The plots of ethylene conversion as a function of reaction time for all the samples are shown in Fig. 7. Photocatalytic activity of the nano-sized TiO_2 quenched in different media is evidently different. The mechanism of photocatalytic decomposition of ethylene was reported by many researchers [35,36]. Yamazaki et al. [35] proposed the reaction sequences based on Langmuir–Hinshelwood model as follows:

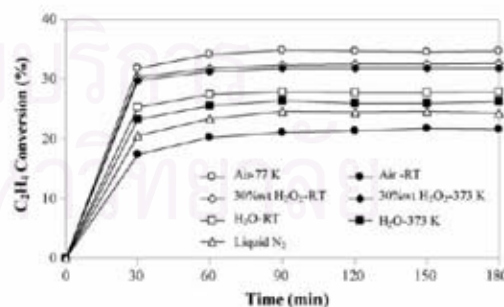


Fig. 7. Results of photocatalytic testing comparing the activities of different TiO_2 samples.



where σ and σ' mean different types of active sites on the TiO_2 surface. From reaction mechanism mentioned above, the hole generated from photo-excitation process plays an important role on creating the reaction intermediate, which react further and form CO_2 as the final product.

From early characterization results (XPS and CO_2 -TPD), it is likely that quenching process can modify surface properties of the TiO_2 samples, i.e., enhancing the amount of surface defects (Ti^{3+}) so that higher photocatalytic activity was obtained. The relationship between the amount of Ti^{3+} surface defect on the TiO_2 samples quenched in different media and ethylene conversion is illustrated in Fig. 8. The surface Ti^{3+} defect sites on TiO_2 photocatalysts has been found to play an important role determining their photocatalytic activity since they can act as photoelectron trapping sites [19,29].

In photocatalysis, light irradiation of TiO_2 powder with a photon energy larger than the band-gap energy produces electrons (e^-) and holes (h^+) in the conduction band and the valence band, respectively. These electrons and holes are thought to have the respective abilities to reduce and oxidize chemical species adsorbed on the surface of TiO_2 particles. For a photocatalyst to be most efficient, different interfacial electron processes involving e^- and h^+ must compete effectively with the major deactivation processes involving e^- - h^+ recombination. Park et al. [29] has reported that modification of TiO_2 surface by increasing the amount of Ti^{3+} surface defects can increase the photocatalytic activity of TiO_2 . It is suggested that the photoelectrons were trapped by the surface defect (Ti^{3+}) leading to inhibition of the e^- - h^+ recombination. In addition, Yu et al. [19] proposed that the doped F atoms convert Ti^{4+} to Ti^{3+} by

charge compensation and that the presence of a certain amount of Ti^{3+} reduces the electron-hole recombination rate and thus enhances the photocatalytic activity.

Recently, Chen et al. [37] reported that the trapping site of photogenerated holes or the surface OH is also an important factor affecting photo-catalytic reaction besides the surface Ti^{3+} . The nano-crystalline TiO_2 particles showed better photocatalytic activities when Ti^{3+}/OH ratios on the TiO_2 surface were close to 1. In this study, Ti^{3+}/OH ratios of the nano- TiO_2 quenched in various media were calculated based on the XPS results and are given in Table 1. It was also found that the TiO_2 quenched in air at 77 K (sample G) with Ti^{3+}/OH ratio=0.93 (closest to 1 among the various samples) exhibited the highest photocatalytic activity. Thus, it is clearly shown from this study that quenching condition and medium during post-synthesis treatment strongly affect photocatalytic activity of the nano- TiO_2 . Considering the TiO_2 samples quenched in the same type of quenching media (i.e., in H_2O , 30% H_2O_2 , or air), it was found that TiO_2 samples quenched at lower temperature exhibited higher photocatalytic activity than those quenched in high temperature ones. For example, TiO_2 quenched in air at 77 K showed higher ethylene conversion than the one quenched in air at room temperature. These results can probably be explained in terms of the thermal shock effect. The large difference in temperature between media and TiO_2 surface may lead to modification of the surface properties, i.e., increasing the amount of Ti^{3+} defects on the TiO_2 surface. Additionally, it is noted that for the used of liquid phase media, the TiO_2 sample quenched in the media containing more -OH group in molecules exhibited higher photocatalytic activity.

4. Conclusions

In this study, we have shown that surface properties as well as photocatalytic activities of the solvothermal-derived nano- TiO_2 can be modified by quenching process post-synthesis treatment whilst the average crystallite size and BET surface area of the samples were essentially similar. It was found that quenching process especially the use of low temperature medium can create a thermal shock effect that as a consequence resulting in more surface Ti^{3+} defects on the TiO_2 sample and hence higher photocatalytic activity.

Acknowledgements

The authors would like to thank the financial supports from the Commission of Higher Education, Ministry of Education, Thailand and the Graduate School of Chulalongkorn University for the 72nd Anniversary of H.M. King Rama IX scholarship for P.S.

References

- [1] A.L. Linsebigler, G. Lu, J.T. Yates Jr., Photocatalysis on TiO_2 surfaces: principles, mechanisms, and selected results, *Chem. Rev.* 95 (1995) 735–758.

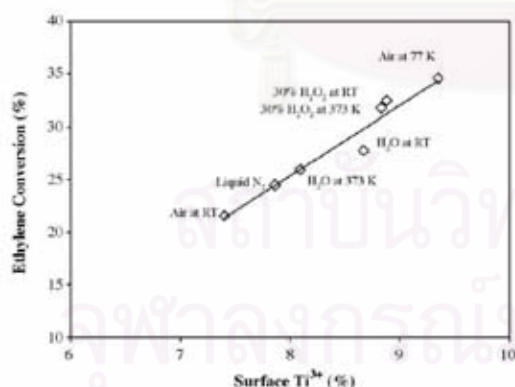


Fig. 8. Ethylene conversions as a function of surface Ti^{3+} on the TiO_2 samples quenched in different media.

- [2] O. Carp, C.L. Huisman, A. Reller, Photoinduced reactivity of titanium dioxide, *Prog. Solid State Chem.* 32 (2004) 33–177.
- [3] V.N.H. Nguyen, R. Amal, D. Beydoun, Effect of formate and methanol on photoreduction/removal of toxic cadmium ions using TiO₂ semiconductor as photocatalyst, *Chem. Eng. Sci.* 58 (2003) 4429–4439.
- [4] D. Chen, A.K. Ray, Removal of toxic metal ions from wastewater by semiconductor photocatalysis, *Chem. Eng. Sci.* 56 (2001) 1561–1570.
- [5] J. Yu, X. Zhao, J. Du, W. Chen, Preparation, microstructure and photocatalytic activity of the porous TiO₂ anatase coating by sol-gel processing, *J. Sol-Gel Sci. Technol.* 17 (2000) 163–171.
- [6] J.-G. Yu, H.-G. Yu, B. Cheng, X.-J. Zhao, J.C. Yu, W.-K. Ho, The effect of calcination temperature on the surface microstructure and photocatalytic activity of TiO₂ thin films prepared by liquid phase deposition, *J. Phys. Chem. B* 107 (2003) 13871–13879.
- [7] C.-S. Kim, B.K. Moon, J.-H. Park, S.T. Chung, S.-M. Son, Synthesis of nanocrystalline TiO₂ in toluene by a solvothermal route, *J. Cryst. Growth* 254 (2003) 405–410.
- [8] C. Wang, Z.-X. Deng, G. Zhang, S. Fan, Y. Li, Synthesis of nanocrystalline TiO₂ in alcohols, *Powder Technol.* 125 (2002) 39–44.
- [9] M. Kang, B.-J. Kim, S.M. Cho, C.-H. Chung, B.-W. Kim, G.Y. Han, K.J. Yoon, Decomposition of toluene using an atmospheric pressure plasma/TiO₂ catalytic system, *J. Mol. Catal. A: Chem.* 180 (2002) 125–132.
- [10] H. Kominami, M. Kohno, Y. Takada, M. Inoue, T. Inui, Y. Kera, Hydrolysis of titanium alkoxide in organic solvent at high temperatures: a new synthetic method for nanosized, thermally stable titanium(IV) oxide, *Ind. Eng. Chem. Res.* 38 (1999) 3925–3931.
- [11] H.-D. Nam, B.-H. Lee, S.-J. Kim, C.-H. Jung, J.-H. Lee, S. Park, Preparation of ultrafine crystalline TiO₂ powders from aqueous TiCl₄ solution by precipitation, *Jpn. J. Appl. Phys.* 37 (1998) 4603–4608.
- [12] C. Su, B.-Y. Hong, C.-M. Tseng, Sol-gel preparation and photocatalysis of titanium dioxide, *Catal. Today* 96 (2004) 119–126.
- [13] P. Yang, C. Lu, N. Hua, Y. Du, Titanium dioxide nanoparticles co-doped with Fe³⁺ and Eu³⁺ ions for photocatalysis, *Mater. Lett.* 57 (2002) 794–801.
- [14] Y. Bessekhouad, D. Robert, J.V. Weber, Synthesis of photocatalytic TiO₂ nanoparticles: optimization of the preparation conditions, *J. Photochem. Photobiol. A: Chem.* 157 (2003) 47–53.
- [15] K. Nakaso, K. Okuyama, M. Shimada, S.E. Pratsinis, Effect of reaction temperature on CVD-made TiO₂ primary particle diameter, *Chem. Eng. Sci.* 58 (2003) 3327–3335.
- [16] H. Kominami, J.-I. Kalo, Y. Takada, Y. Doushi, B. Ohtani, S.-I. Nishimoto, M. Inoue, T. Inui, Y. Kera, Novel synthesis of microcrystalline titanium(IV) oxide having high thermal stability and ultra-high photocatalytic activity: thermal decomposition of titanium(IV) alkoxide in organic solvents, *Catal. Lett.* 46 (1997) 235–240.
- [17] T. Umebayashi, T. Yamaki, S. Yamamoto, A. Miyashita, S. Tanaka, T. Sumita, K. Asai, Sulfur-doping of rutile-titanium dioxide by ion implantation: photocurrent spectroscopy and first-principles band calculation studies, *J. Appl. Phys.* 93 (2003) 5156–5160.
- [18] M. Anpo, M. Takeuchi, The design and development of highly reactive titanium oxide photocatalysts operating under visible light irradiation, *J. Catal.* 216 (2003) 505–516.
- [19] J.C. Yu, J. Yu, W. Ho, Z. Jiang, L. Zhang, Effects of F-doping on the photocatalytic activity and microstructures of nanocrystalline TiO₂ powders, *Chem. Mater.* 14 (2002) 3808–3816.
- [20] D. Li, H. Haneda, Photocatalysis of sprayed nitrogen-containing Fe₂O₃-ZnO and WO₃-ZnO composite powders in gas-phase acetaldehyde decomposition, *J. Photochem. Photobiol. A* 160 (2003) 203–212.
- [21] A. Corma, A. Martínez, C. Martínez, The effect of sulfation conditions and activation temperature of sulfate-doped ZrO₂, TiO₂ and SnO₂ catalysts during isobutane/2-butene alkylation, *Appl. Catal. A: Gen.* 144 (1996) 249–268.
- [22] E. Barraud, F. Bosc, D. Edwards, N. Keller, V. Keller, Gas phase photocatalytic removal of toluene effluents on sulfated titania, *J. Catal.* 235 (2005) 318–326.
- [23] H. Liu, H.T. Ma, X.Z. Li, W.Z. Li, M. Wu, X.H. Bao, The enhancement of TiO₂ photocatalytic activity by hydrogen adsorption, *Chemosphere* 50 (2003) 39–46.
- [24] P.B. Amama, K. Itoh, M. Murabayashi, Gas-phase photocatalytic degradation of trichloroethylene on pretreated TiO₂, *Appl. Catal. B: Environ.* 37 (2002) 321–330.
- [25] I. Nakamura, N. Negishi, S. Kutsuna, T. Ihara, S. Sugihara, K. Takeuchi, Role of oxygen vacancy in the plasma-treated TiO₂ photocatalyst with visible light activity for NO removal, *J. Mol. Catal. A* 161 (2000) 205–212.
- [26] M.A. Henderson, An HREELS and TPD study of water on TiO₂(110): the extent of molecular versus dissociative adsorption, *Surf. Sci.* 355 (1996) 151–166.
- [27] W. Payakgul, O. Mekasuwandumrong, V. Pavarajarn, P. Praserttham, Effects of reaction medium on the synthesis of TiO₂ nanocrystals by thermal decomposition of titanium(IV) *n*-butoxide, *Ceram. Int.* 31 (2005) 391–397.
- [28] T.L. Thompson, O. Diwald, J.T. Yates Jr., CO₂ as a probe for monitoring the surface defects on TiO₂(110)-temperature-programmed desorption, *J. Phys. Chem. B* 107 (2003) 11700–11704.
- [29] D.-R. Park, J. Zhang, K. Ikeue, H. Yamashita, M. Anpo, Photocatalytic oxidation of ethylene to CO₂ and H₂O on ultrafine powdered TiO₂ photocatalysts in the presence of O₂ and H₂O, *J. Catal.* 185 (1999) 114–119.
- [30] M. Lewandowski, D.F. Ollis, Halide acid pretreatments of photocatalysts for oxidation of aromatic air contaminants: rate enhancement, rate inhibition, and a thermodynamic rationale, *J. Catal.* 217 (2003) 38–46.
- [31] S.S. Watson, D. Beydoun, J.A. Scott, R. Amal, The effect of preparation method on the photoactivity of crystalline titanium dioxide particles, *Chem. Eng. J.* 95 (2003) 213–220.
- [32] P.M. Kumar, S. Badrinarayanan, M. Sastry, Nanocrystalline TiO₂ studied by optical, FTIR and X-ray photoelectron spectroscopy: correlation to presence of surface states, *Thin Solid Films* 358 (2000) 122–130.
- [33] J. Yu, X. Zhao, Q. Zhao, Effect of surface structure on photocatalytic activity of TiO₂ thin films prepared by sol-gel method, *Thin Solid Films* 379 (2000) 7–14.
- [34] J. Pouilleau, D. Devilliers, H. Groult, P. Marcus, Surface study of a titanium-based ceramic electrode material by X-ray photoelectron spectroscopy, *J. Mater. Sci.* 32 (1997) 5645–5651.
- [35] S. Yamazaki, S. Tanaka, H. Tsukamoto, Kinetic studies of oxidation of ethylene over a TiO₂ photocatalyst, *J. Photochem. Photobiol. A: Chem.* 121 (1999) 55–61.
- [36] A. Sirisuk, C.G. Hill, M.A. Anderson, Photocatalytic degradation of ethylene over thin films of titania supported on glass rings, *Catal. Today* 54 (1999) 159–164.
- [37] X.-Q. Chen, H.-B. Liu, G.-B. Gu, Preparation of nanometer crystalline TiO₂ with high photo-catalytic activity by pyrolysis of titanyl organic compounds and photo-catalytic mechanism, *Mater. Chem. Phys.* 91 (2005) 317–324.

Dependence of Quenching Process on the Photocatalytic Activity of Solvothermal-Derived TiO₂ with Various Crystallite Sizes

Piyawat Supphasrironjaroen, Wilasinee Kongsuebchart, Joongjai Panpranot, Okorn Mekasuwandumrong, Chairit Satayaprasert, and Piyasan Prasertthadam*

Center of Excellence on Catalysis and Catalytic Reaction Engineering, Department of Chemical Engineering, Faculty of Engineering, Chulalongkorn University, Bangkok, 10330 Thailand

In the present work, the effect of quenching on surface defect and photocatalytic activity of the solvothermal-derived nanocrystalline TiO₂ with average crystallite sizes between 9 and 13 nm was extensively studied. On the basis of CO₂-TPD (TPD = temperature-programmed desorption) and XPS (XPS = X-ray photoelectron spectroscopy) results, it was found that the amount of Ti³⁺ surface defects and photocatalytic activities of the prepared TiO₂ depended strongly on the type of quenching media used in the following order: H₂O₂-RT > H₂O₂-373K > H₂O-RT > H₂O-373K > air-RT > air-373K, where RT = room temperature. However, the TiO₂ sample that was slowly cooled after calcination (the nonquenched sample) also possessed a significant amount of Ti³⁺ surface defects and high photocatalytic activity to a degree similar to that quenched in H₂O-RT. The effect of quenching was more pronounced on the smaller crystallite size TiO₂ than on the larger ones due probably to its higher surface energy so that oxygen atoms were released more easily.

1. Introduction

Titanium(IV) dioxide or titania (TiO₂) has been the focus of many research interests during the past decade due to its scientific and technological importance. It is a low-cost, widely available, nontoxic, and biocompatible substance that is widely used in domestic applications (e.g., increasing paint durability, cleaning wastewaters, etc.).^{1–2} It has been demonstrated to be useful in various areas because of its versatile properties such as catalytic activity,³ photocatalytic activity for pollutant removal,⁴ good stability toward adverse environment,⁵ sensitivity to humidity and gas,⁶ dielectric character,⁷ photoelectrochemical conversion,⁸ nonlinear optics,⁹ and photoluminescence.¹⁰ TiO₂ has been an important component for cosmetics, pigments, filter coating, gas and humidity sensors, dielectric ceramics, catalyst support, solar cells, and so on.¹¹ Its performance in these applications depends to a large extent on its physical and chemical properties which are related to the synthetic conditions. These conditions dictate the properties such as crystal structure, morphology, grain size, thermal stability, and surface structure of the TiO₂ products.

The photocatalytic activity of TiO₂ is greatly influenced by its crystal structure, particle size, surface area, incident light intensity, and porosity. Among these factors, crystal structure and crystallinity of TiO₂ are considered the important factors. Amorphous titania has negligible photocatalytic activity because of the recombination between the pair of photoexcited electron and hole in the amorphous structure.¹² Anatase crystalline TiO₂ is generally accepted to have significant photocatalytic activity. However, much effort indicates that rutile TiO₂ and metal-doped rutile TiO₂ also exhibit high photocatalytic activity especially under visible light irradiation.^{13–15} With the decrease in particle size of powder to nanometer scale, the catalytic activity of titania is enhanced because the optical band gap is widened due to surface defect^{16,17} and an increased in surface area.^{18,19}

Many methods have been proposed to synthesize nanocrystalline TiO₂ in anatase polymorph such as sol-gel²⁰ and

hydrothermal method.²¹ Although the sol-gel method is widely used to prepare nanosized TiO₂, calcination of the gel inevitably causes the grain growth and reduction in the specific surface area of the TiO₂ particles and even induces phase transformation. Solvothermal synthesis, in which chemical reactions can occur in aqueous or organic media under the self-produced pressure at low temperature (usually lower than 250 °C), can solve those problems encountered during the sol-gel process.²² This method has been used to successfully synthesize various types of nanosized metal oxides with large surface area, high crystallinity, and high thermal stability.^{23–24}

In the present work, nanocrystalline TiO₂ powders with various crystallite sizes (9–13 nm) were prepared by the solvothermal method using titanium butoxide as the precursor. Then the TiO₂ products were subjected to a rapid quenching process in various quenching media such as air, water, and hydrogen peroxide at two different temperatures (303 and 373 K). The quenching process has shown to result in a variety of surface defects, strains, and reconstructions of materials.²⁵ It is believed that surface defects on the TiO₂ samples as well as their photocatalytic activity can be modified by rapid quenching process. The properties of TiO₂ samples were characterized using various analytical methods such as X-ray diffraction (XRD), N₂ physisorption, CO₂-temperature programmed desorption (CO₂-TPD), and X-ray photoelectron spectroscopy (XPS). Photocatalytic activity of the TiO₂ was tested in gas-phase decomposition of ethylene under UV irradiation.

2. Experimental Section

2.1. Preparation of Nanocrystalline TiO₂. Nanocrystalline TiO₂ was prepared using the solvothermal method according to that of Payakgul et al.²⁶ using titanium(IV) *n*-butoxide (TNB) as starting material. In general, an amount of 15–25 g of TNB was suspended in 100 cm³ of toluene in a test tube, which was then placed in a 300 cm³ autoclave. The gap between the test tube and the autoclave wall was filled with 30 cm³ of the same solvent used in the test tube. The autoclave was purged completely by nitrogen before heating up to the desired temperature, in the range of 573–593 K at a rate of 2.5 K/min.

* To whom all correspondence should be addressed. Tel.: 66-2218-6883. Fax: 66-2218-6877. E-mail: piyasan.p@chula.ac.th.

Table 1. Phase Compositions and Structural Properties of the TiO₂ Synthesized by Solvothermal Method after Quenching in Various Media

synthesis conditions	quenching medium	crystallite size (nm)	S _{BET} (m ² /g)	sample nomenclature
TNB, 15 g	air at 373 K	8.6	96	9A
toluene, 100 mL	air at RT*	9.4	94	9B
temp, 573 K	H ₂ O at 373 K	9.0	99	9C
holding time, 30 min	H ₂ O at RT	8.9	104	9D
	H ₂ O ₂ at 373 K	10.0	92	9E
	H ₂ O ₂ at RT	10.5	91	9F
TNB, 25 g	air at 373 K	9.6	85	11A
toluene, 100 mL	air at RT	10.6	93	11B
temp, 573 K	H ₂ O at 373 K	10.4	95	11C
holding time, 2 h	H ₂ O at RT	10.5	112	11D
	H ₂ O ₂ at 373 K	13.2	90	11E
	H ₂ O ₂ at RT	13.3	94	11F
TNB, 15 g	air at 373 K	10.4	60	13A
toluene, 100 mL	Air at RT	13.4	67	13B
temp, 593 K	H ₂ O at 373 K	13.4	67	13C
holding time, 6 h	H ₂ O at RT	13.2	69	13D
	H ₂ O ₂ at 373 K	14.6	61	13E
	H ₂ O ₂ at RT	14.7	63	13F

Autogenously pressure during the reaction gradually increased as the temperature was raised. Once the prescribed temperature was reached, the temperature was held constant for 0.5–6 h. After the system was cooled down, the resulting powders were repeatedly washed with methanol and dried in air.

2.2. Quenching Process. Prior to quenching, the synthesized TiO₂ was dried in air atmosphere at 573 K with a heating rate of 10 K/min for 1 h, and then it was taken out and immediately quenched in various quenching media. In this study, both liquid-phase and gas-phase media were employed. For quenching in gas-phase media, air at room temperature and 373 K were used (samples A and B). For quenching in liquid-phase media, hydrogen peroxide at room temperature and 373 K (samples C and D) and water at room temperature and 373 K (samples E and F) were used. After the samples were quenched in the media for 30 min, all the TiO₂ samples were dried in air at room temperature and stored in a desiccator.

2.3. Characterization. The XRD patterns of the TiO₂ samples were recorded using a SIEMENS D5000 X-ray diffractometer using Cu K α radiation with a Ni filter in the range of 20–80° 2 θ . The crystallite size of TiO₂ was determined from half-height width of the 101 diffraction peak of anatase using the Scherrer equation. The specific surface area (S_{BET}) was calculated using BET single-point method on the basis of nitrogen (N₂) uptake measured at 77 K in a Micromeritics ASAP 2000. Temperature-programmed desorption using CO₂ as a probe molecule was performed to determine the Ti³⁺ site existing on the surface of TiO₂ particle.²⁷ It was carried out using 0.05 g of a TiO₂ sample. TiO₂ was dosed by 1 vol % CO₂ in helium for 1 h and then desorbed from 143 to 273 K with the rate of 21.5 K/min. The XPS measurement was carried out using an AMICUS photoelectron spectrometer equipped with an Mg K α X-ray as a primary excitation and KRATOS VISION2 software. XPS elemental spectra were acquired with 0.1 eV energy step at a pass energy of 75 kV. All the binding energies were referenced to the C 1s peak at 285.0 eV of the surface adventitious carbon.

2.4. Photocatalytic Activity Measurement. Catalytic decomposition of ethylene was carried out in order to determine photocatalytic activity of the TiO₂ using a horizontal quartz fixed bed reactor. High purity grade air containing 0.1 vol % ethylene was continuously fed at a constant flow rate with a gas hourly space velocity (GHSV) of 120 h⁻¹. An air stream with 0.1 vol % ethylene was first passed through the reactor without irradiation until reaching gas–solid adsorption equilibrium.

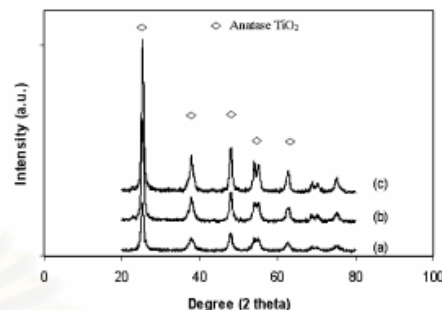


Figure 1. The XRD patterns of the various TiO₂ samples after quenching in air at room temperature: (a) 9 nm, (b) 11 nm, (c) 13 nm.

Then, UV light was irradiated on the surface of the catalyst using a 500 W mercury lamp (Philips, HPL-N). The outlet gas was taken every 30 min. Its composition was analyzed using a Shimadzu GC-14B gas chromatograph equipped with the flame-ionized detector until the reaction reached steady state.

3. Results and Discussion

3.1. Structure and Surface Properties of TiO₂ Quenched in Different Media. In this study, the effects of quenching medium as well as quenching temperature on the properties of nanocrystalline TiO₂ synthesized by solvothermal method are extensively investigated. Quenching process was applied as a postsynthesis treatment with the aims being to create more defects on the TiO₂ surface and, as a consequence, improve their photocatalytic activities. Physical properties of the various TiO₂ such as the BET surface areas and the average TiO₂ crystallite sizes after quenching in different media are shown in Table 1. Due to the different preparation conditions, the TiO₂ samples possessed different crystallite sizes and specific surface areas. The average crystallite size of TiO₂ samples increased from 9 to 13 nm as the BET surface area of the TiO₂ samples decreased from ca. 95 to 65 m²/g. Quenching treatment, however, did not significantly alter the specific surface area and the average crystallite size of the TiO₂. The anatase TiO₂ crystalline phase was preserved after quenching. All the TiO₂ samples consisted of only pure anatase phase TiO₂ (major XRD peaks at 25.36, 37.82, and 48.18° 2 θ). XRD patterns of the TiO₂ with various crystallite sizes after quenching in air at room temperature are shown in Figure 1. The crystallite sizes of the TiO₂ from XRD are in good agreement with those observed from the TEM micrographs of the samples (Figure 2).

The surface structure of TiO₂ was characterized by temperature-programmed desorption of CO₂. All the TiO₂ samples exhibited two main desorption peaks at temperatures ca. 145 and 170 K which could be attributed to adsorption of CO₂ on two different structures of TiO₂ surface.²⁷ For example, the CO₂-TPD profiles of TiO₂ samples with average crystallite size of 11 nm after quenching in various media are shown in Figure 3. The desorption peak at ca. 145 K was attributed to CO₂ molecules binding to the regular five-coordinate Ti⁴⁺ site which was considered as the perfected TiO₂ structure. The second peak at ca. 170 K has been considered as desorption of CO₂ molecules binding to Ti³⁺ defect sites of TiO₂. On the basis of the CO₂-TPD results, it was found that, for a given TiO₂ crystallite size, the peak areas for CO₂ desorption at ca. 170 K (representing the amount of Ti³⁺ defective sites) depended on the type of quenching media employed in the following order: air at 373 K < air at RT < H₂O at 373 K < H₂O at RT < H₂O₂ at 373

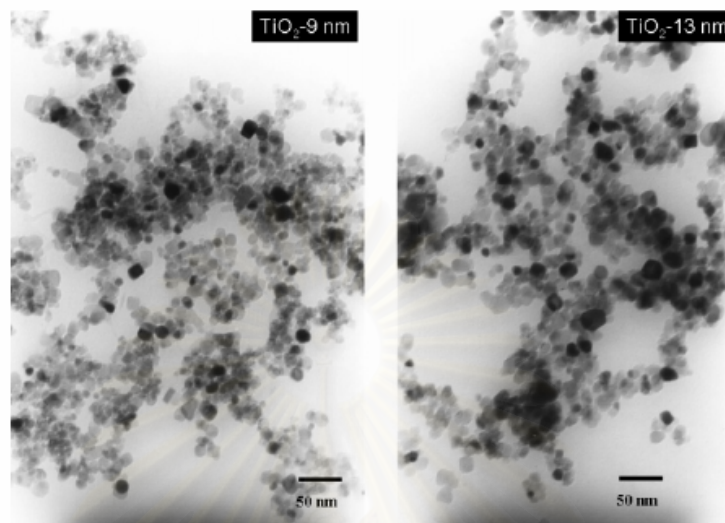


Figure 2. TEM micrographs of TiO_2 -9 nm and TiO_2 -13 nm (nonquenched).

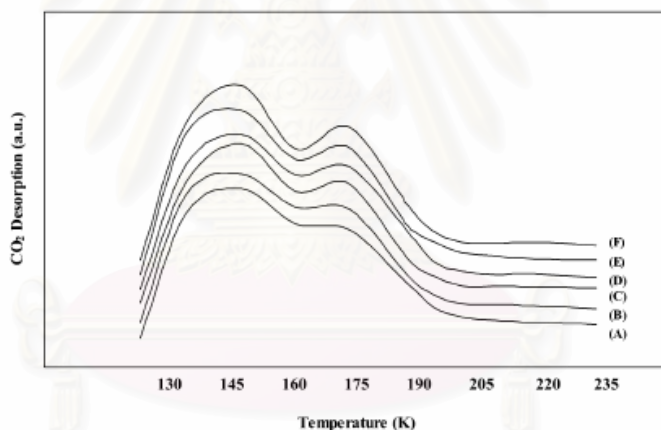


Figure 3. CO_2 -temperature-programmed desorption results of the TiO_2 -11 nm quenched in different media: (A) air at 373 K, (B) air at RT, (C) H_2O at 373 K, (D) H_2O at RT, (E) H_2O_2 at 373 K, and (F) H_2O_2 at RT (RT = room temperature).

$\text{K} < \text{H}_2\text{O}_2$ at RT. It is known that quenching treatment of a metal can create nucleation of dislocations, surface defect, and concentration of stress on the metal surface.²⁸ The results in this study have shown that quenching process can be applied as a postsynthesis treatment for controlling the amount of surface defects on nanocrystalline TiO_2 . The $\text{Ti}^{3+}/\text{Ti}^{4+}$ ratios calculated from CO_2 -TPD results of the various quenched TiO_2 samples and the nonquenched one are illustrated in Figure 4. It was found that the nonquenched sample also possessed a significant amount of Ti^{3+} to a degree similar to that quenched in H_2O at room temperature. However, when compared with the TiO_2 sample quenched in H_2O_2 and H_2O , it is noticed that the TiO_2 sample quenched in liquid-phase media that contained more -OH group in molecules exhibited higher $\text{Ti}^{3+}/\text{Ti}^{4+}$ and higher photocatalytic activity. Recently, Xiao-Quan et al.²⁹ reported that the trapping site of photogenerated holes or the surface -OH is also an important factor affecting photocatalytic reaction besides the surface Ti^{3+} .

The presence of Ti^{3+} on the TiO_2 samples was also studied by X-ray photoelectron spectroscopy. For example, high-resolution XPS spectra of Ti 2p and O 1s recorded from the TiO_2 samples quenched in H_2O_2 at room temperature are shown in Figure 5. The Ti 2p spectrum can be fitted with Gaussian-Lorentzian functions into two spin-orbit components at binding energies of 457.2, and 459.2 eV, corresponding to Ti_2O_3 (Ti^{3+}) and TiO_2 (Ti^{4+}) fractions on the TiO_2 surface, respectively. The component binding energy values are in agreement with those reported in the literature.³⁰ The O 1s peak is often believed to be composed of three to five different oxygen species such as Ti-O bonds in TiO_2 and Ti_2O_3 , hydroxyl groups, C-O bonds, and adsorbed H_2O . It is shown that the O 1s peak is asymmetric, suggesting that at least three peaks related to three different chemical states of oxygen are present. The binding energies of each individual component are 530.8 (Ti^{4+} -O), 531.8 (Ti^{3+} -O), and 533.3 eV (O-H).³¹⁻³² The shapes of the XPS spectra of Ti 2p and O 1s for all the TiO_2 samples are quite similar,

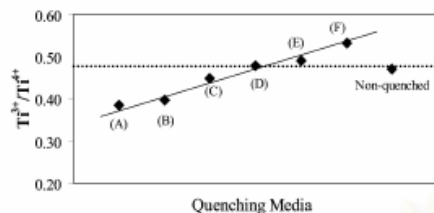


Figure 4. Ti^{3+}/Ti^{4+} ratios calculated from CO_2 -TPD results of the TiO_2 -11 nm quenched in different media: (A) air at 373 K, (B) air at RT, (C) H_2O at 373 K, (D) H_2O at RT, (E) H_2O_2 at 373 K, and (F) H_2O_2 at RT (RT = room temperature).

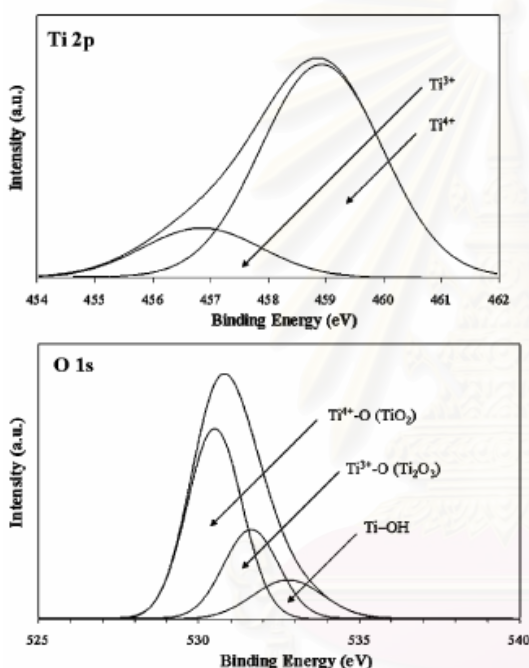


Figure 5. XPS spectra of Ti 2p and O 1s for TiO_2 -11 nm quenched in H_2O_2 at room temperature.

and it was found that the amount of surface Ti^{3+} sites increased in a trend similar to those observed from CO_2 -TPD results.

In photocatalysis, defect sites on the surface of TiO_2 are known as adsorption sites,^{33,34} electronic promoters,³⁵ or electron traps.^{36,37} In general, light irradiation of TiO_2 powder with photon energy larger than the band gap energy produces electrons (e^-) and holes (h^+) in the conduction band and the valence band, respectively.^{38,39} These electrons and holes are thought to have the respective abilities to reduce and oxidize chemical species adsorbed on the surface of TiO_2 particles. For a photocatalyst to be most efficient, different interfacial electron processes involving e^- and h^+ must compete effectively with the major deactivation processes involving e^- - h^+ recombination. Surface Ti^{3+} defect sites (oxygen vacancies) are the sites that oxygen adsorption occurs as well as that the photogenerated electrons are trapped,⁴⁰⁻⁴² so they are effective sites for interface electron transferring. The relationship between the amount of Ti^{3+} defects on TiO_2 surface and their photocatalytic activities has been reported by many authors.⁴³⁻⁴⁶

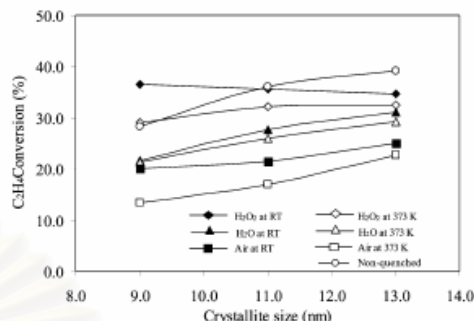


Figure 6. Results of the photocatalytic activities of TiO_2 samples quenched in different media.

3.2. Photocatalytic Activity of the TiO_2 Quenched in Different Media. Photocatalytic activities of the TiO_2 samples with various crystallite sizes after quenching in different media were evaluated in the decomposition of ethylene in gas-phase and the results are shown in Figure 6. Ethylene conversions at steady state (after 180 min of run) for the quenched TiO_2 samples with various crystallite sizes were ranged from ca. 20–37%, while that of TiO_2 Degussa P25 under similar reaction conditions gave ca. 30% ethylene conversion. It was found that, for a given TiO_2 crystallite size, ethylene conversions were strongly dependent on the quenching media and were found to be in the following order: H_2O_2 at RT > H_2O_2 at 373 K > H_2O at RT > H_2O at 373 K > air at RT > air at 373 K. Such results were in good agreement with the amount of Ti^{3+} surface defect on the TiO_2 samples in which those with higher amounts of Ti^{3+} surface defect exhibited higher photocatalytic activities for ethylene decomposition. For a similar quenching medium, the TiO_2 quenched at low temperature resulted in a larger amount of Ti^{3+} and exhibited higher photocatalytic activity compared to those quenched at high temperature. This can probably be explained by a thermal shock effect that a large difference in temperature of the TiO_2 surface and quenching medium can create more surface defects. However, compared to the TiO_2 sample that was slowly cooled down after calcination (the nonquenched sample), only the smaller crystallite size TiO_2 (TiO_2 , 9 nm) that quenched in H_2O_2 exhibited higher photocatalytic activities. The effect of quenching was less pronounced on the larger TiO_2 crystallite size and the nonquenched samples showed higher activities.

4. Conclusions

The surface properties and photocatalytic activities of nano-sized TiO_2 powders synthesized by solvothermal method with various crystallite sizes (9–13 nm) were significantly influenced by quenching media and quenching conditions. For the use of similar quenching media, the TiO_2 quenched in a low-temperature medium has been shown to result in more Ti^{3+} surface defects on the TiO_2 surface and consequently higher photocatalytic activity than those quenched in a high-temperature one. The amount of Ti^{3+} and photocatalytic activity of the quenched samples depended on the type of quenching medium in the following order: H_2O_2 > H_2O > air. Compared to the nonquenched sample (the one slowly cooled after calcination), quenching in H_2O_2 has shown to result in higher Ti^{3+} and photocatalytic activity of the TiO_2 with small crystallite size (9 nm). There was less effect of quenching on larger crystallite size TiO_2 .

Acknowledgment

Financial support from the Thailand Research Fund (TRF) and the Graduate School of Chulalongkorn University is gratefully acknowledged. The authors also thank the Cooperative Research Network (CRN) of the Thai Ministry of Education for the scholarship for P.S.

Literature Cited

- Chen, C. H.; Kelder, E. M.; Schoonman, J. Electrostatic sol-spray deposition (ESSD) and characterization of nanostructured TiO₂ thin films. *Thin Solid Films* 1999, 342, 35.
- Ollis, D. E.; Al-Ekabi, H., Eds. *Photocatalytic Purification and Treatment of Water and Air*; Elsevier: Amsterdam, 1993.
- Tsubota, S.; Nakamura, T.; Tanaka, K.; Haruta, M. Effect of calcination temperature on the catalytic activity of Au colloids mechanically mixed with TiO₂ powder for CO oxidation. *Catal. Lett.* 1998, 56, 131.
- Senogles, P.-J.; Scott, J. A.; Shaw, G.; Stratton, H. Photocatalytic degradation of the cyanotoxin cylindrospermopsin, using titanium dioxide and UV irradiation. *Water Res.* 2001, 35, 1245.
- Tonejc, A. M.; Goti, M.; Gržeta, B.; Musici, S.; Popovi, S.; Trojko, R.; Turkovi, A.; Mušević, I. Transmission electron microscopy studies of nanophase TiO₂. *Mater. Sci. Eng. B* 1993, 40, 177.
- Traversa, E.; Gnappi, G.; Montenero, A.; Guzmano, G. Ceramic thin films by sol-gel processing as novel materials for integrated humidity sensors. *Sens. Actuators B* 1996, 31, 59.
- Ohtani, B.; Nishimoto, S.-I. Effect of surface adsorptions of aliphatic alcohols and silver ion on the photocatalytic activity of TiO₂ suspended in aqueous solutions. *J. Phys. Chem.* 1993, 97, 920.
- Raja, K. S.; Mahajan, V. K.; Misra, M. Determination of photo conversion efficiency of nanotubular titanium oxide photo-electrochemical cell for solar hydrogen generation. *J. Power Sources* 2006, 159, 1258.
- O'Regan, B.; Grätzel, M. A low-cost, high-efficiency solar cell based on dye-sensitized colloidal TiO₂ films. *Nature* 1991, 353, 737.
- Fujihara, K.; Izumi, S.; Ohno, T.; Matsumura, M. Time-resolved photoluminescence of particulate TiO₂ photocatalysts suspended in aqueous solutions. *J. Photochem. Photobiol. A* 2000, 132, 99.
- Ha, H. Y.; Nam, S. W.; Lim, T. H.; Oh, I.-H.; Hong, S.-A. Properties of the TiO₂ membranes prepared by CVD of titanium tetraisopropoxide. *J. Membr. Sci.* 1996, 111, 81.
- Ohtani, B.; Ogawa, Y.; Nishimoto, S.-I. Photocatalytic activity of amorphous-anatase mixture of titanium(IV) oxide particles suspended in aqueous solutions. *J. Phys. Chem. B* 1997, 101, 3746.
- Liu, H.; Gao, L. Co-doped rutile TiO₂ as a new photocatalyst for visible light irradiation. *Chem. Lett.* 2004, 33, 730.
- Sopyan, I.; Watanabe, M.; Muraşawa, S.; Hashimoto, K.; Fujishima, A. Efficient TiO₂ powder and film photocatalysts with rutile crystal structure. *Chem. Lett.* 1996, 25, 69.
- Liu, H. Y.; Gao, L. Synthesis and properties of CdSe-sensitized rutile TiO₂ nanocrystals as a visible light-responsive photocatalyst. *J. Am. Ceram. Soc.* 2005, 88, 1020.
- Shifu, C.; Gengyu, C. The effect of different preparation conditions on the photocatalytic activity of TiO₂-SiO₂/beads. *Surf. Coat. Technol.* 2006, 200, 3637.
- Suriye, K.; Praserttham, P.; Jongsonjitt, B. Impact of Ti³⁺ present in titania on characteristics and catalytic properties of the Co/TiO₂ catalyst. *Ind. Eng. Chem. Res.* 2005, 44, 6599.
- Madhusudan Reddy, K.; Gopal Reddy, C. V.; Manorama, S. V. Preparation, characterization, and spectral studies on nanocrystalline anatase TiO₂. *J. Solid State Chem.* 2001, 158, 180.
- Toyoda, T.; Kawano, H.; Shen, Q.; Kotera, A.; Ohmori, M. Characterization of electronic states of TiO₂ powders by photoacoustic spectroscopy. *Jpn. J. Appl. Phys., Part 1* 2000, 39, 3160.
- Alam, M. J.; Cameron, D. C. Preparation and characterization of TiO₂ thin films by sol-gel method. *J. Sol-Gel Sci. Technol.* 2002, 25, 137.
- Kolen'ko, Y. V.; Burukhin, A. A.; Churagulov, B. R.; Oleynikov, N. N. Synthesis of nanocrystalline TiO₂ powders from aqueous TiOSO₄ solutions under hydrothermal conditions. *Mater. Lett.* 2003, 57, 1124.
- Carp, O.; Huisman, C. L.; Keller, A. Photoinduced reactivity of titanium dioxide. *Prog. Solid State Chem.* 2004, 32, 33.
- Kongwudhithi, S.; Praserttham, P.; Silveston, P. L.; Inoue, M. Influence of synthesis conditions on the preparation of zirconia powder by the glycothermal method. *Ceram. Int.* 2003, 29, 807.
- Mekasuwandumrong, O.; Silveston, P. L.; Praserttham, P.; Inoue, M.; Pavrajaram, V.; Tanakulnugsak, W. Synthesis of thermally stable micro spherical γ -alumina by thermal decomposition of aluminum isopropoxide in mineral oil. *Inorg. Chem. Commun.* 2003, 6, 930.
- Henderson, M. A. An HREELS and TPD study of water on TiO₂-(110): The extent of molecular versus dissociative adsorption. *Surf. Sci.* 1996, 355, 151.
- Payakgul, W.; Mekasuwandumrong, O.; Pavrajaram, V.; Praserttham, P. Effects of reaction medium on the synthesis of TiO₂ nanocrystals by thermal decomposition of titanium (IV) n-butoxide. *Ceram. Int.* 2005, 31, 391.
- Thompson, T. L.; Diwald, O.; Yates, J. T., Jr. CO₂ as a probe for monitoring the surface defects on TiO₂(110)-temperature-programmed desorption. *J. Phys. Chem. B* 2003, 107, 11700.
- Watson, S. S.; Beydoun, D.; Scott, J. A.; Amal, R. The effect of preparation method on the photoactivity of crystalline titanium dioxide particles. *Chem. Eng. J.* 2003, 95, 213.
- Xiao-Quan, C.; Huan-Bin, L.; Guo-Bang, G. Preparation of nanometer crystalline TiO₂ with high photocatalytic activity by pyrolysis of titanil organic compounds and photo-catalytic mechanism. *Mater. Chem. Phys.* 2005, 91, 317.
- Kumar, P. M.; Badrinarayanan, S.; Sastry, M. Nanocrystalline TiO₂ studied by optical, FTIR and X-ray photoelectron spectroscopy: Correlation to presence of surface states. *Thin Solid Films* 2000, 358, 122.
- Yu, J.; Zhao, X.; Zhao, Q. Effect of surface structure on photocatalytic activity of TiO₂ thin films prepared by sol-gel method. *Thin Solid Films* 2000, 379, 7.
- Pouilleau, J.; Devilliers, D.; Groult, H.; Marcus, P. Surface study of a titanium-based ceramic electrode material by X-ray photoelectron spectroscopy. *J. Mater. Sci.* 1997, 32, 5645.
- Diebold, U. The surface science of titanium dioxide. *Surf. Sci. Rep.* 2003, 48, 53.
- Sorescu, D. C.; Yates, Jr., J. T. First principles calculations of the adsorption properties of CO and NO on the defective TiO₂(110) surface. *J. Phys. Chem. B* 2002, 106, 6184.
- Liu, G.; Rodriguez, J. A.; Hrbek, J.; Long, B. T.; Chen, D. A. Interaction of thiophene with stoichiometric and reduced rutile TiO₂(110) surfaces: Role of Ti³⁺ sites in desulfurization activity. *J. Mol. Catal. A* 2003, 202, 215.
- Sakai, N.; Fujishima, A.; Watanabe, T.; Hashimoto, K. Enhancement of the photoinduced hydrophilic conversion rate of TiO₂ film electrode surfaces by anodic polarization. *J. Phys. Chem. B* 2001, 105, 3023.
- Park, D.-R.; Zhang, J.; Ikeda, K.; Yamashita, H.; Anpo, M. Photocatalytic oxidation of ethylene to CO₂ and H₂O on ultrafine powdered TiO₂ photocatalysts in the presence of O₂ and H₂O. *J. Catal.* 1999, 185, 114.
- Schwitzgebel, J.; Ekerdt, J. G.; Gerischer, H.; Heller, A. Role of the oxygen molecule and of the photogenerated electron in TiO₂-photocatalyzed air oxidation reactions. *J. Phys. Chem.* 1995, 95, 5633.
- Brinkley, D.; Engel, T. Active site density and reactivity for the photocatalytic dehydrogenation of 2-propanol on TiO₂(110). *Surf. Sci.* 1998, 415, 1001.
- Diebold, U.; Lehman, J.; Mahmoud, T.; Kuhn, M.; Leonardelli, G.; Hebenstreit, W.; Schmid, M.; Varga, P. Intrinsic defects on a TiO₂-(110)(1 × 1) surface and their reaction with oxygen: A scanning tunneling microscopy study. *Surf. Sci.* 1998, 411, 137.
- Schaub, R.; Thostrup, P.; Lopez, N.; Lægsgaard, E.; Stensgaard, I.; Nørskov, J. K.; Besenbacher, F. Oxygen vacancies as active sites for water dissociation on rutile TiO₂(110). *Phys. Rev. Lett.* 2001, 87, 2661041.
- Schaub, R.; Wahlström, E.; Romau, A.; Lægsgaard, E.; Stensgaard, I.; Besenbacher, F. Oxygen-mediated diffusion of oxygen vacancies on the TiO₂(110) surface. *Science* 2003, 299, 377.
- Li, F. B.; Li, X. Z. Photocatalytic properties of gold/gold ion-modified titanium dioxide for wastewater treatment. *Appl. Catal. A-Gen.* 2002, 228, 15.
- Li, F. B.; Li, X. Z.; Ao, C. H.; Lee, S. C.; Hou, M. F. Enhanced photocatalytic degradation of VOCs using Ln³⁺-TiO₂ catalysts for indoor air purification. *Chemosphere* 2005, 59, 787.
- Kongsuechart, W.; Praserttham, P.; Panpranon, J.; Sirisuk, A.; Supphasirongjaroen, P.; Satayaprasert, C. Effect of crystallite size on the surface defect of nano-TiO₂ prepared via solvothermal synthesis. *J. Cryst. Growth* 2006, 297, 234.
- Suriye, K.; Praserttham, P.; Jongsonjitt, B. Control of Ti³⁺ surface defect on TiO₂ nanocrystal using various calcination atmospheres as the first step for surface defect creation and its application in photocatalysis. *Appl. Surf. Sci.* 2007, 253, 3849.

Received for review May 17, 2007

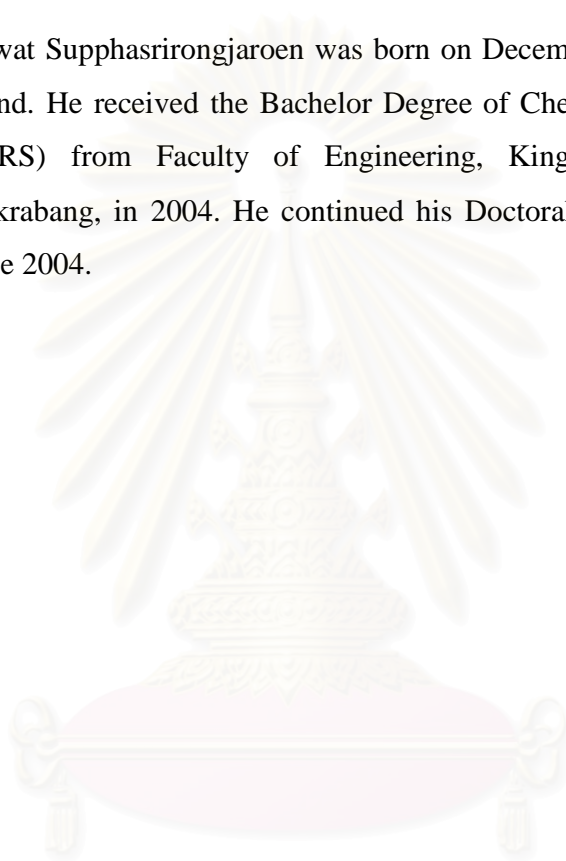
Revised manuscript received September 5, 2007

Accepted October 17, 2007

IE070705A

VITA

Mr. Piyawat Supphasrironjaroen was born on December 1, 1981 in Surat Thani Province, Thailand. He received the Bachelor Degree of Chemical Engineering (FIRST CLASS HONORS) from Faculty of Engineering, King's Mongkut Institute of Technology Ladkrabang, in 2004. He continued his Doctoral's study at Chulalongkorn University in June 2004.



สถาบันวิทยบริการ
จุฬาลงกรณ์มหาวิทยาลัย